TU Delft

Delft University of Technology

Enhancing the performance of active and passive systems in visible light communication

Xu, M.

DOI
10.4233/uuid:de365b76-bea8-489a-a75a-023a04ff1bc8

Publication date
2024

Document Version
Final published version

Citation (APA)
Xu, M. (2024). *Enhancing the performance of active and passive systems in visible light communication*. [Dissertation (TU Delft), Delft University of Technology]. https://doi.org/10.4233/uuid:de365b76-bea8-489a-a75a-023a04ff1bc8

Important note
To cite this publication, please use the final published version (if applicable).
Please check the document version above.

Copyright
Other than for strictly personal use, it is not permitted to download, forward or distribute the text or part of it, without the consent of the author(s) and/or copyright holder(s), unless the work is under an open content license such as Creative Commons.

Takedown policy
Please contact us and provide details if you believe this document breaches copyrights.
We will remove access to the work immediately and investigate your claim.

This work is downloaded from Delft University of Technology.
For technical reasons the number of authors shown on this cover page is limited to a maximum of 10.

Enhancing the Performance of Active and Passive Systems in Visible Light Communication

Enhancing the Performance of Active and Passive Systems in Visible Light Communication

Dissertation

for the purpose of obtaining the degree of doctor
at Delft University of Technology,
by the authority of the Rector Magnificus Prof. dr. ir. T.H.J.J. van der Hagen,
chair of the board for Doctorates,
to be defended publicly on
Wednesday 30 October 2024 at 10:00 o'clock

by

Talia Xu

Master of Applied Science in Electrical Engineering, University of Toronto, Canada,
born in Guangzhou, China.

This dissertation has been approved by promotors.

promotor: Dr. M.A. Zúñiga Zamalloa
copromotor: Dr. Q. Wang

Composition of the doctoral committee:

Rector Magnificus,	Chairman
Dr. M.A. Zúñiga Zamalloa,	Delft University of Technology, promotor
Dr. Q. Wang	Delft University of Technology
Independent members:	
Prof. dr. K.G. Langendoen	Delft University of Technology
Prof. dr. A. Markham	University of Oxford
Prof. dr. C.A. Boano	Graz University of Technology
Prof. dr. H. Flores	University of Tartu

Dr. M.A. Zúñiga Zamalloa and Dr. Q. Wang have contributed significantly to the realization of the thesis.



Keywords: Passive VLC System, Active VLC System

Printed by:

Front & Back:

Copyright © 2024 by T. Xu

ISBN 978-94-6384-670-7

An electronic version of this dissertation is available at
http://repository.tudelft.nl/.

CONTENTS

Summary **vii**

1 Introduction **1**
1.1 Wireless Communication . . . 1
1.2 Communication with Light . . . 3
1.2.1 Artificial Light . . . 3
1.2.2 Natural Light . . . 5
1.3 Contribution . . . 6

2 Seeing Around Corners: Joint Sensing And Communication With Light Using IRS **9**
2.1 Introduction . . . 10
2.2 System Overview . . . 12
2.3 Surface Design . . . 12
2.3.1 Designing a Passive Reflective Surface . . . 12
2.3.2 Designing an Active Reflective Surface . . . 16
2.4 IRS for Around-the-Corner Sensing . . . 19
2.4.1 Sensing Mechanism . . . 19
2.4.2 Around-the-Corner Sensing . . . 21
2.4.3 Sensing Multiple Events . . . 22
2.5 IRS for Communication . . . 23
2.5.1 System Design . . . 23
2.5.2 Evaluation of Passive Surface . . . 25
2.5.3 Evaluation of Active Surface . . . 27
2.5.4 IRS Under Low-Light Condition . . . 28
2.6 Joint Sensing and Communication . . . 29
2.7 Related Work . . . 31
2.8 Conclusion . . . 33

3 Exploiting Digital Micro-Mirror Devices for Ambient Light Communication **35**
3.1 Introduction . . . 36
3.2 System Analysis . . . 37
3.2.1 Maintaining the luminous flux . . . 38
3.2.2 Ray-tracing model . . . 39
3.2.3 Insights & Guidelines . . . 39
3.3 Transmitter Design . . . 42
3.3.1 LC limitations . . . 42
3.3.2 DMD basics . . . 43
3.3.3 Limitations of inexpensive DMDs . . . 44
3.3.4 PhotoLink controller . . . 45

3.4 Optical Link . . . 46
3.4.1 Modulation . . . 46
3.4.2 Demodulation . . . 47
3.5 Evaluation . . . 48
3.5.1 Receiver Design & Data Rate . . . 48
3.5.2 Analyzing the Luminous Flux . . . 51
3.5.3 Issues with DMDs . . . 52
3.6 Related Work . . . 54
3.7 Conclusion . . . 56

4 Sunlight-Duo: Exploiting Sunlight for Simultaneous Energy Harvesting & Communication 57
4.1 Introduction . . . 58
4.2 System Overview . . . 60
4.3 State-of-the-Art analysis . . . 61
4.3.1 Passive RF & positive-energy sensing . . . 61
4.3.2 Solar Cell as a Data Receiver . . . 62
4.3.3 Sunlight as a Signal Source . . . 63
4.3.4 The novelty of our approach . . . 63
4.4 Analysis of Charger and Solar Cell . . . 63
4.4.1 Controlled evaluation setup and metrics . . . 64
4.4.2 Step 1: Choosing a solar cell charger . . . 65
4.4.3 Step 2: Defining Solar Cell Configurations . . . 65
4.4.4 Step 3: Analyzing the Pre-charging Stage . . . 66
4.4.5 Step 4: Analyzing the Charging Stage . . . 67
4.4.6 Step 5: Operation in Fully-charged Stage . . . 69
4.4.7 Summary . . . 70
4.5 Design of Reconfigurable Receiver . . . 70
4.5.1 Receiver Hardware . . . 70
4.5.2 Dynamic Reconfiguration . . . 71
4.6 System Evaluation . . . 72
4.6.1 Comparison with the SoA . . . 73
4.6.2 Experiment Setup in Outdoor Evaluation . . . 73
4.6.3 Link Range and Reliability . . . 74
4.6.4 Bi-Directional Link and Longer Range . . . 75
4.6.5 Stability of Bi-directional Link . . . 76
4.6.6 Discussion . . . 77
4.7 Conclusion . . . 78

5 Conclusion 79
5.1 Dissertation Work . . . 79
5.2 Future Work . . . 81

Acknowledgments 83

Bibliography 85

SUMMARY

Communication technology has continually adapted to new challenges. RF communication, with its established infrastructure, supports technologies like Bluetooth, Wi-Fi, and LoRa. However, the rise of IoT devices has lead to problems in traditional RF communication such as increasing spectrum congestion and interference. In this context, Visible Light Communication (VLC) emerges as a promising alternative to traditional RF systems. VLC uses the unlicensed light spectrum, modulating light intensity at speeds invisible to the human eye to transmit data, which is then received and decoded by photodetectors. While RF communication can also utilize unlicensed bands, VLC operates in an entirely separate region that experiences fewer regulatory constraints and interference issues compared to the crowded RF spectrum.

VLC systems can be classified based on their light source into *active VLC* and *passive VLC*. Active VLC systems use LEDs to transmit data through rapid light modulation controlled by circuitry, enabling fast communication. A key advantage of active VLC is its dual-purpose function, serving both illumination and communication, thereby maximizing resource use. However, the illumination of LEDs is often *obstructed* by walls or furniture affecting the coverage of active VLC systems. On the other hand, passive VLC systems use sunlight for data transmission, offering a *pervasive* and *energy-efficient* communication method, as sunlight provides a continuous source of illumination without additional energy costs. Passive VLC systems use external modulating surfaces to modulate ambient light properties to transmit data but face challenges due to the variable nature of ambient light, leading to links with lower performance compared to active VLC.

In this thesis, we address the *obstruction* challenges of active VLC and the *low performance* of passive VLC through a comprehensive approach that combines novel hardware designs and strategic system integration.

Chapter 2 addresses the obstruction challenge in active VLC by using intelligent reflecting surfaces (IRS). It introduces the Dual-Mirrors platform, a solution designed to tackle Non-Line-of-Sight (NLOS) communication and sensing issues in active VLC systems. This platform utilizes both passive and active IRS to enhance VLC coverage. Passive IRS splits light into multiple beams to cover various spots, while active IRS dynamically adjusts beam direction to maintain connectivity in changing environments. Additionally, retro-reflectors are integrated to detect human presence in areas not directly visible to the light source, extending the sensing range of VLC systems. Practical testing demonstrates that the Dual-Mirrors platform significantly improves communication coverage and reliability in NLOS areas, effectively addressing limitations posed by obstructions like walls and furniture.

Chapter 3 and Chapter 4 address the challenges in passive VLC systems. Chapter 3 focuses on enhancing the communication efficiency of passive VLC systems by introducing a novel transmitter design using Digital Micromirror Devices (DMDs). This im-

plementation achieves data transmission rates up to 30 times faster than conventional methods. An optical model is also developed to understand the fundamental limits and opportunities of ambient light communication, showing that maintaining directional light patterns is crucial for passive links. The research demonstrates that DMDs can maintain high data rates even with ambient light noise, making them a robust solution for real-world applications.

While Chapter 3 proposes a novel transmitter design, Chapter 4 focuses on the receiver. In that chapter, we explore the use of solar cells for both communication and energy harvesting in passive VLC systems, addressing the trade-off between these two functions. The chapter introduces the Sunlight-Duo system, featuring a receiver that dynamically adjusts key solar cell parameters to optimize both energy harvesting and data communication. The prototype demonstrates a self-powered receiver capable of maintaining a bi-directional link for up to 11 meters, with stable data rates even under varying sunlight conditions. This research confirms that with dynamic reconfiguration, VLC systems can achieve stable communication and efficient energy use, highlighting the potential for a sustainable VLC technology in embedded IoT devices.

By advancing the capabilities of both active and passive VLC systems, this thesis demonstrates that VLC can be a viable and sustainable alternative to traditional RF communication, meeting the growing connectivity demands of the digital age while leveraging existing light infrastructure for enhanced efficiency and reduced energy consumption.

1

INTRODUCTION

Imagine a typical morning in the digital age: A smart alarm gently wakes you, while simultaneously adjusting the house's thermostat based on the day's forecast and your personal schedule. In the kitchen, prompted by the same alarm, your coffee maker starts brewing your morning cup. Meanwhile, many miles away in a remote greenhouse, many sensors continuously track humidity and temperature, automatically fine-tuning the environment to ensure optimal plant growth. This seamless integration of IoT devices, from common household appliances to advanced agricultural systems, highlights the crucial need for reliable connectivity. Staying connected has become a fundamental necessity in these dynamic settings, where a myriad of devices rely on robust wireless communication systems for efficient operation throughout the day. As our reliance on such interconnected devices grows, it places increasing demands on our communication infrastructures. Networks supporting these smart systems must therefore evolve to meet the diverse and expanding connectivity needs of our increasingly digitized lives.

1.1. WIRELESS COMMUNICATION

The evolution of communication technology has always been driven by the need to address ever-changing challenges. One notable milestone is Alexander Graham Bell's invention of the Photophone in 1880, which was an early attempt to transmit sound using sunlight reflections. Despite its innovative approach and potential, the Photophone was quickly overshadowed by the emergence of RF communication, which offered greater reliability and broader applicability at the time.

RF communication became the backbone of wireless data transmission, supporting a wide range of applications from Bluetooth to WiFi and LoRa. Extensive infrastructure has been developed to support RF communication. However, as our daily environments have become increasingly populated with IoT devices—from smart home systems to advanced agricultural monitors—the limitations of RF communication, such as spectrum congestion and interference, as shown in Figure 1.1, have become increasingly pronounced [1]. This situation not only challenges existing frameworks but also high-

1

lights the sustainability issues, as RF communication remains the sole pillar for wireless communication.

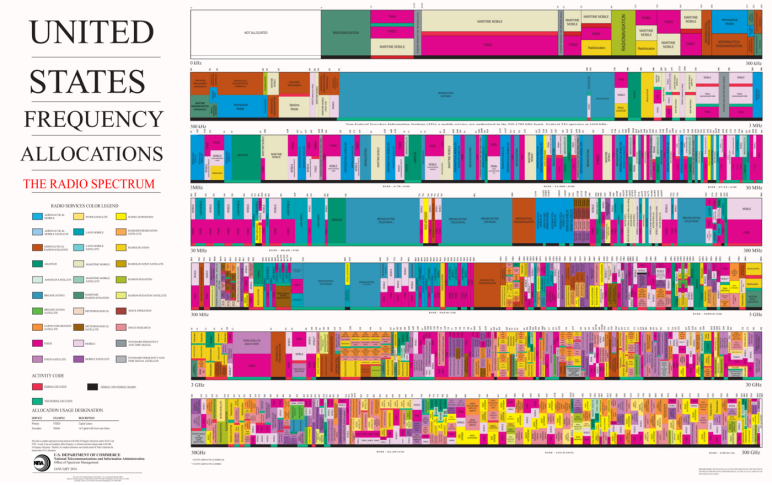


Figure 1.1: U.S. frequency allocation chart for the radio spectrum as of January 2016 [2]

In this context, Visible Light Communication (VLC) stands out as a compelling alternative to traditional RF systems. VLC operates by modulating the intensity of light at speeds imperceptible to the human eye, converting these light variations into data signals that can be received and decoded by photodetectors. Operating on an unlicensed spectrum, VLC avoids the regulatory constraints and interference issues associated with the crowded RF spectrum. This provides VLC with a less crowded channel for communication, as it doesn't compete for bandwidth with the myriad of devices operating in the RF spectrum. Another significant strength of VLC is its ability to utilize a variety of light sources, such as sunlight, streetlights, and indoor lighting, which are commonly available in environments where human activities take place. This capability allows VLC to piggyback on existing illumination infrastructure for data transmission, thereby minimizing the need for additional power and enhancing energy efficiency as light serves dual purposes of illumination and communication. Thus, VLC not only provides potentially higher bandwidth than RF but does so in a way that is inherently more energy-efficient. By utilizing light already in operation, VLC provides a smooth and sustainable way to improve connectivity, proving particularly valuable in settings where RF communication faces limitations.

VLC can support a wide range of capabilities depending on the nature of the light source, as shown in Table 1.1. It's important to note that Table 1.1 does not encompass the full range of possibilities for active and passive VLC systems. Instead, it serves as a generalized overview of their typical performance characteristics, highlighting the common advantages with each approach. *Active VLC* systems, utilizing LEDs, are ideal for high-speed data transmission over short ranges. They are particularly efficient when the same light source is used for both illumination and communication, making them suitable for indoor environments with existing lighting infrastructure. On the other hand,

passive VLC systems harness sunlight, providing very energy-efficient communication over longer ranges. This makes them highly effective in outdoor settings or environments where natural light is abundant.

Table 1.1: Comparison of typical performance parameters for active and passive VLC Systems

Type	Light Source	Range	Speed	Energy Efficiency
Active VLC	Directly Controllable (LED)	Short	High	Efficient (when light is used for both illumination and communication)
Passive VLC	Uncontrollable Ambient Light (Sunlight)	Long	Low	Very Efficient

However, VLC's dependence on light as a transmission medium comes with its own set of challenges. Unlike RF signals, which are designed specifically for communication, light is primarily meant for illumination. Adapting it to serve dual purposes without compromising its primary function requires careful consideration. For instance, natural light like sunlight, while abundant and readily available, is unpredictable and can lead to high noise levels in communication due to its omnipresence and variability. This complexity extends to indoor settings as well; VLC needs to be carefully integrated with existing lighting schemes and adapted to the functional design of spaces, which can restrict its deployment across various indoor environments. While we can add multiple WiFi access points to enhance coverage without affecting aesthetics, adding light bulbs disrupts the lighting design. Light bulbs serving both illumination and communication purposes, require strategic placement to ensure effective data transmission and adequate lighting, making their addition more complex than WiFi access points.

These challenges necessitate creative system solutions to ensure that VLC operates effectively within the constraints of natural and artificial light.

1.2. COMMUNICATION WITH LIGHT

In the modern era, light-based communication technologies are steadily evolving. This section explores various aspects of VLC, focusing on the different ways light is used for data transmission, the corresponding challenges, and how this thesis aims to address them.

1.2.1. ARTIFICIAL LIGHT

The most straightforward way of using light to communicate is by directly turning the light on and off at a speed imperceptible to the human eye. As shown in Figure 1.2, active VLC systems employ LEDs that emit signals controlled by modulating circuitry. This method provides dynamic control of the light source, allowing for rapid switching to create precise data patterns for reliable and efficient transmission. However, it requires modifications to the existing lighting infrastructure. Specifically, the light switches and control systems need to be upgraded to support high-speed modulation, which can involve significant changes to the electrical and control systems of buildings.

1

ARTIFICIAL LIGHT FOCUSING ON COMMUNICATION

Although the premise of VLC systems is to use light for both communication and illumination, several studies focus primarily on optimizing the communication capabilities of VLC systems, with less emphasis on their illumination role. For example, Tsonev et al. demonstrated that using a colored Gallium Nitride μLED could achieve a communication speed of 3 GB/s [3]. Similarly, Yeh et al. achieved a communication speed of 37 MB/s with a custom phosphor-LED array [4]. However, these studies use custom or colored LEDs that are not typically used for general illumination. Later research showed that using laser diodes could push communication rates further to nearly 100 GB/s [5], but this approach also sacrifices the lighting function for higher data rates by using laser. By isolating the communication function, these studies have made significant advancements in speed and efficiency. On the down side, however, this approach comes with a high energy overhead, as the light is used exclusively for communication purposes, neglecting the dual functionality that VLC systems ideally aim to provide.

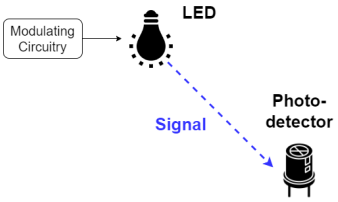


Figure 1.2: System overview of an active VLC system focusing on communication. Only the communication capability is of interest

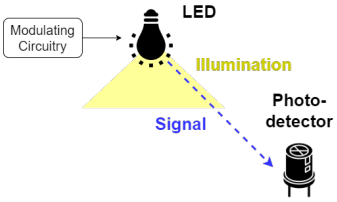


Figure 1.3: System overview of an active VLC system providing illumination and communication

ARTIFICIAL LIGHT FOR BOTH ILLUMINATION AND COMMUNICATION

The core advantage of active VLC occurs when light is used for both communication and illumination simultaneously, as shown in Figure 1.3. This dual-purpose use leverages existing lighting infrastructure to transmit data, introducing only a slight increase in energy usage. Compared to Figure 1.2, the system components remain the same; however, lights must be strategically placed to ensure both effective data transmission and adequate lighting.

This efficient use of light maximizes resource utilization. However, additional constraints related to deployment and coverage must be considered. For example, lights are usually placed in the center of the room, but for communication and sensing, they can be blocked by furniture and walls. When there is a blockage, these lights cannot be easily reinstalled in different locations, and new lights cannot be easily installed to circumvent the obstacles. This inflexibility in placement adds complexity to the system and can limit its effectiveness. One way to mitigate this is to use Intelligent Reflecting Surface (IRS). IRS are reflective surfaces that can reflect light in a controlled manner, effectively redirecting the communication signals around obstacles. By strategically placing IRS in the environment, it is possible to enhance coverage and ensure that data transmission is not impeded by physical barriers.

This leads us to ask the following research question:

How can IRS be tailored to overcome Non-Line-of-Sight (NLOS) communication and sensing challenges in active VLC?

In *Chapter 2*, we explore the integration of IRS into active VLC systems. This research focuses on addressing the challenge of NLOS communication by evaluating both passive and active IRS configurations. The primary objective is to improve communication reliability in environments where direct lines of sight are obstructed. By incorporating IRS prototypes, the study aims to enhance coverage and control, significantly strengthening NLOS communication and sensing capabilities.

1.2.2. NATURAL LIGHT

We previously focused our discussion on artificial light, which only accounts for part of our illumination needs. Many scenarios, such as green house farming and outdoor environments, rely heavily on sunlight. Utilizing sunlight for communication is the most energy-efficient method due to its abundance. Sunlight, being a free and renewable resource, provides an inexhaustible source of illumination without additional energy costs. By harnessing sunlight for data transmission in passive VLC, we can further reduce the energy footprint associated with active VLC.

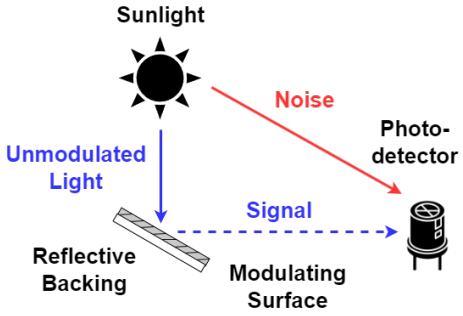


Figure 1.4: System overview of a passive VLC system

The system overview of passive light communication is illustrated in Figure 1.4. In the figure, unmodulated ambient light is directed towards a modulator, which alters its properties to encode data. The modulated light then carries the signal to a receiver, while noise, represented by the red arrow, presents an inherent challenge that must be managed to maintain signal integrity. Instead of generating new light, passive VLC systems modulate the properties of available sunlight to transmit data.

However, compared to active VLC, passive VLC is more challenging because the inherent noise coming from the ambient light source can interfere with the signal integrity. In passive VLC systems, although we use ambient light for communication, its property, such as brightness, is beyond our control. Consequently, variations in the intensity and quality of natural light due to environmental factors such as weather conditions, time of day, and the presence of obstacles can introduce significant noise. This noise can degrade the Signal-to-Noise Ratio (SNR), making it more difficult to correctly decode the transmitted data.

1

In a passive VLC system, we face a unique challenge: optimizing the system's overall performance requires considering both the transmitter and the receiver, as they are inherently intertwined in their reliance on ambient light. To address these interconnected aspects, we pose the following research questions:

How can the transmitter design in passive VLC systems be optimized to increase data transmission rates using ambient light?

In *Chapter 3*, we focus on enhancing the communication efficiency of VLC systems by improving the transmitter design to increase the data rate of passive systems. This chapter introduces a novel transmitter approach using Digital Micromirror Devices (DMD), which allows for significantly higher data transmission rates using ambient light. The implementation of DMD achieves data transmission rates up to 30 times faster than current state-of-the-art studies.

How can passive VLC receivers optimize the system's overall performance and energy efficiency?

Building on advancements in solar cell technology, *Chapter 4* shifts focus to the receiver side. This chapter explores methods to use sunlight for both communication and energy harvesting by designing a receiver with solar cells and a control scheme that optimizes both functions simultaneously. We employ solar cells for the dual purpose of energy harvesting and data reception, leveraging ambient light to enhance the system's overall energy efficiency and performance.

1.3. CONTRIBUTION

As part of our contributions, we have authored several publications related to this thesis.

Chapters 2, 3, and 4 are presented in the following papers:

- **Talia Xu**, Harald Haas and Marco Zúñiga. Seeing Around Corners: Joint Sensing And Communication With Light Using IRS.

  Under submission.

- **Talia Xu**, Miguel Chávez Tapia and Marco Zúñiga (2022). Exploiting Digital Micro-Mirror Devices for Ambient Light Communication. *USENIX Symposium on Networked Systems Design and Implementation (NSDI).*

- **Talia Xu**, Mirco Muttillo, Miguel Chavez Tapia, Patrizio Manganiello, Harald Haas and Marco Zúñiga (2024). Sunlight-Duo: Exploiting Sunlight for Simultaneous Energy Harvesting & Communication. *The International Conference on Embedded Wireless Systems and Networks (EWSN).*

During my thesis I also work on other topics related to VLC, those publications are not part of the thesis but they are listed below. The studies marked with an asterisk (*) are the result of MSc theses I advised during my PhD.

- Miguel Chávez Tapia, **Talia Xu** and Marco Zúñiga (2022). SunBox: Screen-to-Camera Communication with Ambient Light. *Proceedings of the ACM on Interactive, Mobile, Wearable and Ubiquitous Technologies (IMWUT).*
- *Oxana Oosterlee, **Talia Xu** and Marco Zúñiga (2022). Inti: Indoor Tracking with Solar Cells. *The International Conference on Embedded Wireless Systems and Networks (EWSN).*
- *Ricardo Ampudia Hernández, **Talia Xu**, Yanqiu Huang, Marco Zúñiga (2023). Firefly: Supporting Drone Localization With Visible Light Communication. *International Conference on Distributed Computing in Smart Systems and the Internet of Things (DCOSS-IOT).*
- *Lucan de Groot, **Talia Xu** and Marco Zúñiga (2023). DroneVLC: Exploiting Drones and VLC to Gather Data from Batteryless Sensors. *The International Conference on Pervasive Computing and Communications (PerCom).*
- Miguel Chávez Tapia, **Talia Xu** and Marco Zúñiga (2024). Sol-Fi: Enabling Joint Illumination and Communication in Enclosed Areas with Sunlight *Information Processing in Sensor Networks (IPSN).*

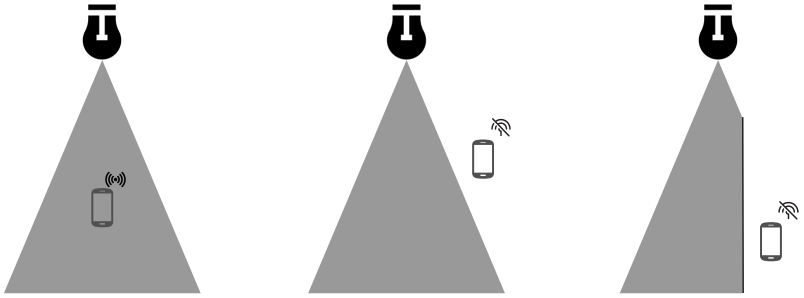
2

SEEING AROUND CORNERS: JOINT SENSING AND COMMUNICATION WITH LIGHT USING IRS

In the introduction of this thesis, we discussed VLC as a promising alternative to traditional RF systems. VLC can use existing lighting infrastructure for both illumination and communication, operating on an unlicensed, less crowded spectrum. However, obstacles can easily block VLC signals, disrupting communication. To address these limitations, we introduce Dual-Mirrors in this chapter, a novel platform to attain joint sensing and communication in scenarios without line-of-sight. Dual-Mirrors provides three main contributions. First, we propose methods to design passive and active surfaces to target different types of static and dynamic scenarios. Second, we design a passive system to detect people's presence using retro-reflectors that could be worn by users or placed in the area of interest. Third, we demonstrate practical links that provide coverage in zones without a line of sight. Combining the above three contributions, we show how a single light bulb –together with our reflective surfaces– can be used in a 12 m×8 m area to sense a person moving around and use the estimated location to provide communication in zones outside the light's coverage.

2.1. INTRODUCTION

The increasing demand for wireless connectivity has motivated researchers to investigate different parts of the electromagnetic spectrum. One of those alternatives is visible light communication (VLC), which exploits a spectrum that is wide, free, and empty. In VLC, the intensity of LEDs is modulated at a high speed, allowing data to be transmitted without compromising the primary lighting function. As LEDs are widely used in both residential and commercial buildings [6], they offer a new approach to address the growing need for fast network speeds in indoor scenarios.



(a) Within coverage (b) Outside coverage (c) Blockage

Figure 2.1: VLC coverage and challenges

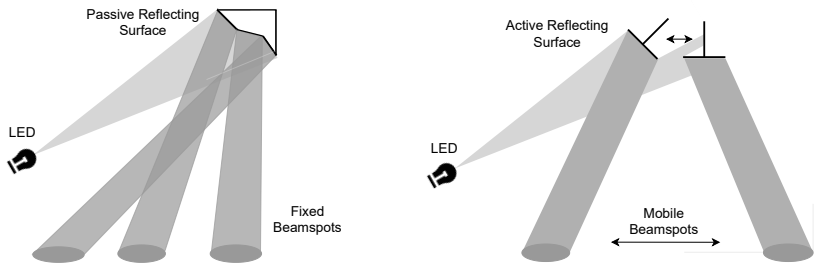
Although VLC offers promising advantages, it also faces important challenges. Contrary to WiFi access points, which can be placed almost anywhere to extend coverage, light fixtures need to follow strict architectural guidelines to fulfill the main role of illumination. These restrictions affect VLC's performance as illustrated in Figure 2.1. Owing to the limited number and strategic placements of light sources, some areas are not covered or could be blocked by walls or furniture, affecting communication due to the line-of-sight requirement of VLC. To enhance the coverage of indoor VLC, a promising strategy involves the use of intelligent reflecting surfaces (IRS). These surfaces are designed to reflect light in predetermined directions. Unlike the restrictions on light bulb deployment, IRS can be easily mounted on walls or other surfaces and do not require modifying the access points (LEDs). Furthermore, the decoupling of IRS from the light infrastructure simplifies deployment, ensuring easier integration into existing indoor environments.

Limitations of the SoA. While IRS in VLC shows potential, the state-of-the-art has two main limitations. *First*, much of the existing research is rooted in theoretical models and simulation-based analysis [7, 8]. These studies consider the impact of the size, position, and orientation of IRS on the wireless channel. The analysis, however, tend to emphasize signal propagation in somewhat idealized, free-space-like environments, which may not fully capture the complexities of real-world settings. For example, these ideal conditions do not include effects present in realistic indoor setups such as the presence of multiple objects or the impact of ambient light. *Second*, the studies focus on communication without considering the potential for sensing. Wireless communication systems based on radio frequencies are increasingly used to sense people [9, 10, 11]. Light-based systems have the same potential but studies mainly focus on developing a communication system or a sensing system, rather than integrating both functions.

Our aim is to bridge two gaps –one between theory and practice, and the other between communication and sensing– by constructing IRS prototypes using standard components and integrating them with a VLC system. This novel approach showcases a more holistic view of IRS's capabilities in real-world applications.

Contributions. Considering the above motivation and challenges, our work, dubbed Dual-Mirrors, demonstrates different types of IRS for both communication and sensing.

Contribution 1: Surface Design [section 2.3]: We present the design, prototyping, and characterization of two types of IRS, passive and active, as shown in Figure 2.2. For the passive case, Figure 2.2a, the IRS divides light into multiple beams, allowing a single access point to cover diverse spots. For the active case, Figure 2.2b, the IRS adjusts the beam's direction, facilitating connectivity in mobile setups. We develop a simulation tool to design an active IRS equipped with mirrors on a pan/tilt rotational platform. With the simulation tool, we determine the expected coverage and generate the necessary motor controls to direct beams to designated points.



(a) Passive IRS (b) Active IRS

Figure 2.2: Two types of IRS

Contribution 2: "Around the corner" sensing [section 2.4]. We assess the sensing capabilities of our IRS by conducting "around-the-corner" experiments in two distinct scenarios. In the first scenario, a user wearing a retro-reflective vest is detected in different areas. In the second scenario, the user does not need to wear any special vest. We place retro-reflective tags on the walls and our active IRS autonomously tracks the users as they pass through the tags.

Contribution 3: "Around the corner" communication [section 2.5]. We build a VLC system using an off-the-shelf LED and photosensor. Under the standard setting of having the receiver placed directly under the LED's coverage, the system can transmit 100 kbps using BFSK modulation. With this optical link, we use "around the corner" scenarios to uncover the trade-offs between coverage and signal-to-noise ratio (SNR) for static and mobile setups using our IRS.

Contribution 4: Joint sensing and communication [section 2.6]. Combining the above contributions, we show a scenario where joint sensing and communication is achieved. We place our transmitter, receiver and IRS in a 12 m × 8 m apartment. The transmitter and IRS have fixed positions but a user moves the receiver to different rooms. We show that our system can track the user as she moves around, and utilizes the estimated lo-

cation to provide communication in rooms that are outside the light's coverage. To the best of our knowledge, this is first demonstration of real IRS with VLC and of simultaneous sensing and communication with light.

2.2. SYSTEM OVERVIEW

Our system is structured around three primary components: the *transmitter*, *surface (IRS)*, and *receiver*.

Transmitter: The *light source*, an LED, acts as the transmitter. Depending on its design, an LED can emit a short and wide beam (short range but wide coverage), or a long and narrow beam (long range but narrow coverage) similar to the behavior of a spotlight. The transmitter also has a photosensor that is used for the sensing tasks, as described later.

Surface (IRS): The IRS acts as a secondary light source, capturing light from the LED and re-directing it towards the receiver. In our design, the IRS is implemented using specular reflective surfaces, similar to mirrors. The reflection of the surface is governed by Snell's law [12].

Receiver: Photodiodes (PDs) and cameras are commonly used as receivers in VLC systems. In our design, we utilize a PD due to its fast response time and lower power consumption compared to a camera. This receiver integrates a TEPT4400 phototransistor, coupled with a single-stage amplifier with variable gain.

***System Setup for Communication and Sensing*:** The configurations for both communication and sensing using IRS are shown in Figure 2.3a and Figure 2.3b. For the sensing phase, the transmitter simply needs to emit light (black arrows). As a target moves around the space, the amount of reflected light reaching the receiver varies (dashed arrows), which is used for tracking. For the communication phase, the LED emits modulated light and the (mobile) receiver decodes the information. The communication link of our system is simplex (only downlink). Commercial VLC systems use infrared or RF signals for the uplink [13, 14]. Using RF signals would suit our platform better[1].

We target scenarios similar to industrial warehouses, where workers may wear reflective vests and the layout of aisles, shelving units, and equipment generate obstructions. Here, IRS could be strategically deployed to bounce light into dim zones, facilitating both visibility and signals for seamless communication and sensing across the warehouse. Leveraging light reflections in such settings might seem straightforward, but next, we show that crafting optimal surfaces for is not simple.

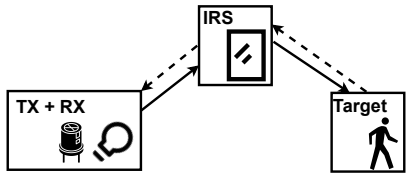
2.3. SURFACE DESIGN

In this section, we present a framework that provides a systematic approach to designing passive and active IRS.

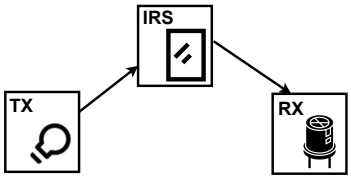
2.3.1. DESIGNING A PASSIVE REFLECTIVE SURFACE

Designing a passive IRS to direct beams to multiple locations is complex because the divided beams can obstruct each other. Manual attempts to configure multiple beams

[1] Note that VLC systems using RF signals for the uplink still reduce the congestion in the RF spectrum because all downlink data uses light.

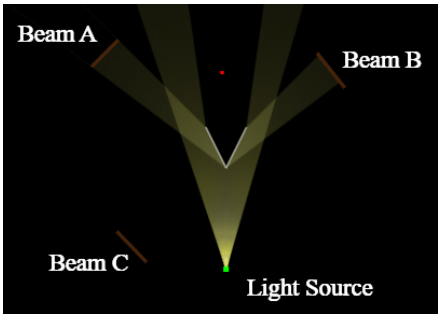


(a) System for sensing

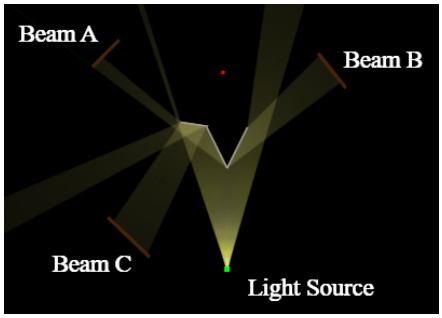


(b) System for communication

Figure 2.3: System setup



(a) Generating two beams



(b) Generating three beams

Figure 2.4: A 2D example showing complications in generating multiple beams with mirrors

can be time-consuming and may not achieve the desired configuration, as illustrated in Figure 2.4, where an initial surface provides coverage to areas A and B, but adding a third area C, inadvertently blocks area A. This complexity escalates with more beams, underscoring the need for a systematic approach that considers the IRS elements as an interconnected whole. To attain that goal, we propose using convex polyhedra for passive IRS design. These geometric entities, characterized by flat faces without concave areas, are well suited for the construction of reflective surfaces.

DESIGN METRICS.

To evaluate passive IRS, we use two primary design metrics, though our framework can be expanded to assess other design aspects as well. First, we examine the *beam deviation*, which quantifies the discrepancy between the generated beams and the target beams. Secondly, we assess the *aspect ratio* of the projected IRS contour. The aspect ratio is central for the IRS to maximize light capture. Considering the overall surface of an IRS, the aim is to create as much overlap as possible between the surface and the incoming light beam. In other words, given that beams from LEDs are usually circular, the projection of the IRS contour onto the plane of the incoming light should aim to have an *aspect ratio* close to one. This ensures maximum light capture.

INITIAL DESIGN APPROACH

In the simulator, we take into account the parameters of the room size, the location of the LED light, the location of the IRS, and the desired characteristics of the beam, as shown in Table 2.1. The parameters in Table 2.1 are based on measurements from our experimental setup. A 3D representation of this setup is shown in Figure 2.6. In this

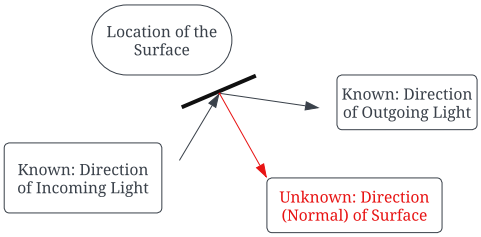


Figure 2.5: Obtaining the surface normal

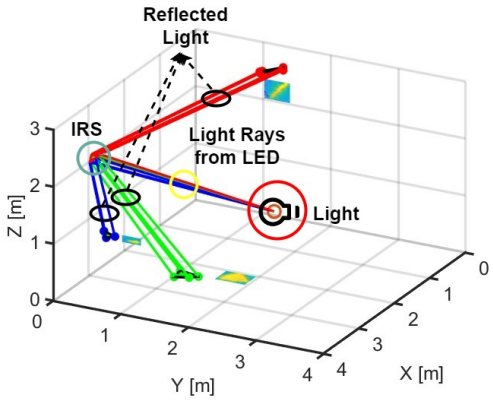


Figure 2.6: 3D representation of setup in Table 2.1

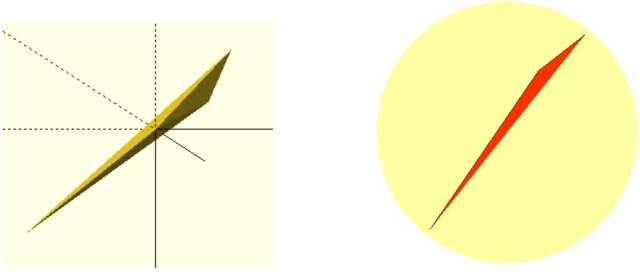
design, the surface splits the incoming light into three beams, one of them has a radius of 0.2 m and the other two a radius of 0.1 m. The differences in beam sizes demonstrate the simulator's capability to generate various configurations.

Once the input parameters are determined, we need to obtain the IRS *surface normals* and the *beam areas*. The *surface normals* can be derived by the positions of both the light source and the reflecting surface by applying geometric relationships, as illustrated in Figure 2.5. The *beam areas* are obtained from the user input. Once the surface normals and associated beam areas are determined, we can reconstruct the convex polyhedra using the mathematical method proposed by Sellaroli [15]. The generated surface is shown in Figure 2.7a, and its projection onto the plane of the incoming light is shown in Figure 2.7b.

This initial design has two problems. *First,* the deviations from the target beams are up to 5.8°, or 37.8 cm, from the intended beam spots projected on the floor or the wall, as captured in Table 2.2. The misalignments primarily arise because the algorithm creates a 3D solid object focused on a single center point, while we utilize its surfaces whose centers deviate from this point. *Second,* due to the long and narrow shape of the IRS (a high aspect ratio), if we were to have a light beam covering its surface, as shown in

Table 2.1: Parameters for simulation

Object	Parameter	Value
Room Size	[x, y, z]	[4 m, 4 m, 3 m]
LED Light	Center of Light	[3.5 m, -1.15 m, 1.36 m]
	Direction of Light	[-0.94 m, 0.31 m, 0.17 m]
IRS	Center of IRS	[0 m, 0 m, 2 m]
Beam	Number of Beam	3
Beam Spot 0	Center	[2.5 m, 1.2 m, 0 m]
	Normal	[0, 0, 1] (beam on floor)
	Radius	0.2 m
Beam Spot 1	Center	[4 m, 0.5 m, 1 m]
	Normal	[-1, 0, 0] (beam on wall)
	Radius	0.1 m
Beam Spot 2	Center	[0 m, 1.2 m, 2.5 m]
	Normal	[1, 0, 0] (beam on wall)
	Radius	0.1 m



(a) Generated IRS after 1st run

(b) The contour of the generated IRS projected onto the light plane

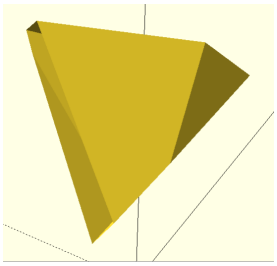
Figure 2.7: Generated IRS surface without optimization

Figure 2.7b, only 2.34% of the light intersects with the surface. This results in a significant portion of the light going unutilized, leading to efficiency losses. To address these two problems, we incorporate an optimization phase that refines the initial design.

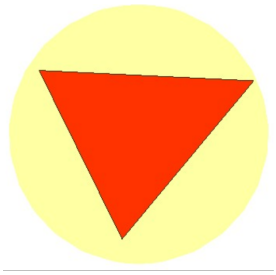
OPTIMIZED DESIGN APPROACH

To overcome the above challenges, we employ the Broyden–Fletcher–Goldfarb–Shanno (BFGS) algorithm, a gradient-based optimization method known for its effectiveness in solving nonlinear optimization problems [16]. The BFGS algorithm is particularly suited for this task due to its ability to efficiently handle the complex relationship between the IRS's shape and the desired beam alignment without requiring the calculation of second derivatives, which can be computationally intensive. Our optimization process, guided by the design metrics outlined in Section 2, specifically targets reducing the cumulative beam deviation and improving the aspect ratio of the IRS with respect to the beam.

The results after optimization are shown in Figure 2.8a, showing a significantly different shape from the surface obtained in the first attempt without optimization. Table 2.2 shows that the maximum beam deviation is now less than 0.01 cm from the designated beam centers for all beams. In addition, we can also observe that the surface intercepts 40.2% of the beam, a significant increase from the previous 2.34%, showing that the optimization step significantly improves surface performance. The 3D design of the opti-



(a) Generated IRS after optimization



(b) The contour of the generated IRS projected onto the light plane

Figure 2.8: Generated IRS surface after optimization

Table 2.2: Beam deviation before and after optimization

Object	Parameter	No Optimization	After Optimization
Beam 0	Angle Deviation	3.0°	0.0004°
	Center Deviation	17.4 cm	N/A [1]
Beam 1	Angle Deviation	1.12°	0.0004°
	Center Deviation	8.98 cm	N/A [1]
Beam 2	Angle Deviation	5.8°	0.0011°
	Center Deviation	37.8 cm	N/A [1]
Surface	LED light coverage	2.34%	40.2%

[1] Negligible, deviation is smaller than 0.01 cm

mized surface was sent to a company so they can manufacture it, and we evaluate the surface in section 2.5. To showcase the framework, we build an IRS with three surfaces. However, the algorithm can generate an arbitrary number of surfaces.

2.3.2. DESIGNING AN ACTIVE REFLECTIVE SURFACE

Considering the warehouse scenario discussed before, the arrangement of objects and shelves can occasionally change. With those dynamics, a fixed reflective surface may be insufficient to provide optimal communication and sensing coverage, as its efficiency would vary with each rearrangement. An active IRS, on the other hand, can adjust its position providing consistent coverage as the environment changes.

Using the pan-tilt mount with motors commonly found in camera and surveillance systems, an IRS could be quickly reoriented. It is important to note that the pan-tilt platform allows efficient adjustments but the mechanical movements are not instantaneous. Our aim is not real-time communication in constantly mobile scenarios. Instead, our focus is on environments that can be reconfigured.

DESIGN TRADE-OFFS AND FRAMEWORK

When designing an active IRS, two important design choices emerge: selecting the motor and determining the surface size. Motors with higher precision offer fine control but are expensive. Similarly, while a larger surface can produce a wider beam, increasing its size also means added weight and rotation complexity, compromising the agility of the system.

Understanding the interplay between motor precision, surface size, and the intended



Figure 2.9: Pan/tilt platforms tested. Left: DF05BB; Middle: RB-Lyn-316; Right: ROB-14391

Table 2.3: Pan/tilt kits and characteristics

Name	Motor	Min. Step Angle	Kit Price	Motor Price
Gravity P/T	DF05BB	1°	€28.92	€10.45
Lynxmotion P/T	HS-85BB	0.5°	€78.65	€28.18
ROB-1439	SG90	12°	€7.11	€3.25

coverage area is crucial for optimizing the design of an active IRS. The system's adaptability, particularly its ability to precisely move and direct beams, hinges on the motors' minimum step angles. To explore this dynamic, we analyze three different pan/tilt platforms, detailed in Figure 2.9 and Table 2.3. These platforms vary in their minimum step angles—from 0.5° with the Lynxmotion Pan/Tilt kit, priced at €78.65, to 12° with the ROB-1439, available for €7.11. Note the clear link between the angular resolution of a platform and its price, highlighting the importance of selecting the appropriate resolution to achieve effective beam coverage within the budget constraints and system requirements.

To facilitate the design of active IRS, we develop a simulation tool based on ray-tracing methods. At each angle step, the emulated mirror rotates using its pan/tilt motors parameters. The simulator then uses the ray-tracing algorithm to trace the path of the light as it reflects off the mirrors and maps it to the final beam spot on the floor or wall. As a sample scenario, we examine the impact of hardware choices on sensing coverage in an area of 5 m by 5 m.

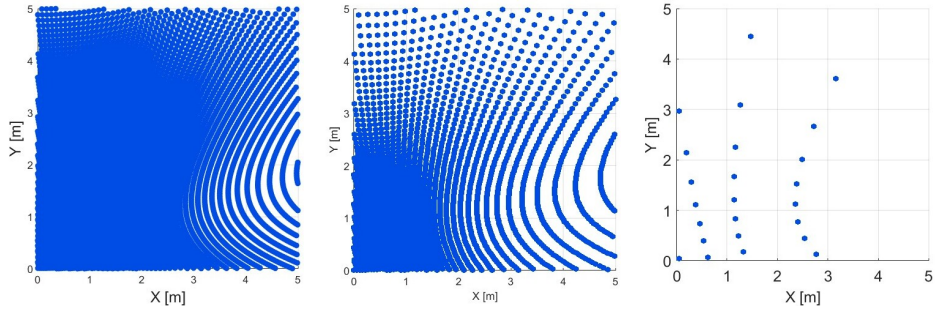
BEAM COVERAGE ANALYSIS

We analyze beam coverage with the input parameters defined in Table 2.4. The results are shown in Figure 2.10. In those figures, the IRS is located at the bottom left corner. In Figure 2.10a, Figure 2.10b and Figure 2.10c, the significance of motor control precision in beam distribution becomes evident. Specifically, a smaller minimum step size results in a denser arrangement of beam spots (better coverage). Additionally, the beam spot density varies with proximity to the IRS; spots are more closely packed near the IRS.

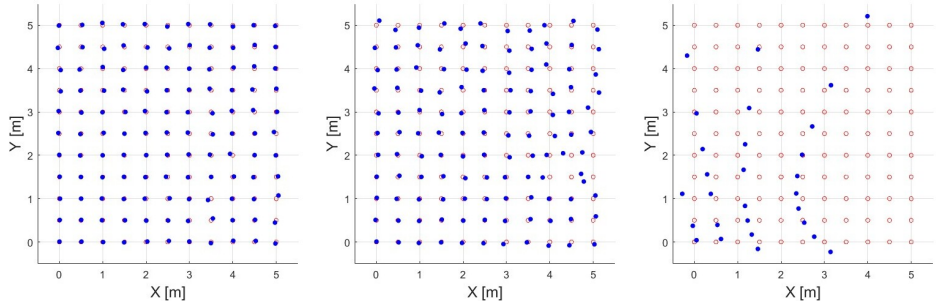
To better quantify beam density, we compare the deviations between actual beams (blue dots) and predefined spots (red dots) spaced 50 cm apart. The results are shown in Figure 2.10d, Figure 2.10e, and Figure 2.10f, with errors detailed in Table 2.5. Smaller step sizes result in significantly reduced errors, underscoring the precision-cost trade-off inherent in servo selection—finer motor adjustments lead to higher costs but better accuracy.

Table 2.4: Simulation parameters for active IRS

Object	Parameter	Value
LED Light	Center of Light	[3.5 m, 0 m, 1.36 m]
IRS	Center	[0 m, 0 m, 1.65 m]
	Angle Step	0.5°, 1°, 10°
	Surface Normal	[1, 0, 0]



(a) Angle step 0.5° (b) Angle step 1° (c) Angle step 10°



(d) Angle step 0.5° (e) Angle step 1° (f) Angle step 10°

Figure 2.10: Beamspots at different IRS locations

A key insight from our analysis is the impact of the reflective surface size on minimizing beam placement inaccuracies. Beams, rather than forming pinpoint spots, generate wider patches significantly influenced by the reflective surface's dimensions. For example, to achieve complete coverage over a 5mx5m area with a motor step size of 10°, a reflective surface measuring 706.4 mm^2 is required to compensate for the beam's dispersion and ensure full coverage. On the other hand, for a finer step size of 1°, a considerably smaller surface area of 102 mm^2 is adequate. This analysis reveals an important trade-off: the IRS's ability to provide full coverage is limited by the motor's precision and the physical dimensions of the IRS surface. As the distance from the IRS increases, a beam directed at a specific target tends to miss its mark more significantly. Increasing the beam's size serves as a countermeasure, reducing the impact of such deviations and thereby expanding the effective coverage area.

In this section, we discussed the design process for both passive and active IRS. We presented a framework that covers the essential design metrics and trade-offs. In the

Table 2.5: Active IRS characteristics for an area of 5 m by 5 m

Object	Parameter	Value
Platform 0	Angle Step	0.5°
	Maximum Error	89 mm
	Cumulative Error	359.8 mm
	Side Length	35.3 mm
Platform 1	Angle Step	1°
	Maximum Error	259 mm
	Cumulative Error	914.9 mm
	Side Length	102 mm
Platform 2	Angle Step	10°
	Maximum Error	1783 mm
	Cumulative Error	8866.3 mm
	Side Length	706.4 mm

following sections, we demonstrate the use of IRSs in sensing and communication applications and provide a closer look at our prototypes and their characteristics.

2.4. IRS FOR AROUND-THE-CORNER SENSING

In warehouse settings, accurately tracking movements presents a notable challenge. RF sensing is well investigated but struggles with interference from metal shelves and electronic devices, which can lead to inaccuracies. This issue prompts a search for more reliable methods. Light-based sensing stands out as a viable alternative, offering improved detection in environments where RF signals are compromised. Yet, the task of tracking people with light is not simple because standard clothing does not always generate the necessary reflections to sense a person effectively.

To address this challenge, our approach leverages retro-reflective materials. These materials, often found in warehouse workers' uniforms and safety vests, enhance light reflection, facilitating tracking. To further refine this method, besides exploiting vests, we can strategically place retro-reflective tags around the warehouse, on assets and key locations, to ensure comprehensive detection coverage. This approach—combining the natural advantage of existing reflective elements with additional strategically placed retro-reflectors—marks a novel strategy to improve light-based sensing effectiveness.

To demonstrate and evaluate the effectiveness of IRS for light-based sensing, we use a residential setup, as shown in Figure 2.11. This setup has interconnected rooms, similar to sections in an industrial facility but on a smaller scale. For example, if a light source is in room F and only covers rooms C, E, and F, our goal is to use IRS to also detect movement in areas not directly visible, like rooms G, H, and I.

2.4.1. SENSING MECHANISM

For sensing with IRS and light, the transmitter and receiver (photosensor) are placed next to each other. We propose two mechanisms to detect the presence of a person in an area of interest: one that requires active user participation (by wearing reflective vests) and another that is passive (no vests required).

Transmitter: We use a 2 W flashlight with 10° FoV. The flashlight transmits a fixed signal at 500 Hz. Using a fixed signal allows us to easily identify variations induced by

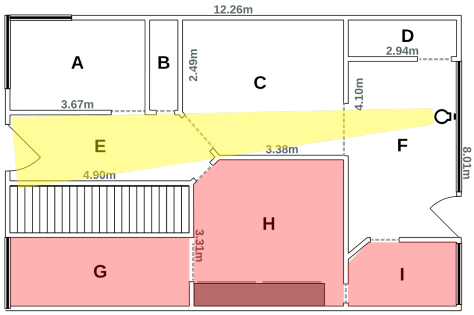
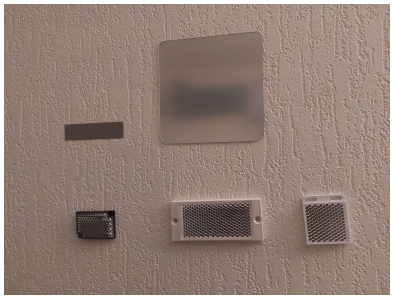


Figure 2.11: Floor plan of a residential house



(a) Retro-reflective tags and fabric



(b) Reflective vest

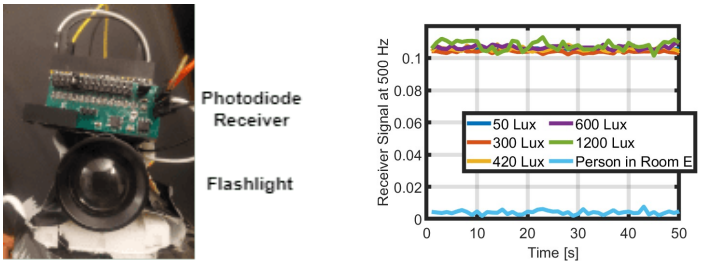
Figure 2.12: Retro-reflective tags and vests

individuals walking by, while effectively filtering out noise from ambient light in the environment.

Receiver: The receiver uses a TEPT4400 photodetector and is colocated with the flashlight, as shown in Figure 2.13a. It detects the light that is reflected back to the transmitter.

Reflectors: The *reflective vest* method is shown in Figure 2.12. The vests reflect light from the transmitter towards the receiver, enabling detection. However, a notable limitation is the dependence on individuals wearing the vest, which may not always occur. Another method is to place *retro-reflective tags* on the walls or floor of the considered areas. As a person walks by and blocks the tags, the signal returning to the receiver will incur noticeable changes.

To evaluate the system's effectiveness against ambient light interference, an experiment is conducted using a flashlight and a retro-reflective tag in an environment where we can control the level of ambient light. The signal intensity is measured under different ambient light conditions, ranging from dim (50 lux) to bright (1200 lux). The analysis involves a 0.1 s sliding window and Fast Fourier Transform (FFT) to focus on the 500 Hz signal strength, and the results are shown in Figure 2.13b. The findings show that the system is robust against ambient light, including sunlight and indoor lighting, with minimal impact on its functionality. At all ambient light intensities, the strength of the tag reflection remains strong and stable, around 0.1. A significant signal reduction (blue curve) is observed when a tag is blocked, indicating the system's ability to differentiate between



(a) Sensing TX light and RX photodetector

(b) Receiver signal for different ambient light intensities

Figure 2.13: System setup and noise resilience

Table 2.6: Detecting Threshold for Sensing

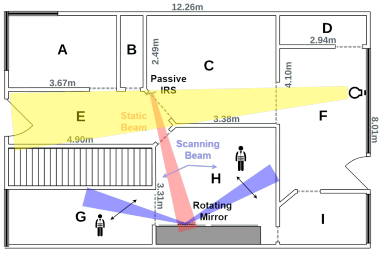
Object	Reference Value	Margin	Treshold Value
Vest	0.002	50%	0.003
Tag	0.018 (High), 0.002 (Low)	20%	0.0068
Fabric	0.008 (High), 0.002 (Low)	20%	0.0148

changes in ambient light conditions and actual movement. This resilience allows using preset thresholds to reliably detect movements.

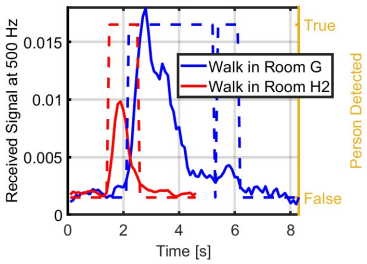
2.4.2. AROUND-THE-CORNER SENSING

This section illustrates the capability of IRS to facilitate sensing beyond direct lines of sight. In Figure 2.14a and Figure 2.15a, we show how the combination of passive and active IRS can increase the coverage to rooms G, H, and I, which cannot be reached directly by the light. In this specific scenario, the passive IRS first redirects the light beam, indicated by the red beam in the figure. After that, the active IRS is set to direct light either towards room G or H, shown by the blue beams, allowing us to sense events in those "blocked" rooms. This configuration enables the detection of movements and events in obscured areas, showcasing the sensing capabilities enabled by the synergistic use of passive and active IRS.

For event detection, a threshold is set by averaging a 10-second signal in a quiet environment, which acts as a reference for inactivity. The retro-reflective vest method, due to its variable reflectivity, uses this mean value as the only reference. In contrast, for stationary retro-reflective tags, we establish both maximum and minimum reference values based on the signal with and without obstruction, detailed in Table 2.6. Although these reference points may need updates with changes in the furniture setup, they remain stable with respect to light fluctuations, reducing the necessity for frequent recalibrations. The variable reflection from vests, caused by the wearer's movement and distance from the IRS, necessitates a detection threshold that accommodates a 50% variation from the reference value, addressing dynamic changes in reflectivity. For stationary retro-reflective tags, event detection employs a threshold set at 20% of the range between the higher and lower reference values, enabling precise monitoring due to their consistent signal outputs. This method provides accurate event detection tailored to the reflective properties of different materials.

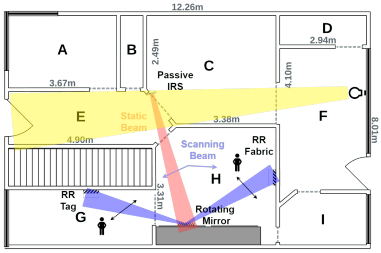


(a) Floorplan with IRS

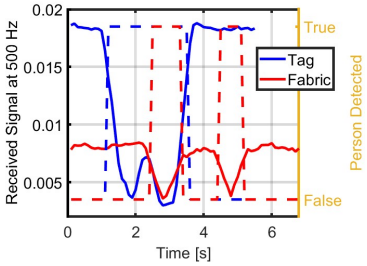


(b) Walking in room G and H

Figure 2.14: Sensing with retro-reflective vest



(a) Floorplan with IRS



(b) Tag and fabric

Figure 2.15: Sensing with retro-reflective tags and fabric

The signal received and the classification results for vests and tags are shown in Figure 2.14b and Figure 2.15b. The solid lines indicate the received signals, and the dashed lines represent the classification results. The data captures two walks: the first between rooms G and H, and the second between rooms H and I. As can be seen, both events are successfully detected with both methods. In addition, there's a distinct difference in the characteristics of the received signal between the vests and the tags and fabrics. With the vest, there's an extended signal, with a longer event detection, especially when the walk is closer, such as in room G. This is because the vest is "visible" to the transmitter as long as light reflected from the vest can reach the transmitter. On the other hand, the signals from the fabric and tag are more defined, almost resembling a binary signal where either the fabric or tag is obstructed or not. Though the tag reflects light more intensely than the fabric, the fabric reflects light over a wider FoV. Empirically, both produce detectable signals up to about 10 meters. This highlights the effectiveness of IRSs in improving the sensing range of light-based systems.

2.4.3. SENSING MULTIPLE EVENTS

In large indoor spaces like warehouses, accurately monitoring simultaneous events, especially beyond direct line-of-sight, is challenging. Traditional sensing systems often struggle to distinguish between concurrent activities in hidden areas, underscoring the need for a system capable of both detecting and differentiating multiple events. To ad-

dress this challenge, we integrate passive and active IRS components.

To test our system, we augment a reflective vest experiment by placing a retro-reflective tag in room E (Figure 2.16a), focusing on two subjects: one individual without a reflective vest entering room E, and another with a vest entering room H. This setup aims to distinguish between these events using a single light transmitter and receiver setup while exploiting distinct reflective properties.

The system employs a rapid "scanning" approach across predefined "anchor points" marked by the retro-reflective tags. Leveraging the servo motors' speed, this scanning captures unique signals from tags and vests simultaneously. To differentiate between these simultaneous events, the system adopts a sequential filtering approach. Initially, it identifies signals from the first event (an individual entering room E) that exceed a predetermined signal threshold. These data points are then excluded from the signal, allowing the system to focus on and analyze the second set of signals. The findings, in Figure 2.16b, illustrate the system's ability to distinguish events by identifying the distinct reflective properties of the tag and vest. This approach, combining IRS components and targeted scanning, enables effective monitoring and differentiation of activities in various areas of a space using a unified sensing setup.

This sensing system tracks multiple events by using retro-reflective tags as scanning "anchor points", aiding in activity detection and differentiation within specific areas. However, using these tags as static anchor points limits coverage, possibly overlooking activities in non-adjacent areas. Expanding coverage may involve adding tags or implementing dynamic scanning patterns. For example, machine learning methods could be applied to identify active zones beyond current tags, guiding autonomous adjustments in scanning routes or optimal placement of new tags, thus improving the system's effectiveness in complex environments.

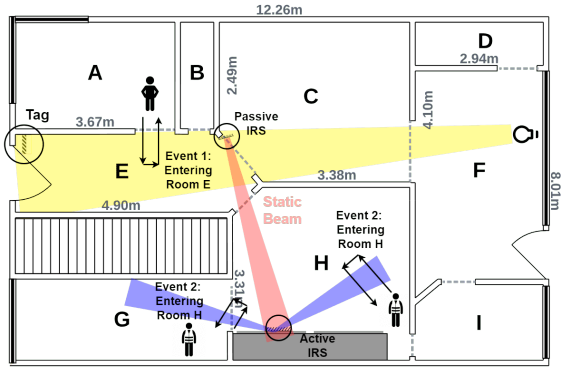
2.5. IRS FOR COMMUNICATION

Following our examination of how reflective surfaces are designed for sensing purposes, we now proceed to examine their application in communication. This transition involves understanding how the principles and techniques previously outlined can be adapted to enhance the coverage of communication systems.

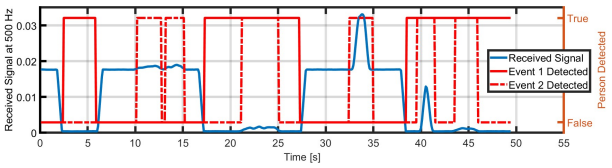
2.5.1. SYSTEM DESIGN

In prior sections, we described the design of the transmitter and the IRS for sensing. For communication purposes, we outline additional components in this section.

Transmitter Configuration: To evaluate the performance of both the passive and active IRS, we begin our tests using the same flashlight as in the prior section, with a narrow field-of-view; and later, we use an LED with a broader field-of-view (to emulate standard light fixtures). The flashlight is adjusted to ensure that its light beam illuminates the entire area of the IRS with 400 lux. Note that this amount of lux is not high, standards require office desks to get 500 lux. The transmitter operates in two modes: emitting a fixed tone for SNR measurements and transmitting packets for link quality assessment. SNR measurements are obtained with the LED transmitting a 3000 Hz modulated signal, and the communication link is evaluated by sending "Hello World!" packets at 100 kbps.

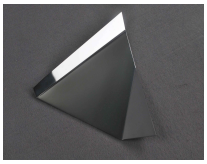


(a) Experiment setup for multiple paths

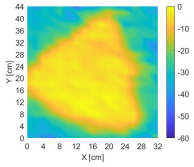


(b) Sensor outputs and categorization

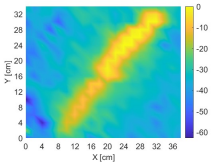
Figure 2.16: Identifying multiple activities



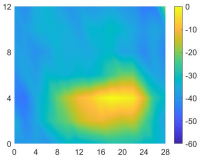
(a) Prototype



(b) Received SNR for surface 1



(c) Received SNR for surface 2



(d) Received SNR for surface 3

Figure 2.17: Prototype and measured SNRs for each surface

Receiver Design: In the context of sensing, the transmitter uses a co-located receiver to detect the reflected tones. However, for communication purposes, a *mobile receiver* is needed to test the wireless link. To evaluate the characteristics of our IRSs, we design the receiver shown in Figure 2.18. This receiver has a lens and a TEPT4400 photodetector, mounted on a MacQueen robot car to test the impact of mobility. In addition, the receiver has an on-board MCU and ADC to decode packets directly.

Modulation: We use binary frequency-shift keying (BFSK) to modulate light. FSK may lead to lower data rates, but it is designed from inception to be resilient to noise [17], which is key for our scenarios because we are exposed to natural and artificial ambient light. The '0' and '1' symbols use frequencies that are triple and quadruple the baud rate, respectively. Our packet structure is simple: it begins with an SYN symbol (01010101), followed by an STX (Start of Text, 00000010), after that comes the payload ("Hello World!"), and ends with an ETX (End of Text, 00000011) and ETB (End of Trans-

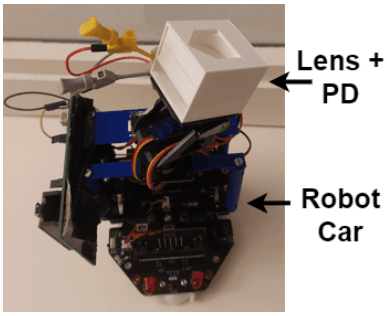


Figure 2.18: Receiver mounted on a robot car

mission Block, 00010111).

Decoding Process: The receiver undertakes the following steps. *Preamble detection*: A continuous moving window, equivalent to a single bit's duration, scans the incoming signal looking for the SYN byte. Within this window, an FFT is carried out to decode the symbols. *Information Decoding*: After an SYN byte is detected, the subsequent bytes undergo a similar decoding process. The decoding ends when an ETX is identified. *Alignment Adjustment*: Should inconsistencies appear between consecutive bits during the initial sequence recognition, the receiver realigns its observation window to synchronize with the transmitter's phase.

2.5.2. EVALUATION OF PASSIVE SURFACE

To demonstrate the communication capabilities of the passive IRS, we constructed the passive surface described earlier in subsection 2.3.1, which divides a single beam into three separate beams. The prototype is shown in Figure 2.17a and the setup is similar to the one presented in Figure 2.6. The prototype was built through a machining process, and polishing of the surface was carried out to obtain a mirror-like finish.

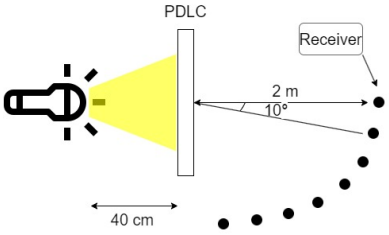
To illustrate the transition of our surfaces from sensing to communication functionalities, we evaluate their performance by presenting normalized SNR values at the expected spots on the walls and floor. The SNRs are presented in Figure 2.17b, Figure 2.17c, and Figure 2.17d. The measured SNRs closely resemble the three shapes of the surfaces, a large triangle that is four times the area of the other two surfaces, an elongated strip, and a smaller triangle shape, with equal areas. These results validate how effectively our surface directs light from the LED source to its designated receiver points.

MODIFYING THE BEAM'S COVERAGE: NARROW & LONG OR WIDE & SHORT

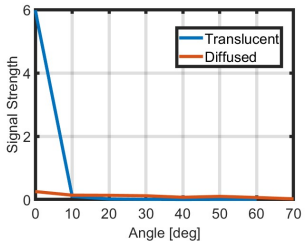
In industrial warehouses, tasks vary widely, necessitating adaptable communication systems for both stationary robots and personnel. Robots performing specific tasks like assembly or inspection may require *long and narrow* beams for precise tracking and data transmission with minimal interference. Conversely, areas with personnel activity, such as inventory management, may benefit from wider coverage to accommodate broader movement patterns. Employing passive tracking technology that can dynamically switch between narrow beams for robots and wider beams for personnel provides a practical approach to address the varied lighting needs within the same environment.

Table 2.7: Measured Light Intensity with PDLC

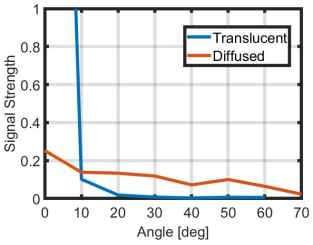
	PDLC Translucent	PDLC Diffused
In front of PDLC	400 lux	410 lux
Behind PDLC	179.4 lux	137.4 lux
30 cm behind PDLC	31.8 lux	17.4 lux



(a) PDLC experiment setup



(b) PDLC signal strength

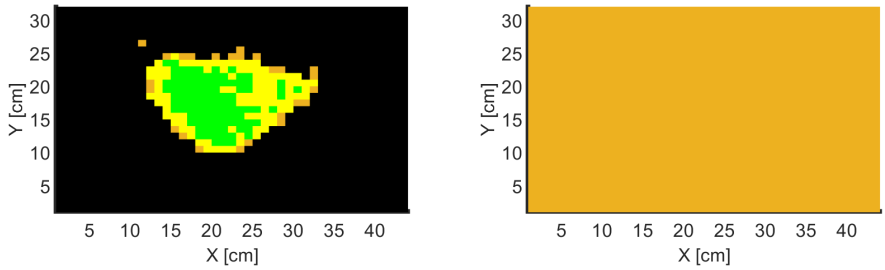


(c) Signal zoomed in

Figure 2.19: PDLC experiment setup and results

Leveraging a technology called Polymer Dispersed Liquid Crystal (PDLC) offers a way to achieve such dynamic beam adjustment. By combining a PDLC film with a passive IRS, we can design a system that can alternate between focused and broad beams, adjusting to specific application demands.

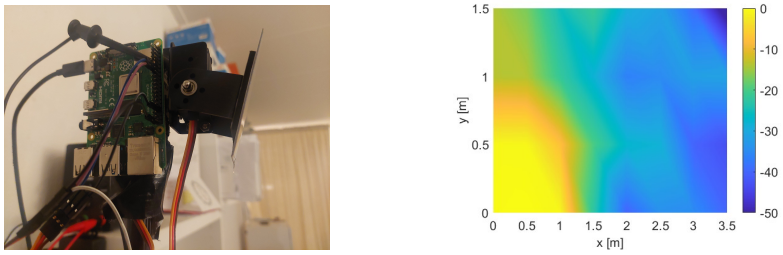
PDLC films have the unique ability to switch between two states: translucent and diffused. In the translucent state, PDLC allows light to pass through unchanged, maintaining the beam's direction. On the other hand, in the diffused state, the film scatters light uniformly in all directions. To investigate how PDLC film behaves in these states, we conducted an experiment as illustrated in Figure 2.19a and Table 2.7. This setup involves shining a flashlight from a distance of 40 cm onto the PDLC film and measuring the intensity of the received light at a 2 m distance, across a range of angles from 0° to 70° in increments of 10°. The results, displayed in Figure 2.19b and Figure 2.19c, reveal that in its translucent state, the PDLC film produces highly focused beams with a strong signal intensity directly in front (0°). The signal intensity, however, decreases significantly as the angle widens, showing a drop of over 99% by 10°. In contrast, the diffused state results in more evenly distributed signals across various angles, albeit with a lower peak intensity compared to the translucent state. At angles greater than 10°, the diffused state yields higher signal levels than those observed in the translucent state. These results highlight the distinct directional and diffusive light patterns achievable through the two states of a PDLC film.



(a) IRS with PDLC at on state

(b) IRS with PDLC at off state

Figure 2.20: Data rate and coverage with PDLC at on/off states. Green: higher than 90 kbps. Yellow: between 90 kbps and 10 kbps. Orange: 10 kbps. Black: No communication



(a) Mirror prototype

(b) Received SNR

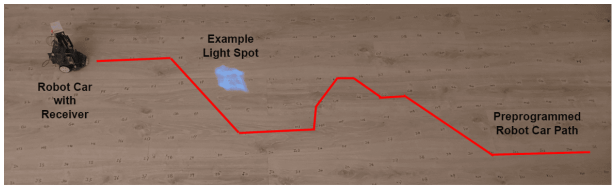
Figure 2.21: Active surface prototype and characterization

To evaluate the performance of PDLC in conjunction with the IRS, we positioned the PDLC in front of one of the surfaces of the passive IRS and measured the communication speed at the receiver. The results, in Figure 2.20, indicate that when the PDLC is on, it creates a sharp, focused beam spot that effectively limits communication (0 kbps) beyond its direct area, as captured by the black region in Figure 2.20a. Conversely, when the PDLC is deactivated, though there's a tenfold decrease in communication speed, the coverage area notably expands by six times, c.f. Figure 2.20b. This demonstrates the potential of combining PDLC with IRS to offer adaptability between focused and broad coverage.

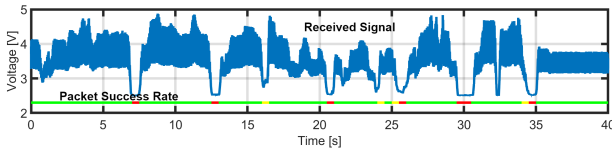
2.5.3. EVALUATION OF ACTIVE SURFACE

To explore the practical application of an active IRS, we design and build a prototype with a 10 cm by 10 cm flexible mirror mounted on a pan/tilt controlled by a Raspberry Pi, as shown in Figure 2.21a. This setup aimed to assess the efficiency of the IRS in directing light toward a receiver across different locations in a 3.5m x 1.5m area. The signal strength measurements depicted in Figure 2.21b show that the directed light maintains strong signal strength at closer distances, with a predictable decrease as the receiver moves further from the IRS.

Considering the challenge of maintaining continuous communication with moving objects in a warehouse, where robots frequently change positions, we conducted an additional experiment to evaluate the performance of active IRS in dynamically sustaining



(a) A robot traveling a designed path



(b) Received signal and packet success rate (PSR) at 100 kbps as robot moves along the path. Green indicates a PSR over 90%, yellow indicates a PSR of 70% to 90%, and red indicates a PSR under 70%

Figure 2.22: Robot car path and packet results

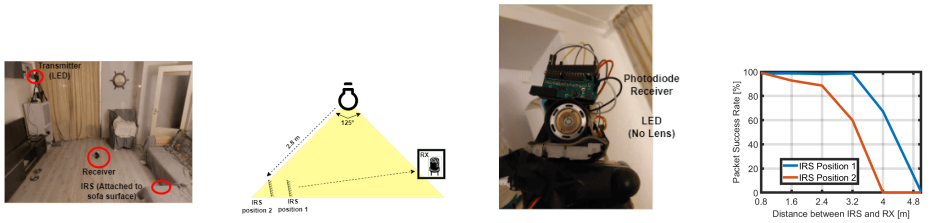
a communication link. In this scenario, illustrated in Figure 2.22a, a robot car follows a set path marked on the floor, with packet success rates recorded by the receiver shown in Figure 2.22b. Despite signal strength variations, the system successfully preserved the communication link along most of the path, achieving over 90% packet success rate (highlighted in green). Temporary disruptions occurred during turns (marked in red and yellow), where misalignment briefly interrupted the connection, yet quick realignment restored communication. These results show that in warehouses, where mobile robots are playing an increasingly important role, our IRS framework could provide adequate coverage in non-line-of-sight (NLOS) areas.

2.5.4. IRS UNDER LOW-LIGHT CONDITION

Until now, our evaluation placed lights illuminating an area in a horizontal way. This setup is not uncommon in industrial setups, which for security reasons place lamps horizontally on walls to attain longer coverages. In many indoor settings, however, lighting fixtures are placed at the top center of an area or room. This design choice often results in peripheral areas, around the walls and corners, receiving significantly less light. To evaluate these typical low-light conditions we consider the setup in Figure 2.23, where we arrange the lights and IRS to emulate a ceiling fixture covering NLOS areas as shown in Figure 2.23b. Another important change in this setup is the light's FoV. We modify our flashlight to produce unfocused light with a wide FoV.

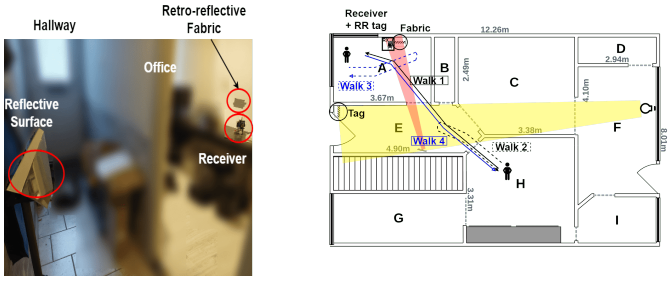
The LED chosen is a Cree XML T6, driven at 2W with a wide beam angle of 120°, as shown in Figure 2.23c. The IRS is placed at the edge of the LED's beam in two different positions, as presented in Figure 2.23b.

By conducting an experiment with this wide LED and by placing the IRS on the edge of the light spread, we mimic a realistic scenario wherein an IRS placed on a peripheral wall receives scarce light. In this context, the intensities measured at IRS positions 1 and 2 are 6 lux and 4 lux, respectively. These values are extremely low and present a considerable challenge for communication via IRS, especially when compared to the 500 lux recommended for workplace lighting. The results in Figure 2.23d show the sys-



(a) Test setup (b) LED pattern (c) TX (d) Packet success rate

Figure 2.23: Communication experiment. The photodiode receiver in (c) is not used in this experiment



(a) Experiment setup (b) Walking paths

Figure 2.24: Joint communication and sensing experiment

tem maintains over 80% packet success up to 3.2 m with 6 lux and up to 2.4 m with 4 lux, despite indoor lighting standards requiring significantly higher illumination. These findings demonstrate the system's resilience and potential for real-world application in environments with limited light.

2.6. JOINT SENSING AND COMMUNICATION

Optimizing resources in smart buildings poses many challenges. One of those challenges is reducing the energy cost of wireless communication by suspending data transfer in unoccupied spaces. Ideally, a wireless transmitter should be active only if users are present in the area. In VLC systems, energy consumption is divided into two parts, illumination and communication. Thus, stopping communication when no users are present saves energy. This section seeks to demonstrate the capability of an IRS communication system to dynamically activate or deactivate based on individual presence, marking a significant step towards smarter, more efficient building operations.

In our experiment, the focus of the IRS system is on monitoring traffic into and out of room A, as illustrated in Figure 2.24, using a retro-reflective tag and fabric placed at strategic points to track movement. *In this experiment, the user does not wear a vest, only normal clothing.* Paths 1 and 4 represent an entry and exit between Rooms H and A. These paths are designed to trigger communication adjustments. In contrast, paths 2 and 3 involve movement near or within Room A that should not alter the system's communication state. At its core, the system employs a two-stage sensing mechanism that first detects a person's approach in hallway E and then the entry into room A (Figure 2.25), effectively reducing false positives by confirming actual room entries.

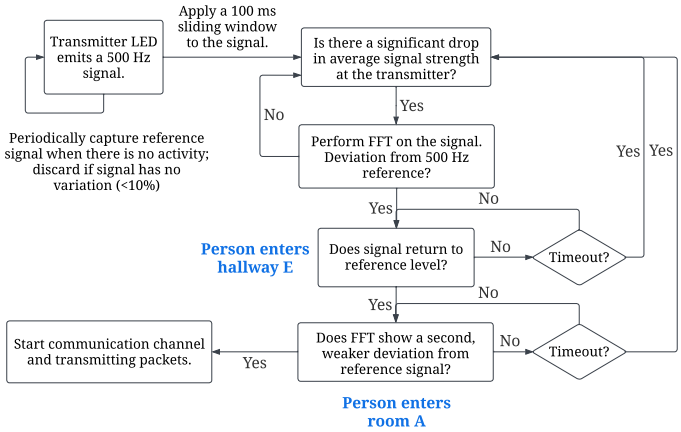


Figure 2.25: Flow chart to start communication

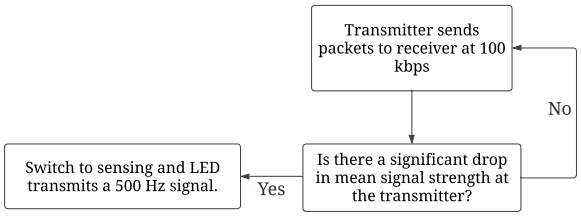
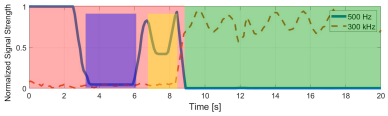


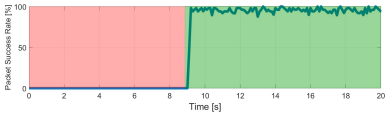
Figure 2.26: Flow chart to end communication

Figure 2.27 presents the received sensing signals, identified events, and packet success rates. The left plots show the strength of the sensing signals captured at the transmitter (via reflections from the tags). The blue curves capture the *sensing* frequency signals at 500 Hz, used to pinpoint events, and the red dashed curves capture the *communication* frequency signals at 300 kHz. The system differentiates between sensing and communication modes using FFT on these frequencies. The right plots show the packet reception rate at the receiver.

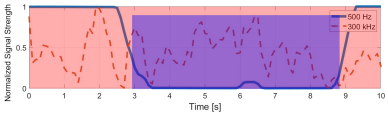
In the scenario depicted in Figure 2.27a and Figure 2.27b, where an individual moves from room H to A, the system initially in sensing mode (red region), transitions to communication mode (green) after detecting an entry into room A. The entry is captured by a signal drop in Hallway E (purple segment) and subsequent change in Room A (yellow segment). Note that after detecting the entry, the packet success rate goes from 0% to nearly 100% because the communication is turned on. Conversely, Figure 2.27c shows the system remaining in sensing mode because the user only walks around the hallway (purple event) without actually entering the room (no yellow event). For that reason, the communication is not enabled, c.f. Figure 2.27d.



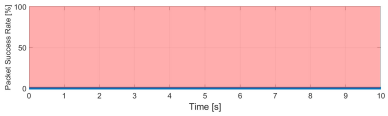
(a) TX: Walk 1 - entering room



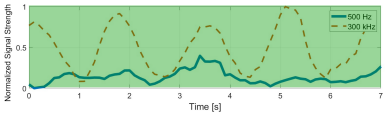
(b) RX: Walk 1 - entering room



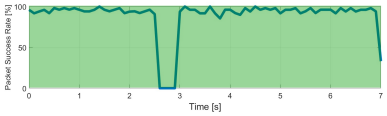
(c) TX: Walk 2 - approaching without entering



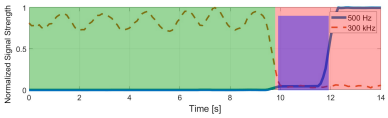
(d) RX: Walk 2 - approaching without entering



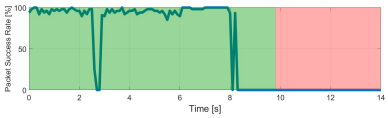
(e) TX: Walk 3 - moves around room



(f) RX: Walk 3 - moves around room



(g) TX: Walk 4 - exiting room



(h) RX: Walk 4 - exiting room

Figure 2.27: Received signal and packet success rates

Once the receiver enters the room and moves around, the communication is maintained, c.f. green regions in Figure 2.27e and Figure 2.27f. In Figure 2.27f, it can be observed that in the middle, the packet success rate drops to zero, as the link is blocked by the person moving within the room. However, since the receiver does not detect any exiting events (as expected), the communication is kept on Figure 2.27e.

The last required step is to detect the moment when a person leaves the room. In the communication mode, sensing the 300 kHz signal becomes challenging due to the reduced SNR. That high frequency significantly surpasses the 500 Hz sensing rate, which causes a significant drop in the signal strength reflected to the transmitter. This decrease in SNR makes it difficult to notice considerable shifts in the reflected signal when someone moves within the room. Therefore, we rely solely on the detection performed in the hallway as a signal to switch off communication, c.f. purple event in Figure 2.26.

The above evaluation highlights the capability of IRS technology to seamlessly integrate communication and sensing. The findings demonstrate the system's ability to respond to real-time variations, like occupancy within a space, emphasizing the role of IRS in fostering more efficient and responsive smart building environments.

2.7. RELATED WORK

IRS Design for Visible Light Communication. IRS designs for light differ significantly from those for RF, due to differences in spectral coverage, bandwidth, and propagation characteristics [18]. While the primary objective of IRS in earlier VLC research has been to overcome non-line-of-sight limitations, IRS can solve various challenges, as il-

lustrated in [19, 20, 21, 22, 23, 24, 25, 26, 27, 28, 29, 8]. This includes power amplification [19], handling multi-user contexts [20], ensuring security [20, 21], enhancing SNR [22], optimizing resources [29, 28], analyzing channels [27], and evaluating various types of surfaces [8]. These studies tackle different applications and provide important insights but they emphasize theoretical and numerical evaluations, without actual implementation. These studies assume the existence of IRS that can follow the proposed theoretical frameworks.

Among the above studies, three are the most relevant and we discuss those in more detail. Mushfique et al. enhance indoor lighting and data transmission with strategically placed mirrors for better coverage and throughput, focusing on simulation outcomes [22]. Abdelhady et al. propose boosting VLC optical power via programmable metasurfaces and mirrors, also through simulated models [8]. Ndjiongue et al. improve VLC range with an LC-based IRS, although their surfaces cater only to line-of-sight scenarios and are based on data from custom LCs [30]. Although these studies shed light on IRS potential, our work is the first to provide a framework to create and test practical IRS. Furthermore, we move beyond communication and add simultaneous sensing.

Around-the-corner Sensing. Some works allow the detection of objects or activities outside the direct line of sight. In the RF sphere, radio signal properties naturally enable such sensing capabilities because they can travel through walls. For example, Fang et al. introduced a method using standard WiFi equipment for this purpose [9]. But, with the RF spectrum becoming more saturated, interference risks rise, potentially affecting sensing accuracy. VLC offers a broad, open and unregulated spectrum. Given light's direct propagation, achieving around-the-corner sensing is more challenging than with RF, but it has been attained using lasers and specialized single-photon receivers [31]. Our work follows a similar direction but with off-the-shelf lights and sensors using a novel IRS framework.

Other studies sense people with light but require line-of-sight. One such system is LiSense, which attains real-time 3D human skeletal mapping through shadow analysis [32]. This system, however, requires direct coverage of the person from various overhead lights. In a different study, Zhang et al. present a model where retailers use ceiling-mounted color sensors to track people [33]. This system is able to identify individuals based on optical signatures, but similar to LiSense, it requires direct coverage of users. Differently from these studies, we provide novel IRS and methods to sense without direct line-of-sight.

Joint Sensing and Communication (JCS). Joint sensing and communication provide an integrated platform to manage resources efficiently. However, using a single light source for both of these purposes remains relatively uncharted in the literature. Amjad et al. provide insight into this domain [34], by proposing a system that leverages LED lights alongside cameras to monitor and communicate with machinery health. Another contribution is from Shi et al. [35], where they propose a method that integrates m-CAP modulation and RSS-based trilateration to provide concurrent communication and localization. These studies provide novel solutions for JCS with light, but require direct line of sight.

2.8. CONCLUSION

We introduce a platform with novel IRS for around-the-corner sensing and communication. Our system offers three main contributions. First, the design of passive and active surfaces suitable for various scenarios. Second, the use of retro-reflectors to sense the presence of people. Third, links that enable static and mobile coverage in areas outside the transmitter's coverage. Combining these elements, we illustrate how a single light bulb, paired with our IRS, can detect movement in a 12 m×8 m area and provide communication on-demand in areas without line-of-sight.

3

EXPLOITING DIGITAL MICRO-MIRROR DEVICES FOR AMBIENT LIGHT COMMUNICATION

In the previous chapter, we focus on artificial light, which only accounts for part of our illumination needs. Now, we turn our attention to *ambient light* for wireless communication. This emerging research area offers two key advantages: it utilizes a free portion of the spectrum and does not require modifications to existing lighting infrastructure. However, most existing designs rely on a single type of optical surface at the transmitter: liquid crystal shutters (LCs). LCs have two inherent limitations, they cut the optical power in half, which affects the range; and they have slow time responses, which affects the data rate. We take a step back to provide a new perspective for ambient light communication with two novel contributions. First, we propose an optical model to understand the fundamental limits and opportunities of ambient light communication. Second, based on the insights of our analytical model, we build a novel platform, dubbed PhotoLink, that exploits a different type of optical surface: digital micro-mirror devices (DMDs).

3.1. INTRODUCTION

In the last two decades, the adoption of wireless communication has gone through an unprecedented expansion. This ever-increasing demand has raised warnings of a looming 'radio frequency (RF) crisis' [36], and various alternative technologies are being explored to mitigate this risk. Among them, visible light communication (VLC) has gained significant attention due to its wide, free and unregulated spectrum. VLC is a sub-area of optical wireless communication (OWC) that focuses on light sources that are incoherent, divergent and multichromatic (such as sunlight and artificial white light). VLC allows standard LEDs to provide illumination and communication and it is enabling several novel applications, from interactive toys [37], indoor positioning systems [38], to LiFi [39]. VLC, however, has an important limitation: it requires direct (*active*) control over the circuitry of the light source to modulate its intensity. Most of the light in our environments comes from sources we cannot control directly, not only the sun but also plenty of artificial lighting.

To exploit the vast presence of *ambient light*, researchers are investigating backscattering (*passive*) communication. Passive VLC modulates ambient light using liquid crystal shutters (LCs). LCs can be seen as light shutters that allow (or block) the passage of light to communicate logical ones (or zeros). Recent studies report ambient light links reaching more than 50 m with data rates around 1 kbps, while consuming only a few mWs [40, 41]. Ambient light communication is a transformative eco-friendly concept because it piggybacks on top of energy that already exists, but current passive VLC studies face two main challenges.

Challenge 1*: There has been no optical analysis of various passive VLC systems.* In a way, our community has rushed into the design of systems without carrying out first a proper optical analysis of the various types of ambient light and their impact on communication. Hence, several designs have been implemented reporting a wide range of *(i)* coverages (from a few meters to several tens of meters), *(ii)* data rates (from hundreds of bps to several kbps), and *(iii)* lighting conditions (from cloudy and sunny days to various types of artificial lighting). However, without an analytical framework, it is difficult to define a common baseline to directly compare and understand which elements contribute to such disparate performance. More importantly, we cannot provide insights about the fundamental opportunities and limits of ambient light communication.

Challenge 2*: Transmitters focus on a single optical device.* State-of-the-art (SoA) designs in passive VLC studies have been mainly constrained to a single type of optical surface, the LCs, but LCs have some inherent limitations. First, even before any type of modulation begins, LCs cut the optical power in half due to the use of polarizers. This undesirable, but necessary, property of LCs reduces the communication range. Second, LCs have inherently slow rise and fall times, which has limited the data rate of all *single-cell* designs to values around 1 kbps [32, 42, 41]. Our design space could broaden greatly if we include other types of optical surfaces.

In this work, we take a step back to rethink passive VLC. First, we propose a simple optical model to gain fundamental insights. Then, based on the outcomes of our model, we explore the use of digital micromirror devices (DMDs), which have different operating principles compared to LCs. In particular, our work makes the following contributions:

***Contribution 1 [section 3.2]**: An optical model for ambient light communication.* Our model includes a key optical principle that has not been considered in ambient light communication: the fact that the performance depends not only on the luminous flux of the light source (output power) but also on its radiation pattern (diffused or directional). For example, this insight explains why a system tested under artificial light can perform better than under diffuse sunlight, even though diffuse sunlight can provide illumination that is an order of magnitude higher than artificial lighting.

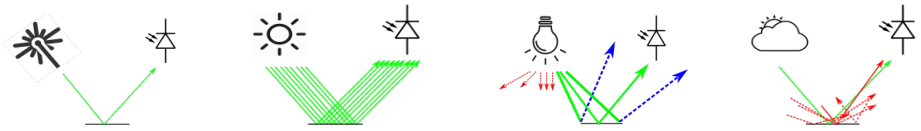
***Contribution 2 [section 3.3]**: A new type of transmitter device.* Our model shows that maintaining directional light patterns is central for passive links, but maintaining such directionality requires the right type of *(i) ambient light* and *(ii) transmitter* (optical surfaces with specular reflection). To attain that goal, we propose a novel transmitter based on DMDs. Inexpensive DMDs, however, are designed for video projection and provide slow update rates, around a few hundred Hz. We design a custom controller to generate carriers up to 220 kHz. Our novel transmitter provides higher contrast and faster switching speed, allowing us to increase the data rate of passive links by a factor of 80 compared to LC transmitters.

***Contribution 3 [section 3.4 and section 3.5]**: An implementation and thorough evaluation of our platform.* We build two transmitters, one with a DMD and the other with an LC; and two receivers, one optimized for LCs and the other for DMDs. Using the same setup for all evaluations, in terms of surface area and illumination, our results show that (i) if we use the receiver optimized for LCs, PhotoLink attains 30 kbps for a distance of six meters and a BER below 1%, compared to the 1 kbps provided by the LC for the same range and BER [42, 17, 41], (ii) if we use the receiver optimized for DMDs, the data rate increases to 80 kbps. This performance is obtained with a power consumption around 45 mW. Furthermore, even if we compare PhotoLink with a *multi-cell* LC system having a surface area that is 500+ times bigger than ours (66 cm^2 vs. 0.13 cm^2) [43], PhotoLink can achieve an order of magnitude higher data rate (80 kbps vs. 8 kbps). To the best of our knowledge, our work is the first to break the 10 kbps barrier with ambient light communication.

3.2. SYSTEM ANALYSIS

A passive VLC system has three basic components, the emitter (light source), the transmitter (modulating surface) and the receiver. Every SoA study adopts a different set of components. Some studies use a light bulb as the emitter, others use a flashlight or the sun. Some studies use a diffuser at the modulating surface, others use retro-reflectors or aluminium plates. Some studies use lenses at the receivers, others do not. This wide range of set ups is, in part, responsible for the equally wide range of performances reported in the literature, with data rates ranging from 0.5 kbps to 8.0 kbps to link distances ranging from 2 m to 80 m [17, 32, 44, 40, 43, 42].

Leaving aside the specific modulation methods of all these studies, we want to gain a fundamental understanding of passive systems and their components. Building upon the models developed for free-space optics [45], we propose a framework to analyze passive communication with ambient light.



(a) Ideal [laser] (b) Directional [direct sunlight] (c) Lambertian [light bulb] (d) Random [diffuse sunlight]

Figure 3.1: The effect of different radiation patterns on the luminous flux. The reflective surface is specular

3.2.1. MAINTAINING THE LUMINOUS FLUX

First, let us start with a guideline that, to the best of our knowledge, has not been stated in any prior passive VLC study: *The most important aim in passive communication is to convey as much* LUMINOUS FLUX *as possible from the emitter to the receiver.* The *luminous flux*, which is measured in *lumen*, is different from *illuminance*, which is measured in *lux* (lux = lumen per unit area). To compare two different systems fairly, one should know at least the area and the illuminance at the transmitter (modulating surface). This represents the amount of energy that is captured by the transmitter (E_C). Unfortunately, few studies report these two pieces of information.

The luminous flux, however, is not the only important parameter. Equally important is the radiation pattern, which determines how much luminous flux is maintained throughout the optical link (i.e., how much of E_C is able to arrive at the receiver). To highlight the importance of the radiation pattern, Figure 3.2 depicts a *specular (mirror-like)* surface under four different types of light sources. The effect on the luminous flux is shown from more to less directive:

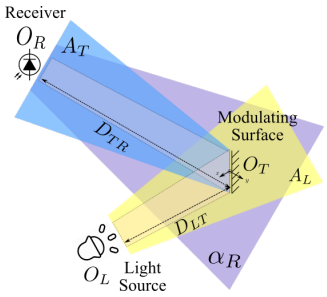
a) Ideal. First, to exemplify an ideal setup, let us use a laser, which is a highly directional source where the luminous flux is hardly lost. Due to this property, lasers are used extensively for long-distance free-space communication. Lasers, however, are a fundamentally different type of light source that is not as pervasive (or safe) as natural or artificial white light, and therefore, it is considered only as a reference in this paper.

b) Directional (sunlight in a clear day). On a clear day, sunlight rays travel in parallel and a specular surface maintains that directionality (luminous flux) towards the receiver. *We found only one study exploiting this setup, but with LCs [41]. Our platform shows the significant gains that can be obtained in this setup using DMDs.*

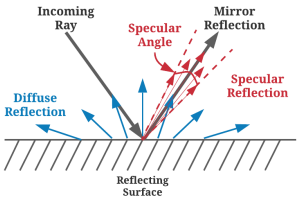
c) Lambertian (light bulbs and flashligths). With light bulbs, only a fraction of the luminous flux radiated by the source reaches the surface (green arrows in Figure 3.1c). Furthermore, since rays are radiated in different angles, when the luminous flux hits the surface, some rays are lost because the impinging angle is either too broad or too narrow to hit the receiver (blue arrows). *This scenario is used by all the backscattering studies reported in the literature [32, 42, 43, 40].*

d) Random (sunlight in a cloudy day). Clouds scatter sunlight, emitting rays uniformly in random directions. Due to this phenomenon, only an infinitesimally small fraction of the rays will impinge the surface at the right angle to reach the receiver (green arrow in Figure 3.1d). *Our model shows that this is the worst case scenario with specular surfaces. No practical links can be obtained in this setup.*

The key point of this preliminary analysis is to highlight the importance of maintaining the luminous flux throughout the optical link. In the next subsection, we present a



(a) A 2D representation of the optical system



(b) Different types of reflections based on the Phong model [47]

Figure 3.2: Optical system and different reflection types

model to capture more detailed insights with a ray-tracing simulator.

3.2.2. RAY-TRACING MODEL

A 2D representation of a typical passive system is shown in Figure 3.2a. The optical link has two main parts. *First*, the link between emitter and transmitter. Light is emitted from the light source O_L, with a (yellow) wavefront represented by A_L. The modulating surface O_T, acting as a transmitter, is at a distance D_{LT} from the light source, and receives a fraction of the luminous flux emitted by O_L. *Second*, the link between transmitter and receiver. The flux reflected by the surface O_T is represented with a (blue) wavefront A_T[1]. The photoreceiver O_R is at a distance D_{TR} from the transmitter, and collects only a fraction of the flux reflected by O_T. Another relevant parameter is the Field-of-View (FoV) of the receiver, which is represented by α_R (purple coverage). A wide FoV can cope with movements at the transmitter, but captures more noise.

Our toolbox, based on the above described model, is built upon Optometrika, a ray-tracing tool [46]. In essence, the toolbox divides the surface of the emitter, transmitter and receiver into small elements and calculates the fraction of rays that are able to reach the receiver. To assign the correct weight to each ray, Optometrika considers important optical parameters such as the angles of radiation, incidence and reflection. To analyze ambient light communication, the key inputs we need to provide to the toolbox are the radiation patterns of the emitter and the modulating surface.

3.2.3. INSIGHTS & GUIDELINES

A passive link is, in essence, a triplet <emitter, transmitter, receiver> that finetunes the parameters of each element to optimize the performance. To analyze the complete design space, including the systems proposed in prior studies, we utilize a few abstractions for the emitters and transmitters, as presented in Table 3.1 and Table 3.2.

Unless indicated otherwise, our analysis assumes that (i) there is no noise, which is similar to conducting experiments in the dark, (ii) the illuminance on the transmitter is fixed at 1800 lx, to provide a common baseline for all cases and *remove the trivial case*

[1] It is important to note that our model also captures the performance of retroreflectors because, from an optical perspective, the reflected radiation patterns are similar to those caused by mirrors.

Table 3.1: Emitters

Source	Type	Size of O_L	D_{LT}
L1	LED	5 cm × 5 cm	1 m
L2	LED	5 cm × 5 cm	4 m
L3	Diffuse Sunlight	N/A	N/A
L4	Direct Sunlight	N/A	N/A

Table 3.2: Transmitters

Modulating Surface	Type	Specular Angle	Size of O_T	Illuminance
T1	Diffuse	N/A	3 cm × 3 cm	1800 lx
T2	Specular	0.3°	3 cm × 3 cm	1800 lx
T3	Specular	1°	3 cm × 3 cm	1800 lx
T4	Specular	5°	3 cm × 3 cm	1800 lx

where the performance is increased by increasing the illuminance, and (iii) the area of the receiver is 1×1 cm^2. The selected area has no real impact on the analysis. The only assumption we make is that the transmitter's area is bigger than the receiver's, which is the case for most systems. Also, for our initial analysis, the receiver's FoV does not play a role because we assume a dark environment. In practice, the FoV plays a critical role and we will discuss it later on.

Regarding the modulating surface, we consider two main reflective patterns, as shown in Figure 3.2b: *diffuse reflection*, caused by rough surfaces that reflect light in all directions, and *specular reflection*, caused by smooth surfaces. We further classify specular surfaces based on their specular angle. If the angle is zero, we call it mirror reflection.

CHOOSING THE RIGHT EMITTER AND TRANSMITTER

The design space of passive links can be divided into six main blocks based on the <emitter, transmitter> pair. Table 3.3 shows previous works categorized in this manner. Considering that direct sunlight provides tens of thousands of lx, overcast sunlight thousands of lx and light bulbs only hundreds of lx, a designer may assume that for any given surface, sunlight will always perform better than light bulbs. Similarly, considering that specular (mirror) surfaces provide stronger reflections than diffuse surfaces, a designer may assume that for any type of ambient light, a specular reflector will always perform better. Neither assumption is correct. In fact, we show that a particular combination of sunlight and specular reflectors gives the worst performance.

Figure 3.3 depicts the signal strength of various scenarios as a function of the transmitter-receiver distance (D_{TR}). We consider all six possible combinations of *emitters*: LED (L1 & L2), overcast day (L3), clear day (L4); and *transmitters*: diffuse (T1), specular (T2). Our results show four design regions, which are described next from worst to best. Our evaluation section validates many of these results empirically.

Region 1: cloudy day & specular surface (L3-T2 in Figure 3.3a, gray area in Table 3.3). This region captures the scenario in Figure 3.1d, where light arrives in a scattered manner and only an infinitesimal amount of the flux reaches the receiver. The signal strength of this setup is so weak and decays so fast, compared to the other scenarios, that it is not

Table 3.3: A taxonomy of passive VLC systems

Light Source \ Surface Type	Specular (includes retro-reflectors)	Diffuse
LED	RetroVLC [32] PassiveVLC [42] RetroTurbo [43] RetroI2V [40]	
Sunlight (Cloudy Day)		Tweeting with Sunlight (TwSL) [48]
Sunlight (Clear Day)	ChromaLux [41]	Luxlink [17]

shown within the range of Figure 3.3a to have a clearer view of the other regions.

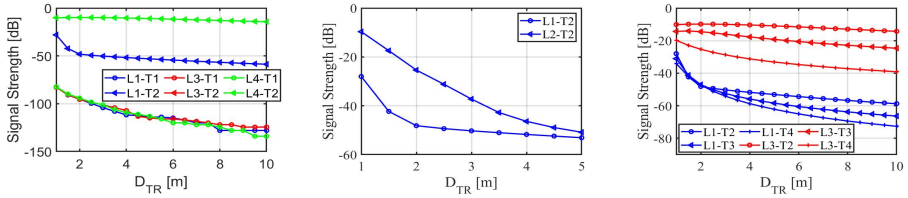
Region 2: any light & diffuse surface (LX-T1, blue area). When a diffuse surface is used, it does not matter the radiation pattern of the light source, so long as the luminous flux at the transmitter's surface is the same. Note that all T1 curves overlap with each other in Figure 3.3a. This occurs because ideal diffusers, such as paper or plaster, distribute the reflections of the impinging flux in all directions.

Region 3: LED & specular surface (L1/L2-T2, red area). This is the second best region, and coincidentally, the main focus of prior work using retro-reflectors. Artificial lights, however, offer a wide range of radiation patterns, resulting in widely different performance. To illustrate this point we use Figure 3.3b, where two emitters are placed at 1 m and 4 m (L1 & L2). *Both emitters attain the same illuminance at the receiver* (1800 lx, a white light illuminance of 1800 lx over an $1\,m^2$ surface is approximately equivalent to the power of a 25 W LED), but L2, which is *further away*, provides a stronger signal strength, which is counter-intuitive. This occurs because the further away the light source is, the more it behaves as a distant point source, leading to more directional beams impinging on the transmitter, and hence, less flux lost towards the receiver, c.f. Figure 3.1c. In practice, L1 could be seen as a light bulb and L2 as a flashlight, which explains why studies using a flashlight attain better results [40, 43].

Region 4: clear day & specular surface (L4-T2, green area). This is the best operation region. Note that the signal strength hardly decays in Figure 3.3a. This occurs because the high directionality of clear sunlight maintains the luminous flux over long distances, which is why heliographs (mirrors) used in the 1800's reached ranges beyond 100 km. This same property can increase the data rate of ambient light links. In practice, air attenuates the signal strength (similar to what happens with lasers), but the benefits of directionality remain strong.

CHOOSING THE RIGHT SPECULAR SURFACE

The above analysis highlights the importance of maintaining directionality throughout the optical link. However, given that there are no perfect mirror-reflectors, how critical is the specular angle? A wide specular angle can be the result of imperfections on the surface. For example, many studies use retro-reflectors, but the quality of retro-reflectors



(a) Signal strength for different light source and surface combinations

(b) Signal strength for LEDs at different distances D_{LT}

(c) Signal strength for different specular angles

Figure 3.3: Different simulation setups

can vary. Figure 3.3c shows the signal strength of surfaces with different specular angles, from narrow (T2, 0.3°) to wide (T4, 5.0°), considering an LED (L1) and direct sunlight (L3). When an LED is used (blue lines), the misaligned radiation pattern of the LED is more relevant than the specular angle, therefore, there is not much difference among the various surfaces. However, for a directional source (red lines), a large specular angle (e.g. 5° for T4) can lead to a significant decrease in the signal strength. Thus, *the more directional the rays, the more critical is the use of high-quality specular surfaces.*

CHOOSING THE RIGHT RECEIVER

Passive VLC systems use cameras and photodiodes as receivers. Cameras are widely available in smartphones, but they are power hungry and slow, allowing only a few hundred frames per second. Photodiodes (PDs), on the other hand, are inexpensive, low-power and have a high bandwidth. Thus, PDs are the preferred choice for high data rate links. A key element in the PD's design is its FoV. The FoV will not only capture the intended signal but the surrounding noise as well (purple coverage in Figure 3.2a). In practice, to maximize the SNR, the receiver's FoV should cover only the modulating surface, but that is difficult to attain. PDs with varying FoV have been used in the literature, ranging from 1° to close to 90° [17, 44]. Many studies using the wide FoV, however, were conducted at night with no interfering ambient light, which is similar to having a nearly perfect FoV of 0°. Given that our system is aimed at working with surrounding ambient light (noise), we borrow the design from [17], which uses a lens at the receiver to reduce the FoV, and thus, limit the noise level. Overall, our analysis uncovers two key design guidelines. First, for the emitter-transmitter link. Direct sunlight, flashlights and light bulbs –in that order– are preferred due to their directionality. Diffuse (cloudy) daylight is the least ideal condition in spite of being the second most powerful source (after direct sunlight). Second, for the transmitter-receiver link. The more directional the light source is, the more critical is to use mirror-like reflectors. The only case where diffuse surfaces are preferred is when the impinging light is diffuse as well.

3.3. TRANSMITTER DESIGN

3.3.1. LC LIMITATIONS

Most passive VLC systems using either transmissive [17, 49] or reflective (backscattering) principles [42, 32] rely on liquid crystal shutters (LCs) as the modulating surface. Unlike

liquid crystal displays (LCDs), LCs do not have embedded light sources. LCs are readily available, economical, and power efficient, but they suffer from two intrinsic limitations.

LIMITATION 1: HIGH SIGNAL ATTENUATION

LCs only allow a single polarization direction to pass through. All other directions are either fully or partially attenuated. Ambient light, however, is not polarized. This implies that only half of the power can pass through a linear polarizer. On the other hand, DMDs have microscopic mirrors with a high reflection coefficient and are polarization insensitive. For example, the DLP2000 module from Texas Instruments has an efficiency of 97% [50]. Thus, considering the same modulating area and incoming illuminance, DMDs radiate almost 100% more light than LCs, which can be exploited to increase the range or the data rate of passive links.

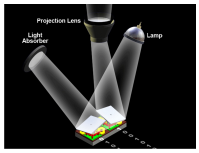
LIMITATION 2: LIMITED BANDWIDTH

The rise and fall times of commercial LCs take a few ms, as shown in Figure 3.4d. These times limit the bandwidth to be under 1 kHz. Furthermore, LCs combine two different operation principles, an electrical signal for the rise time and mechanical inertia for the fall time. This asymmetric operation makes the fall time much slower and it is usually the main bottleneck to increase the bandwidth. Active research has been carried out to squeeze as much data rate as possible from that limited bandwidth, but community efforts are still restricted to around 1 kbps for single-cell designs [32, 42, 17, 41] and 8 kbps for more sophisticated multi-cell designs [40, 43]. DMDs, on the other hand, use the same (fast) operating principle for the rise and fall times. We exploit this fast switching speed to increase the data rate of passive links by an order of magnitude or more.

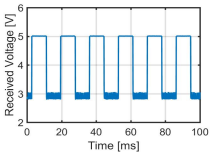
3.3.2. DMD BASICS

A DMD is an optical micro-electro-mechanical system (MEMS) that contains between a few hundred thousand and several millions of highly reflective microscopic mirrors of less than 10 microns each. A DMD can be controlled by electrical pulses, which flip each mirror to one of two fixed directions, for example, $+12^\circ$ and -12°. DMDs usually come integrated within a sophisticated projector system called Digital Light Processing (DLP). Besides the DMD, the DLP has a lamp, a light absorber and a projection lens, as shown in Figure 3.4a. A micro-mirror is *on* if its angle is tilted towards the projection lens, and *off* if the angle is tilted towards the light absorber. All these optical and electrical components are tightly synchronized by the DLP controller.

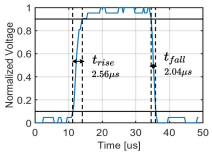
There are multiple types of DLPs, as shown in Table 3.4. All these DLPs tackle *Limitation-1* because DMDs have a high reflective coefficient by design, but exploiting the DMDs' potential for higher bandwidth is harder to attain (*Limitation-2*). On one hand, there are inexpensive units, such as the DLP2000 (~ 100 €), but their screen refresh rate is too slow. The refresh rate can be seen as the equivalent of the rise (or fall) time in an LC. At 120 Hz, the DLP2000 is even slower than the LC shown in Figure 3.4d, which provides 320 Hz ($\frac{1000\times 2}{1.38+4.82}$). On the other hand, there are units providing refresh rates above 20 kHz, but with prices beyond 4K€, they are prohibitively expensive compared to LC-based systems, which cost a few tens of Euros. A single DMD device (instead of an integrated unit) has comparable cost (26 €) to a LC.



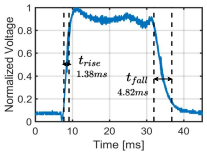
(a) States: ON/OFF (right/left pixel). Reprinted from [51]



(b) Maximum data rate of out-of-the-box DMD



(c) DMD rise/fall time with custom controller



(d) LC rise/fall time

Figure 3.4: DMD Pixel states and DMD and LC timing characteristics

3

Table 3.4: Commercial DMD modules

Name	Clock Rate	Data Bus	Screen Refresh Rate	# of Pixels	Module (DLP) Price	DMD Price	# of pins
DLP2000	60-80 MHz	12(bits)x1	120 Hz	640x360	109.01€	26.14€	42
DLP4500	80-120 MHz	24(bits)x1	4.2 kHz	912x1140	1106.49€	144.69€	80
DLP7000	200-400 MHz	16(bits)x2	32.5 kHz	1024x768	4144.09€	866.96€	203
DLP9500	200-400 MHz	16(bits)x4	23.1 kHz	1920x1080	4403.30€	2693.38€	355

The inability to exploit DMDs is an important barrier in passive VLC. While there are multiple studies utilizing LCs, there are only a few utilizing DMDs. One of those studies uses the same DMD we use, the DLP2000, but attains only a few bits per second because they only use the default refresh rate (120 Hz) and utilize a smartphone camera as a receiver, which is inherently slow [52]. The other studies utilize the more sophisticated DLP4500 (1100€) [53, 54], which provides a maximum refresh rate of 4.2 kHz. Those studies, however, do not exploit that refresh rate for digital communication, but to generate analog signals of just a few tens of Hz (sine, square, triangle, saw-tooth) for localization and audio transmissions. We design a controller for the inexpensive DMD inside the DLP2000 (26€) and increase its refresh rate to 220 kHz, almost a factor of ten faster than the most expensive DLP (DLP9500, 4400€). Next, we describe the main limitation of the DLP2000 for ambient light communication, and subsequently, the design of the PhotoLink controller.

3.3.3. LIMITATIONS OF INEXPENSIVE DMDS.

The DMD from the DLP2000 is the most readily available and economical product, but it is designed for display applications. Hence, for ambient light communication, logical 1s and 0s can only be conveyed as a series of white and black images in a video, which leads to the slow update rate shown in Figure 3.4b. In a video application, the pixel's color is obtained by (i) multiplexing RGB beams and (ii) changing the duty cycle of the mirror for each color beam. DMDs provide incredible images, with up to 16.7 million colors, thanks to the fine-grained duty cycle provided by the micro-mirrors. *The micro-mirrors can be flipped at very high speeds between their on/off status*, enabling short operational periods τ, with $\tau \ll T$. These short periods allow a large number of (primary color) combinations. The operation of DMDs, however, is designed for the human eye, which has a slow response. As long as the $3T$ period takes less than 8.3 ms (120 Hz), people will only see high quality videos. Photodiodes, on the other hand, have MHz bandwidth and do not need to capture colors. For PhotoLink, we need control of τ, not T. Thus, our goal is to remove the controller in the original system and design a new one that gets us as close

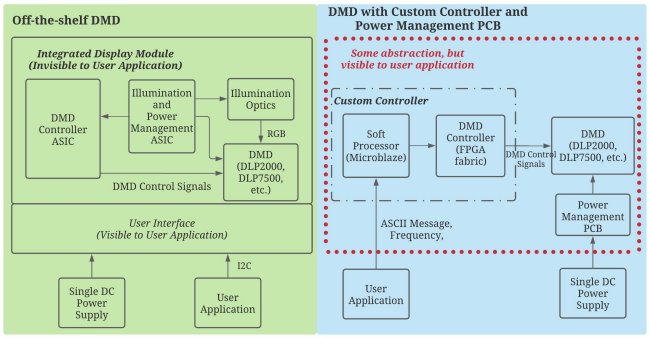


Figure 3.5: The block diagrams of an off-the-shelf DMD (green, left), and our custom PhotoLink controller (blue, right)

as possible to the bare fast switching speed of the micro-mirror.

3.3.4. PHOTOLINK CONTROLLER

There are two main obstacles preventing the use of inexpensive DMDs for ambient light communication: no suitable *hardware abstractions* or *operational modes*. Next, we describe each obstacle and the solutions we provide.

HARDWARE ABSTRACTION

Most commercial DLPs do not expose control and power signals to user applications, as illustrated in Figure 3.5. There are two ASIC components preventing direct access to these signals: the controller and power management. The *controller* implements the logic to set each micro-mirror and an I2C interface. The interface is the only means to communicate with user applications and hides all control signals. It is therefore impossible to extend beyond the supported frame rate by the controller (120 Hz for the DLP2000). The *power management* controls the DMD power and the integrated RGB light source, which is not needed for ambient light communication.

To increase the refresh rate of the DMD, we remove all hardware components from the original DLP design and use only the DMD. As shown in Figure 3.5 (blue side), our main components are: (i) the power management unit, which provides the necessary voltage supplies for different DMD operations without requiring a light source; (ii) an FPGA, which supplies the data and logic for updating the DMD; and (iii) the Microblaze module (soft-processor), which runs on the FPGA and provides a user interface but without hiding the control logic. This interface is used to configure the packet format and the transmitting frequency (explained in section 3.4).

OPERATIONAL MODES.

Creating a new hardware abstraction is necessary but insufficient to use the DLP2000 for ambient light communication. The next step is to apply the appropriate operational mode to switch the mirrors as fast as possible. The manufacturer does not disclose all the required information to tackle this step, so we base our design on two references: the data sheet of the DMD [50] and a basic description of micro-mirrors [51].

The switching of the mirrors involves two steps: the *memory state* and *micro-mirror state*. In the memory state, the value of each mirror is set (on/off), but the mirror does not tilt. In the micro-mirror state, an actuation pulse tilts the mirrors to their new value. These states define two operational modes.

Individual pixel mode. In this mode, every pixel acts as an individual binary reflector. This allows the DMD to be configured as a fine-grained video projector. The DLP2000 has more than 230 thousand pixels, whose memory has to be written sequentially. As a result, the memory state takes a few hundred μs before any actuation (transmission) can be performed.

Global mode. Considering that the bulk of the delay is in the *memory state*, it would be ideal to by-pass it. In ambient light communication, a fine-grained control of the DMD is not necessary, as photodiodes are used as receivers[2] It is sufficient to update all pixels at once and use the DMD as a single-pixel device, which we dub the global mode. In this mode, we do not write the memory of each pixel, but instead write a global '0' or '1' to all pixels. Attaining this operation requires a careful coordination of various signals[3], but the bandwidth increases dramatically compared to the original DLP design, as shown in Figure 3.4c: 60 Hz vs 217.4 kHz, a factor of 3600+[4]. Compared to the LC, the global mode reduces the rise time by a factor of 540 (2.56 µs vs. 1.38 ms) and the fall time by a factor of 2360 (2.04 µs vs. 4.82 ms), which translates to almost a 1350 increase in bandwidth.

SUMMARY OF CONTRIBUTIONS.
Our novel controller allows inexpensive DMDs to be decoupled from their integrated video-projection system. We design a global mode to take full advantage of the fast switching times of micro-mirrors. Compared to LCs, our approach increases the transmitter bandwidth by more than three orders of magnitude. Our controller also achieves a higher refresh rate, even when compared to the high-end DLPs shown in Table 3.4. Since all DMDs manufactured by TI follow the same operating principles [51], our controller's design would also apply to those DLPs, which could allow them to increase their refresh rates to attain even a better performance than the one obtained with the low-end DLP2000.

3.4. OPTICAL LINK

3.4.1. MODULATION

The majority of modulation schemes fall within two categories: amplitude-based [32, 42] and frequency-based [17]. Amplitude-based methods work well in dark scenarios but are prone to errors when external light sources are present. Frequency-based modulation, on the other hand, has the inherent property of being more resilient to external noise. However, prior LC studies using frequency-based methods had difficulties creating stable periodic signals because the rise and fall times of LCs are asymmetric [17]. DMDs

[2] To take advantage of the individual pixel model, a camera has to be used as a receiver, which is slow (hundreds of frames per second) and requires the use of large screens as transmitters to be efficient.
[3] The hardware and firmware of our controller will be made open source.
[4] The refresh rate of the DLP2000 is 120 Hz, which considers only the time taken by the rise or fall time, the bandwidth considers both times.

Table 3.5: The structure of the data link layer

00010101	00000010	ASCII Byte Array	00000011	00010111	00010101
SYN	STX	ASCII Text Message	ETX	ETB	SYN

Table 3.6: Parameters for different bit rates

Bit rate	Symbol	Frequency	# of cycle
24 kbps/30 kbps/ 40 kbps/60 kbps/ 80 kbps/100 kbps	00	12/15/20/30/40/50 kHz	1
	01	24/30/40/60/80/100 kHz	2
	10	36/45/60/90/120/150 kHz	3
	11	48/60/80/120/160/200 kHz	4

have symmetric times, which allows the generation of stable periodic signals.

To increase the data rate, we use M-ary FSK (MFSK) with two bits per symbol. This high frequency band of PhotoLink (217.4 kHz) allows us to define different modulation parameters and data rates, as shown in Table 3.6. For example, for a data rate of 30 kbps, we set the four modulating frequencies to 15 kHz, 30 kHz, 45 kHz and 60 kHz. The different modulation parameters permit a thorough evaluation of PhotoLink under different ranges and with different receivers, as discussed in the next section. To avoid abrupt transitions between two frequency signals, the transition between the MFSK frequencies only occurs after a full oscillation period, as depicted in Figure 3.6. Considering that the only prior work using MFSK for passive VLC is [17], we use it as a baseline for comparison. We implement a similar data link layer (shown in Table 3.5) and receiver design (shown in Figure 3.7b and described in section 3.5). Our packet starts with a SYN symbol (00010101) that uses only the lower transmitting frequencies (00 & 01). These low frequencies have the highest amplitude, and hence, it is easier for the receiver to discover the signal and synchronize to the phase of the transmitter. The ASCII payload is preceded by a STX (Start of Text, 00000010) and followed by ETX (End of Text, 00000011) and ETB (End of Transmission Block, 00010111).

3.4.2. DEMODULATION

The receiver knows the transmitting frequencies and takes the following steps to demodulate the signal.

Preamble detection: A sliding window, equivalent to one symbol, applies a Fourier transform (FFT) to the received signal and decodes the symbol. Every time a byte (four symbols) is decoded, the byte is compared to SYN.

Data demodulation: After a SYN byte is identified, the receiver decodes the incoming message using the same FFT process. If an ETX is received, the packet transmission ends.

Phase correction: If a received two-bit symbol is '00', during the preamble detection or data demodulation, the receiver leverages the presence of this high-amplitude symbol to synchronize to the phase of the transmitter and adjust to any frequency shift that could have been induced by the channel.

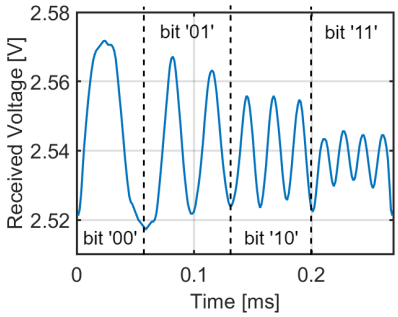
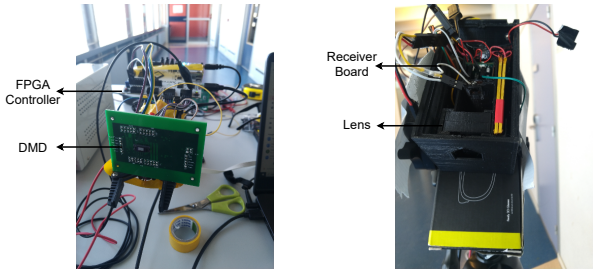


Figure 3.6: The received signal for different symbols for 100 kbps. Each symbol carries two bits.



(a) Transmitter setup (b) Receiver setup

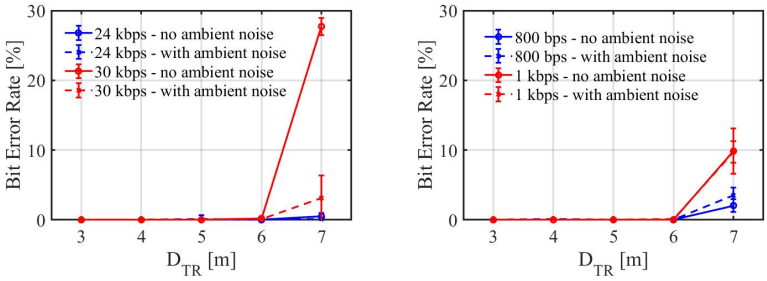
Figure 3.7: Transmitter and receiver setup

3.5. EVALUATION

Our transmitter runs the methods described in section 3.3 using a custom FPGA controller board and a custom PCB with power management circuits for the DMD. Next, we evaluate our simulation toolbox and controller under various aspects.

3.5.1. RECEIVER DESIGN & DATA RATE

The design of a low-power optical receiver needs to balance a trade-off between gain and bandwidth. If we optimize for sensitivity (high-gain), small changes in light intensity can be detected, which is advantageous for long-distance communication; but the response is slow (low-bandwidth), which limits the ability to decode high frequency carriers. The opposite trade-off holds for a high-bandwidth receiver. A low-bandwidth receiver is not a concern when LCs are used as transmitters, as the bandwidth of the LC is low, but it can severely restrict the performance of DMDs. In this subsection, we compare the performance of PhotoLink with LCs used in state-of-the-art studies. We quantify the performance of PhotoLink with two receivers, one optimized for LC operation and the other for DMD. LCs can be used in different ways depending on the type of application: as part of a reflective tag, where either a diffusive or retro-reflective material is placed behind the LC to reflect light, or as part of a transmissive tag, where the LC is used solely as an optical shutter without additional reflective surfaces. To ensure a fair comparison between DMDs and LCs, in the following evaluation, we carry out experiments with both optical devices, but without adding any additional surfaces.



(a) DMD (b) LC

Figure 3.8: Bit error rate of DMD and LC with artificial light

Table 3.7: Rise and fall time for different sensors and resistors

Photoreceiver	Feedback resistor	rise time	fall time
TEPT4400	69/50/20 kΩ	100/64/24 µs	140/105/48 µs
PD204-6C	1000/400/100kΩ	6.4/3.5/2.5 µs	6.2/3.2/2.1 µs

Experiment 1: Receiver optimized for LCs. PhotoLink increases the data rate by a factor of 30

In this experiment, we use a receiver similar to the one used in [17], consisting of a convex lens with a diameter of 2.5 cm and a TEPT4400 photosensor placed at the focal distance of the lens. The TEPT4400 is a high-gain low-bandwidth photoresistor well-suited for long-range communication with LCs. Using the same illumination environment, we test this receiver using a DMD and an LC as transmitters. The LC and the DMD have the same physical setup, surface area, modulation and demodulation schemes.

We evaluate the DMD and LC in two scenarios. First, we use a bike flashlight (Simson USB Headlight "Future") to illuminate the transmitting surface in a dark room, such that repeatable experimental results can be obtained. The flashlight is placed 1 m away from the transmitter, and the illuminance at the transmitter is 1800 lx. Then, we use the same setup but turn on the indoor lights located on the ceiling and allow natural ambient light to enter the room (in addition to the flashlight). These additional light rays are not aligned with the receiver and act as ambient noise. The illuminance of the ambient noise (excluding the flashlight) is around 700 lx at the transmitter.

In each experiment, a "Hello world!" packet is sent 100 times. Each experiment is repeated 30 times, and the mean and standard variation of the bit error rates are shown in Figure 3.8. With the DMD, we obtain an average BER of less than 1% at 7 m for a data rate of 24 kbps and 6 m for a data rate of 30 kbps. With the LC, we obtain an average BER of less than 1% at 6 m for a data rate of 800 bps and 1 kbps. The data rates achieved with the LC are in line with what has been reported for single-pixel systems [32, 42, 17, 41]. Overall, under the same illumination and modulation conditions, DMDs achieve a data rate of more than 30 times that of LCs.

Experiment 2: Receiver optimized for DMDs. PhotoLink increases the data rate by a factor of 80.

Considering that the maximum data rate achieved by the SoA is 8 kbps [43], a 30 kbps

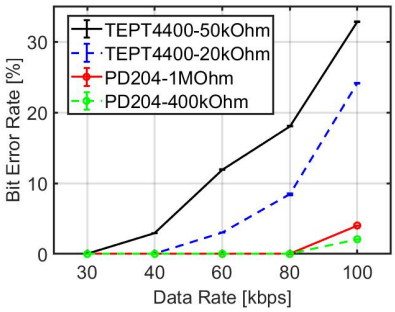


Figure 3.9: Bit error rate with different sensors and resistors

link is a significant improvement. However, using a receiver optimized for LCs does not exploit fully the capabilities of DMDs. Note from Table 3.6 that the maximum frequency used for a 30 kbps data rate is 60 kHz, but as stated in section 3.3, the global mode can reach frequencies above 200 kHz. The limitation of low-bandwidth sensors is that they cannot capture fast transitions: even though the *transmitted* signal has rise and fall times below 3 µs (Figure 3.1c), the *received* signal delivers rise and fall times above 100 µs.

At the core of this phenomenon are two parameters, the parasitic capacitance C_P, which is inherent to the sensor and cannot be modified; and the feedback resistor R_F, which can be modified. A large R_F and C_P improve the receiver's SNR (high-gain), but reduces the bandwidth. We analyze the effect of the feedback resistor on two photosensors: the TEPT4400 (high C_P, low-bandwidth) and the PD204-6C (low C_P, high-bandwidth). Table 3.7 shows the ability of each receiver-resistor pair to measure the fast DMD transitions for the rise and fall times. The first pair is the configuration used for LCs in [17], and thus, we use it as our baseline. We can see that the PD204 has a bandwidth that is big enough to capture transitions in the few microseconds range.

To showcase the importance of designing an optimal receiver for DMDs, we select four pairs from Table 3.7, and repeat the same experiment and setup described in subsection 3.5.1 but for a fixed distance d_{tr}=2 m. The results are presented in Figure 3.9. We know from *Experiment 1* that the TEPT4400 with a 69 kΩresistor can attain 30 kbps (baseline). A 50 kΩresistor is not low enough to increase the bandwidth significantly, but a resistor of 20 kΩcan increase the data rate to 40 kbps. The lower capacitance of the PD204, however, increases the bandwidth to a value that is high enough to double the data rate, reaching 80 kbps. Note that the improvement in data rate comes at the cost of reducing the range (lower gain). For the TEPT4400, the range is reduced from 6 m (30 kbps) to 2 m (40 kbps). For the PD204 with 100 kΩ(last pair in Table 3.7), the data rate reaches 100 kbps but at ranges shorter than 2 m, and thus, is not presented in Figure 3.9. The limited range, however, is not a fundamental problem because it can be increased by adding more amplifier stages at the receiver (our receiver has a single stage) or by using focusing lenses at the transmitter. In the case of the LCs, the bandwidth of any photodetector is much higher than the the bandwidth of the LCs, however, that is not the case for DMDs. We expect that an even higher data rate can be achieved if a photodetector with a high gain bandwidth is used together with multiple stages of signal amplification.

The data rate, on the other hand, has been a fundamental limitation for passive VLC and PhotoLink provides a ten-fold improvement over the most sophisticated LC-system in the SoA. Regarding the cost, DMD-based and LC-based systems can make use of the same photo-receivers, a DMD (€ 28.62) costs € 22 more than an LC (€ 6.56). We use an Artix-7 FPGA, which cost € 50, but a less expensive controller can be used as well. A microcontroller that costs € 13.6 was used in Luxlink [55].

3.5.2. ANALYZING THE LUMINOUS FLUX

Our work has two main contributions, the controller evaluated in the prior subsection and the toolbox presented in section 3.2. The main insight of our toolbox is the importance of maintaining the luminous flux throughout the optical link. To capture this phenomena, we consider two scenarios.

Scenario 1: Normalized flux (indoor setup). In this scenario, we use the baseline receiver (TEPT4400 with a 69 kΩresistor) and transmit a fixed carrier frequency. The frequency is empirically chosen to be 30 kHz because this signal can be clearly detected at 4 m without saturating the receiver at 1 m. To calculate the amount of luminous flux maintained in the optical link, the signal intensity measured at 4 m is normalized with respect to the intensity measured at 1 m for *the same* light source. This normalization process and careful setup quantify the impact of the radiation pattern of each light source independent of its emitted power.

Under this setup, we evaluate four different light sources *indoors*, as shown in Table 3.8, and simulate the same illumination conditions with our toolbox. In the test setups, the direct and diffuse sunlight arrive at the DMD through a large glass window. To obtain realistic simulation results, we apply the parameters in Table 3.9, which correspond to the actual physical properties of PhotoLink. The normalization method is also applied to the simulations[5], and the results are shown in Figure 3.10. The plots show a strong agreement between the experimental and simulated flux under all illumination conditions. With diffuse sunlight, we are not able to detect a signal even at 1 m, despite measuring a 2000 lx illuminance on the surface of the DMD. This aligns with our analysis in section 3.2, which states that diffuse light has the lowest performance with reflective surfaces. The results also show that direct sunlight performs best at retaining the luminous flux (losing 30% at 4 m), followed by artificial lights (losing more than 80%). And with artificial lights, more luminous flux is retained at the receiver when the light is placed further away from the transmitter (setup 2). All these results are in agreement with the insights provided by our model in section 3.2.

Scenario 2: Absolute flux (outdoor setup). In this scenario, we do not perform a normalization process, instead, we transmit 100 packets of "Hello world!" at 30 kbps and present the received voltage and BER. We evaluate the two best light sources identified by our toolbox, flashlight and direct sunlight. The evaluation with direct sunlight is done *outdoors* during a clear day with good sunlight (several thousand lux), and then, moving the setup indoors and placing a flashlight in a dark room.

With sunlight, a BER of $0.9x10^{-3}$ is achieved at 1 m and a BER of $0.8x10^{-3}$ is achieved at 2 m. The errors can be attributed to the fact that a link in the outdoor environment

[5] Since photodiodes have a quasi-linear response to light intensity, we assume a linear correlation between the obtained signal strength in the toolbox and the voltage obtained in our experiment.

Table 3.8: Measuring the power drop-off with respect to distance

Setup	Light Source	D_{LM}	D_{TR}	Measured Normalized Signal	Simulated Normalized Signal
1	Direct Sunlight	N/A	1 m and 4 m	0.70	0.73
2	Flashlight	4 m		0.17	0.20
3	Flashlight	1 m		0.04	0.06
4	Diffuse Sunlight	N/A		N/A	N/A

Table 3.9: Key parameters used in simulator

Light Source	Dimension	2.7 m x 2.7 m
	Half Angle	30°
Modulating Surface	Dimension	4.8 mm x 2.7 mm
	Light-absorbing area	8 mm by 8 mm
	Spreading Angle	0.3°
Receiver	Lens Dimension	2.5 cm
	Tangent Sphere Radius	(4 cm, -5 cm)
	Lens Material	bk7
	FoV	1°
	Photodiode Diameter	3 mm

is subjected to occasional disturbance. With flashlight, the BER is 0 at 1 m, however, at 4 m, the BER increases to $19.4x10^{-3}$. In Figure 3.11, we present a direct comparison of the flux reaching the receiver with the flashlight and sunlight using the SYN symbols in the packet. At 1 m, the flux reaching the sensor with the flashlight is slightly lower than that with sunlight (around 0.18 V vs. 0.2 V), which shows that the flashlight and sunlight result in similar voltage range. However, at 4 m, the luminous flux reduces by 60% with flashlight, due to a less directional pattern, while direct sunlight loses only 10%[6]. This result highlights the importance of expanding passive VLC studies towards the exploitation of natural light.

3.5.3. ISSUES WITH DMDS

DMDs have not been designed for ambient light communication, and hence, present some limitations. We now discuss what we consider the main shortcomings of this MEMS technology for passive VLC.

Issue 1: Directionality. DMDs operate with two fixed angles, which raises up the issue of directionality. If the light source changes its location, the impinging light rays will no longer be aligned with the predefined angles at the DMD, breaking the link. This issue can be overcome with light concentrators. As a proof of concept, we build a simple concentrator with two optical components, as show in Figure 3.12a. The first component is a Compound Parabolic Concentrator (CPC). The CPC is a special parabolic lens that collects light from different angles and concentrates it on a small output area. We use a CPC with an input and output circular area of 14 mm and 4 mm diameter respectively, and a

[6]Note that the flashlight loss is higher than the loss predicted in Figure 3.10 for 1 m because we place the light closer to the DMD, 30 cm instead of 1 m

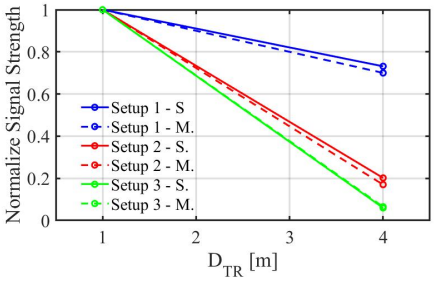
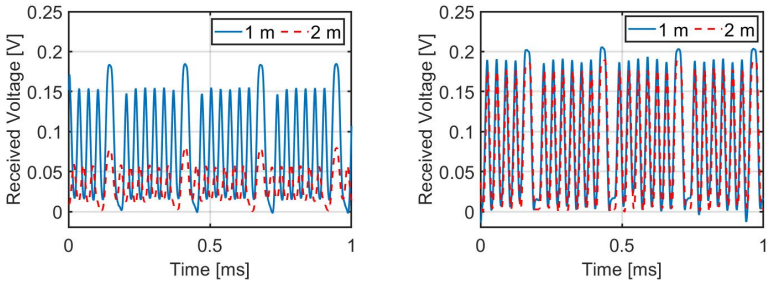


Figure 3.10: Simulated and measured voltage dropoff



(a) Flashlight (b) Sunlight

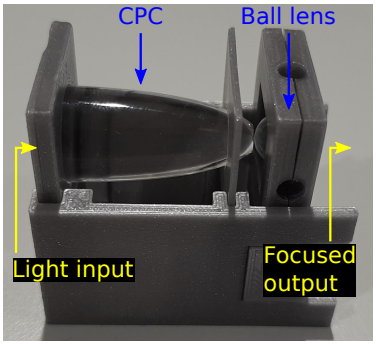
Figure 3.11: Signal strength

concentration factor of 10. The second component is a ball lens of 8 mm diameter, which is used as a coupler and collimator, to further focus the collected light. We manufacture a 3D-case to align the CPC and the ball lens, and aim its output to the DMD.

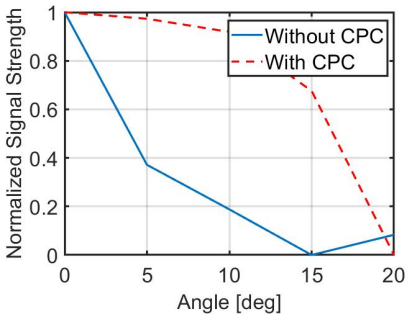
Figure 3.12b presents the results obtained with and without the light concentrator. A flashlight is positioned at different incidence angles and the signal strength is measured at the receiver. Without the concentrator, the signal strength decays below 0.9 with deviations around +/- 1 degree. With the concentrator, the signal remains above 0.9 for angles around +/- 10 degrees. This is a simple implementation, more sophisticated designs can increase the FoV to any desired degree. Thus, while an ideal DMD design for passive VLC could consider flexible angles, it is not a strict requirement.

Issue 2: Power consumption. Perhaps the most limiting factor of current DMD designs is the relationship between its small area and relatively high power consumption. The performance of passive VLC depends on the area of the transmitting surface. For example, a standard light bulb consumes 1 watt to emit 90 lumen, but with an area of 13 mm^2, the DLP2000 would emit only between 0.1 and 0.5 lumen.

Regarding the power consumption, current DMD designs have two levels of overhead. The first level is related to the *memory state*, which is not required for PhotoLink and consumes 57 mW in the DLP2000. The second level is the actuation of the micromirrors and consumes 45.5 mW. We are, thus, left with a surface that emits between 0.1 and 0.5 lumen (depending on daylight conditions), while consuming 45 mW. Considering that LCs consume less than 1 mW, and that low-power LEDs consume less than 100 mW, it is central to consider power consumption in the comparison with LCs and LEDs. To



(a) Design



(b) Evaluation

Figure 3.12: CPC

perform that analysis, let us consider a low-power LED that has been used in prior VLC studies [56], the VLMB1500, which consumes 75 mW and emits 0.2 lumen. We perform a theoretical comparison between LCs, DMDs and LEDs based on the Shannon-Hartley theorem $C = B\log_2(1+SNR)$. The analysis assumes a luminous flux of 0.2 lumen for the DMD.

First, let us consider LCs, which have areas that are two orders of magnitude bigger than DMDs, and hence, receive two orders of magnitude more lumen. Assuming that the LC receives 20.2 lumen on its incoming area (20 from the light source and 0.2 from the 'extra' LED), the outgoing flux would be 10.1 lumen because LCs cut the power in half (Limitation-1 in section 3.3). Hence, the SNR of an LC-system would increase by a factor of 50 (10.1/0.2), but the SNR only contributes logarithmically to the capacity. Overall, the extra SNR would contribute with a factor of 6, compared to the factor of 1350 contributed by the BW of the DMD, making the DMD still two orders of magnitude more competitive.

To consider the option of using the LED with active-VLC, we measure its rise and fall times, which are 3.5 µs and 1.6 µs: a period of 5.1 µs compared to the period of 4.6 µs for DMDs. Recalling that the LED and DMD emit a similar lumen, the DMD is only slightly more competitive. This result, however, should consider that current DMDs are not designed for ambient light communication. The mirrors of the DLP have a size of microns and use *electrostatic* actuation, larger area mirrors (bigger than 2 mm) "benefit from *electromagnetic* actuation proportional to the mirror area" [57], leading to bigger surfaces with lower power consumption.

Thus far, the passive VLC community has faced a major obstacle, even with big LC surfaces, no system can provide data rates above 10 kbps. PhotoLink shows that current (suboptimal) DMDs can provide 100 kbps. Synergies with MEMS researchers could enable the design of bigger modulating surfaces to create wireless networks operating solely with natural light and with low power budgets.

3.6. RELATED WORK

Passive VLC systems using LCs. There have been several studies on passive VLC systems, which are summarized in Table 3.10. To date, LCs have been widely used as an optical transmitter in SoA passive VLC systems. There are two categories: one uses LCs in com-

Table 3.10: Comparison of PhotoLink with the most relevant systems in the state of the art

Name	O_L	O_L Power or Illuminance	D_{LT}	O_T	Surface Type	O_R	FoV	Data Rate	Range
RetroVLC [32]	LED	12 W	Variable[1]	LC+RR[2]	Specular	Photodiode	50°	0.5 kbps[2]	2.4 m
PassiveVLC [42]	Flashlight	3 W	Variable	LC+RR	Specular	PD	4°	1 kbps	1 m
RetroTurbo [43]	Flashlight	4 W	Variable	LC+RR	Specular	PD	20°	8(4) kbps	7.5(10.5) m
RetroI2V [40]	Flashlight	30 W	Variable	LC+RR	Specular	PD	30°	125(1000) bps	101(80) m
Chromalux [41]	Sunlight(Direct) / Flashlight	3-6 klux / 400-700 lux	N/A / N/S	LC and Metal Sheet	Specular	Color Sensor	Variable	1 kbps	50 m / 10 m
Luxlink [17]	Sunlight(Direct) / LED	10-26 klux / 2 klux	N/A / N/S[3]	LC and Diffuser	Diffuse	PD	1°	80 bps / 1 kbps	65 m / 3 m
TwSL [48]	Sunlight(Diffuse)	3 klux	N/A	Paper	Diffuse	PD	N/S	127 bps	4 m
[53]	LED	15 W	čms	DMD	Specular	PD	N/S	4.2 kbps	170 cm
[54]	LED	15 W	čms	DMD	Specular	PD	N/S	9 bps	2.5 m
[52]	Sunlight(Direct)	330 lux	N/A	DMD	Specular	Camera	N/S	1 bps	60 cm
PhotoLink	Flashlight	1800 lx	1 m	DMD	Specular	PD	1°	30(80) kbps	6(2) m

[1] For work involving retro-reflectors as a transmitter, $D_{LT} = D_{TR}$
[2] RR stands for Retro-reflectors
[3] For work involving retro-reflectors, uplink data rate is quoted
[4] N/S stands for 'not specified'

bination with retro-reflectors, where the light source and the receiver are co-located; the other adopts only the LC as a transmitter, where the light source and the receiver can be placed at different locations, opening up the possibility to take advantage of natural light.

The studies in the former category typically have a constrained data rate and range. The earlier studies [32, 42], achieve a data rate of 0.5 kbps and 1 kbps with ranges up to a few meters. More recently, RetroI2V [40] achieves a range of 80 m. However, it uses a powerful 30 W light to achieve a data rate around 1 kbps. RetroTurbo [43] has a surface area of 66 cm^2 and uses an advanced modulation scheme to overcome the slow time response of LCs. RetroTurbo achieves a data rate of 8 kbps with a moderate light source (4W flashlight) up to 7.5 m [40]. However, retro-reflectors cannot be used with ambient light, as the light source and the receiver have to be co-located.

On the other hand, the studies in the latter category take advantage of the strong illumination from sunlight and are able to achieve a long range without a dedicated illuminator, such as in the case of Luxlink [17] and Chromalux [41]. Luxlink is able to reach a range of 65 m with sunlight, but the data rate is limited to 80 bps. It also demonstrates that with an LED, a data rate of 1 kbps can be achieved up to 3 m. Chromalux [41] takes advantage of the transient state in LCs, and is able to achieve a range of 50 m with a data rate of 1 kbps with sunlight, and up to 10 m with a flashlight. While LCs are energy efficient, they suffer from a high attenuation loss due to the use of polarizers, and a limited bandwidth because of its slow rise and fall times. On the other hand, a higher data rate can be achieved with DMDs, but using more power. And in addition to demonstrating a novel system, we provide an analytical framework to understand the performance of different studies.

Applications of DMDs. Like LCs, the main application of DMDs is video projection, and thanks to their competitive advantages (high reflective efficiency and switching times) they dominate the market. But DMDs are also used in other applications: microscopy, holography, data storage, and also as spatial modulators with lasers [58]. The use of DMDs for ambient light modulation, however, is restricted to a handful of studies in-

volving localization [53] and communication [54, 52]. And all these studies suffer from a limited data rate (1 bps, 9 bps and 4 kbps), as well as a limited communication range (60 cm, 2.5 m and 170 cm). These systems use the off-the-shelf DMD controllers with their default refresh rates, which fail to take advantage of the fast switching times of the DMDs.

Channel modelling for VLC systems. There have been an array of studies on channel modelling techniques for indoor active VLC systems [45], several of which are ray-tracing based [59, 60]. The focus of those studies is to achieve an accurate impulse response considering the dynamics of the VLC system and its indoor environment. They remain a theoretical exercise in most cases, as an accurate description of the indoor space is difficult to obtain. This differs from our work, as our study focuses on the interactions between different types of surfaces and ambient light.

Ambient RF backscatter systems. In RF backscatter, passive devices can communicate with each other utilizing surrounding RF sources. The first study exploited TV tower signals and showed a data rate of 1 kbps at distances of 2.5 feet outdoors and 1.5 feet indoors [61]. Subsequent studies have shown that WiFi, BLE and LoRa signals can also be backscattered, attaining even higher data rates and/or ranges [62, 63]. RF backscattering is an exciting area but requires *man-made* signal (radio towers and antennas), and antennas typically have a limited bandwidth. Ambient light backscattering not only allows exploiting a different part of the electromagnetic spectrum but it can also exploit *natural* sunlight.

3.7. CONCLUSION

In this work, we propose an optical model to analyze ambient light communication, and based on the insights it provides, we explore the use of a DMD as an optical transmitter. We propose a novel platform that optimizes the retention of the luminous flux to attain the best optical performance. This approach allows us to achieve a data rate that is 30 times higher compared to LCs under the same working conditions. Furthermore, with optimally designed receivers, the data rate reaches 80 kbps. While current DMD designs still face limitations to operate with ambient light, it is a component that expands the possibilities of the nascent area of passive VLC.

4

SUNLIGHT-DUO: EXPLOITING SUNLIGHT FOR SIMULTANEOUS ENERGY HARVESTING & COMMUNICATION

Having discussed a passive transmitter in the prior chapter, we now turn our attention to the receiver. Sunlight has been used for decades to *harvest energy* and more recently to *transmit wireless data*. We present a novel system that exploits sunlight to achieve both *energy harvesting* and *communication*, enabling in that way a sustainable system that relies *solely* on natural light. Sunlight can be modulated with different optical devices, but demodulating sunlight with solar cells playing the dual role of energy harvesters and data receivers presents a challenge that has not been tackled yet. This challenge exposes a fundamental trade-off between energy harvesting and communication. High sunlight intensity favors energy harvesting but also creates a high source of interference because sunlight provides both, the signal (S) and noise (N). Thus, *an open research question is whether solar cells can operate as harvesters and receivers with sunlight*. To answer this question, we perform a thorough analysis of various solar cell configurations suitable for embedded IoT devices. Our analysis reveals that sunlight can be used for simultaneous energy harvesting and data reception, but the receiver must adjust key solar cell parameters on the fly. Based on our analysis, we build a *self-powered* prototype and test it in different conditions. Our prototype maintains a bi-directional link for up to 11 m, with a data rate of 1200 bps for downlink and 800 bps for uplink. Additionally, our system maintains a stable link over 2 m throughout the daytime. To the best of our knowledge, this is the first work using sunlight simultaneously for energy harvesting and communication.

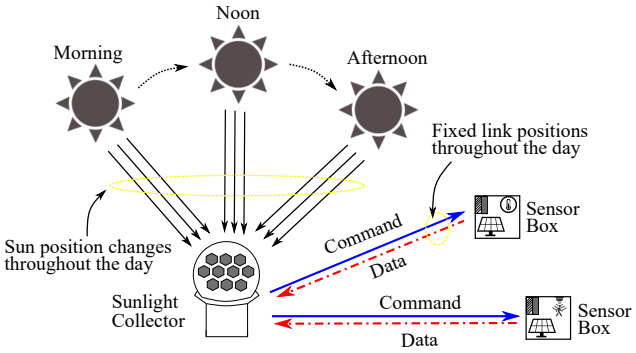


Figure 4.1: An overview of our approach

4.1. INTRODUCTION

Since its invention in the 19th century, wireless communication has predominantly relied on the RF spectrum. However, during the last decade, there has been an unprecedented demand on this spectrum [36]. In response to this challenge, researchers have started exploring visible light communication (VLC). By modulating the intensity of an LED at a high speed, wireless transmissions can be achieved without disturbing illumination, offering a yet unexploited spectrum [6, 64]. *In indoor scenarios*, VLC is practical because there is not much interference from sunlight and a small energy overhead is needed to add communication over illumination. *In outdoor scenarios*, VLC is less effective due to the strong presence of ambient light. Receivers based on *photodiodes* tackle interference through the use of elaborate optical enclosures and automatic gain control mechanisms. To mitigate the shortcomings of photodiodes, researchers have demonstrated the potential of solar cells to serve the dual purpose of energy harvesters and data receivers [65, 66, 14]. Given that solar cells are designed, from inception, to handle high illumination, it is advantageous to re-purpose them as receivers. However, *the fundamental limitation of the SoA is that solar cells are used as receivers but only with transmitters using high-power lights [14] or carefully selected lasers [65, 66].* Using artificial light sources for transmission misses the opportunity to leverage the pervasive presence of sunlight as a wireless carrier.

An alternative approach in leveraging the omnipresence of sunlight for communication is termed *passive VLC*. Unlike VLC, passive VLC does not need to modulate an artificial light directly [67]. Instead, it modulates ambient light using optical surfaces, such as liquid crystal shutters (LCs). *The limitation of passive VLC systems is that the receivers still use photodiodes, which miss the opportunity for energy harvesting and necessitate the use of elaborate optical designs to limit sunlight interference.*

Motivation. We envision a new communication paradigm for embedded IoT devices to harness sunlight for communication and energy harvesting. This paradigm merges the most sustainable features of passive VLC (using sunlight to transmit data) and outdoor-VLC (employing solar cells to harvest energy and receive data).

Our prototype introduces a novel use of sunlight collectors, as illustrated in Figure 4.1. Sunlight collectors capture natural light and redirect it to *indoor* spaces, but

we show that these collectors can also be exploited outdoors[1]. The beams radiated by the sunlight collector are modulated using liquid crystals, and the receiver is a battery-less device that uses solar cells to obtain energy and data from the sunlight beams. The receiver also has a reflective surface to communicate back to the transmitter, creating a bi-directional link. A potential application of our system is within the realm of smart farming, where a central unit (sunlight collector) could issue commands to retrieve data from nearby sensors.

*Our system is **not** envisaged to replace low-power RF, but rather to provide a new perspective.* A key advantage of light communication is the access to an open and unrestricted spectrum; and considering the increasing use of solar cells in small IoT devices, these cells could be dubbed as receivers.

Key challenge. Exploiting sunlight for communication and energy harvesting exposes a challenge that has not been investigated before: *We need to optimize solar cells not only as harvesters but also to decode a signal that is embedded in sunlight.* Sunlight provides the signal (S) but also noise (N). In outdoor-VLC, sunlight interference is reduced by using artificial sources, such as lasers [65, 66], that transmit data within the weakest portions of the sunlight spectrum. With such configurations, the spectra and intensity of the transmitter (laser) are carefully designed to differ as much as possible from sunlight. In passive VLC, sunlight interference is limited by creating optical enclosures around photodiodes; and the only task is communication, there is no harvesting. In our scenario, the signal and noise share the same spectrum and similar intensity, affecting the operation of solar cells to perform both as receivers and harvesters.

Contributions. Considering the above motivation and challenges, our work makes the following contributions.

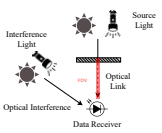
Contribution 1 [section 4.4]: Analysis of solar cell chargers and configurations. To gain a deep understanding of the charging and communication behavior of solar cells, we carry out a thorough analysis considering different ambient light intensities and solar cell configurations. This analysis provides key insights for designing a front end that can meet different charging and communication needs.

Contribution 2 [section 4.5]: Dynamic reconfiguration scheme. After identifying the configurations that perform best, we evaluate the performance of our passive link over a complete *charging cycle*. Based on the insights, we design a dynamic reconfigurable scheme that maintains a high level of energy harvesting while optimizing for communication.

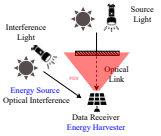
Contribution 3 [section 4.6] Prototype and evaluation. Using sunlight for simultaneous energy harvesting and communication, our prototype achieves more than 90% packet success rate at a distance of 11 m for both uplink and downlink, with a data rate of 1200 bps and 800 bps, respectively. Our results also show that we can establish a stable link from 9 am to 7 pm. During this time, our receiver harvests enough power to support the decoding process and three extra sensors and an e-ink display. This is the first demonstration of a link relying solely on sunlight for communication and power.

Historical context. In 1880, Alexander G. Bell built the first sunlight link. The trans-

[1] A sunlight collector consists of a lens system and a motor to follow the sun's position. While it's feasible to develop a compact, custom-made sunlight collector, we chose a commercial variant to reduce the design time.



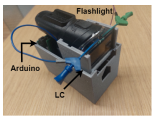
(a) Passive VLC system with PD as receiver



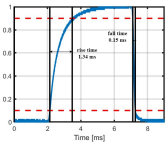
(b) Passive VLC system with solar cells as receiver



(c) Himawari sunlight collector



(d) Transmitter prototype with flashlight



(e) Rise and fall time of the LC

Figure 4.2: System overview and components

mitter was a megaphone connected to a reflective surface to modulate voice using sunlight, and the receiver was a rudimentary photosensor. Bell called his invention the Photophone and in a letter to his father wrote *"I have heard articulate speech by sunlight! I have heard a ray of sun laugh and cough and sing!"*. Sunlight-Duo (Sunlight-Duo) is a stepping stone towards converting the Photophone into an eco-friendly link using sunlight for transmission and solar cells for reception and energy.

4.2. SYSTEM OVERVIEW

Similar to most passive VLC studies, our system has three components: the *light source*, the *transmitter*, and the *receiver*. *Our main contribution is on the receiver*. In this section, we describe these components and the challenge of designing a solar cell receiver.

Light Source: Various elements can emit ambient light, functioning as a *source*, *interference*, or both, as shown in Figure 4.2a. The source's light is modulated by an optical surface (transmitter). In most passive VLC studies, the source and interference are distinct. For example, in [43, 40], a flashlight is used as the source and other light bulbs act as interference. This setup provides stable links because the source light is much stronger and more focused than the ambient light, and they have different spectra. In other studies, the source and interference come from the same point, typically the sun [17, 41]. This setup is more complex because the source and interference have the same spectrum, completely mixing the signal and noise. Furthermore, the sun intensity changes throughout the day. This more challenging setup is the one tackled in our work, with the added complexity of using solar cells as receivers, instead of photodiodes.

Transmitter: The transmitter is an optical device that modulates ambient light by changing some of its properties. Two types of optical surfaces have been studied as transmitters, liquid crystals (LCs) [32, 42, 40, 43] and Digital Micromirror Devices (DMDs) [68]. DMDs achieve a higher data rate but require a complex driver. Since most studies rely on LCs, we build upon the SoA designs using LCs due to their simpler modulation.

An LC has two states, which either block or allow light to pass through depending on the voltage applied to its pins. LCs are simple to drive but have slow rise/fall times. Most systems employing LCs and photodiodes have demonstrated data rates between 100 bps and 8 kbps [32, 42, 40, 41, 17, 43]. Since our focus is on the receiver, we build upon the SoA designs consisting of *single* LCs [32, 42, 17]. Our platform uses a PI-cell LC with a switching speed around 600 Hz, c.f. Figure 4.2e (1.34 ms and 0.15 ms for the rise and fall times). This speed is sufficient to attain full contrast. Since we use frequency-shift keying modulation, we can attain faster switching speeds, at the cost of lowering the contrast,

as described in section 4.5.

Our work uses two setups to analyze interference: controlled and in-the-wild. The *controlled* setup is used in section 4.4, where we rely on artificial lights to emulate an outdoor lighting scenario. This controlled setup allows a systematic assessment of solar cell performance in terms of their charging and communication behaviors. Figure 4.2d depicts the transmitter used in this setup, where the beam emitted by a flashlight is modulated via an LC controlled with an Arduino. The *on-the-wild* setup is used in our final evaluation (section 4.6). In that setup, the sun provides the interference and the flashlight is replaced with the output of the sunlight collector to radiate a natural light beam towards the LC. The output of the sunlight collector has bundles of optical fibers to direct the light from the tracking lenses to the desired direction (Figure 4.2c). This final evaluation exclusively uses sunlight for both energy harvesting and communication.

Receiver: Prior passive VLC studies leveraging sunlight for communication employ photodiodes. However, photodiodes require substantial power and a complex optical design to prevent saturation outdoors [17, 41]. Moreover, in strong sunlight conditions, outdoor-VLC studies indicate that solar cells outperform photodiodes as receivers [69]. Contrary to the power-consuming nature of photodiodes [70], solar cells generate power while receiving information, but they introduce a challenge in the design, as demonstrated in Figure 4.2b. Unlike photodiodes, which allow for reducing the field-of-view (FoV) to eliminate interference, solar cells inherently have a broad FoV that cannot be reduced without significantly hampering their energy-harvesting potential.

Overall, our work targets a scenario that has not been considered before, one where *sunlight is the common source of three components: energy, data, and interference.* Therefore, it is important to analyze different levels of ambient light and solar cell configurations to achieve joint energy harvesting and communication.

4.3. STATE-OF-THE-ART ANALYSIS

In this section, first, we position our work within the general areas of ambient backscattering and positive energy sensing, and after that, we discuss in detail the areas of outdoor- and passive VLC.

4.3.1. PASSIVE RF & POSITIVE-ENERGY SENSING

Ambient RF energy harvesting for battery-less transmissions has gained traction. That approach exploits ubiquitous RF signals (e.g., TV, WiFi, BLE, LoRa) to create passive wireless links [61, 62, 63]. RF backscattering relies on energy-intensive man-made signals, unlike natural light, which uses an energy-free wireless carrier.

Positive-energy sensing involves sensors harvesting energy for their own operation and additional tasks. Some studies use photodiodes (PDs) [71] while others use solar panels [72] for energy harvesting and close-proximity hand gesture recognition. These techniques require gestures to be made a few centimeters away and capture under 10 samples per second. While these approaches utilize ambient light, they don't fully exploit solar cells' sensing capabilities in speed and range.

4.3.2. SOLAR CELL AS A DATA RECEIVER

A taxonomy highlighting the novelty of our work w.r.t. the most relevant studies in the SoA is presented in Table 4.1 and a quantitative comparison in Table 4.2.

Table 4.1: Relevant Communication Systems in the SoA

Signal Source \ Energy Source	Sunlight	Artificial Light	External Power[1]
Sunlight	① This work		② Passive VLC
Artificial Light (LED, Laser)	③ Outdoor VLC	④ Indoor VLC	⑤ Solar Cell as Data Receiver

[1] External power required, not provided by the receiver (PD or solar cell)

Solar Cells as Data Receivers: cell (5) in Table 4.1. As solar cells have been traditionally used as energy harvesters, early research efforts aimed at demonstrating the potential of solar cells to work as data receivers. For instance, Wang et al. showcased impressive communication speeds of 7.01 Mbps and 11.84 Mbps over 39 cm using an LED transmitter and a 4.5 W solar cell receiver [73, 44]. Moreover, Lorrière et al. showed that solar cells could outperform PDs under intense sunlight [69]. These studies, however, use solar cells *solely* as receivers, requiring external batteries to operate, and neglect their inherent energy harvesting potential. Other studies explore workarounds such as alternating between charging and sensing, yet this method reduces efficiency and requires careful synchronization between the transmitter and receiver [74, 75].

*Simultaneous charging and communication, but using **only artificial light** as an energy and signal source:* (4) in Table 4.1. Mir et al. conducted a study where an LED transmitted information to a solar cell receiver that could simultaneously harvest energy and decode data [14]. The study analyzes the impact of various solar cell configurations. Their findings indicate that a parallel configuration of solar cells performs more effectively for charging, while a series configuration excels in communication. While these insights are valuable, they are derived from an *indoor scenario using light bulb and without interference.* In our work, we show that these findings are not applicable in outdoor scenarios as the performance of both, charging and communication, degrades significantly outdoors.

*Simultaneous charging and communication, but using sunlight as an energy source and **artificial light as a signal source**:* (3) in Table 4.1. A few outdoor-VLC studies demonstrate the potential for simultaneous communication and energy harvesting using solar cells. However, these studies rely on *artificial* light sources for the signal. Das et al. created an outdoor link with a 940 nm laser [65, 66]. This wavelength is chosen because

Table 4.2: Comparison of Sunlight-Duo with the most relevant systems in SoA

Name	Signal	Power	Signal Strength	Sunlight Interference	Speed	Range	Solar Cell Model	Location	Sim. S/C	System
[73]	LED	External	$3.5W/m^2$	Yes (<10% signal)	7.01 Mbps	39 cm	SX305M (4.5W)	Indoor	No	active
[44]	LED	External	$7W/m^2$	No	11.84 Mbps	N/S[1]	SX305M	Indoor	No	active
[14][2]	LED	LED	N/S	No	N/S	N/S	Variable	Indoor	Yes	active
[69]	LED	External	5080 lux	Yes ($400W/m^2$)	1.2 MHz	23 cm	Solar Frontier PV Module	Outdoor	No	active
[65]	Laser	Sunlight	$8.7W/m^2$	Yes	8 Mbps	30 m	5 W Silicon Solar Cell	Outdoor	Yes	active
[66]	Laser	Sunlight	N/S	Yes	6.34 Mbps	3.5 m	5 W Silicon Solar Cell	Outdoor	Yes	active
[17]	Sunlight	External	Variable	Yes	80 bps	50+ m	N/A[3]	Outdoor	No	passive
[41]	Sunlight	External	Variable	Yes	1.2 kbps	50+ m	N/A[3]	Outdoor	No	passive
Sunlight-Duo	Sunlight	Sunlight	Variable	Yes	1.2 kpbs	11 m	KXOB25-14X1F	Outdoor	Yes	passive

[1] N/S stands for 'not specified'
[2] This studies implements a LiFi downlink and an RF uplink
[3] Photodiodes were used in place of solar cells

sunlight is highly attenuated by the atmosphere in that portion of the spectrum. In this way, the communication link performance is guaranteed due to minimal interference. Contrary to this approach, we propose a system where sunlight is used for data transmission, eliminating the requirement for a separate artificial source for communication.

4.3.3. SUNLIGHT AS A SIGNAL SOURCE

This section describes the relevant work on passive VLC systems, (2) in Table 4.1. These systems capitalize sunlight solely as a signal source, but not as an energy source. Luxlink [17] and Chromalux [41] leverage the intense illumination from sunlight to enable long-range communication without the need for artificial sources. Luxlink achieved a range of 65 m using sunlight, although with a limited data rate of 80 bps. Chromalux, meanwhile, covered a distance of 50 m achieving a data rate of 1 kbps. Despite these achievements, both studies opt for photodiodes (PDs), which do not harvest energy and perform sub-optimally as outdoor receivers compared to solar cells [69].

4.3.4. THE NOVELTY OF OUR APPROACH

Overall, our work advances the SoA in two main ways, cell (1) in Table 4.1. Compared to studies requiring external power –using either PDs, as in (2), or solar cells solely as sensors, as in (5)– our platform is self-powered by the receiver. And compared to studies using solar cells for simultaneous energy harvesting and decoding –either indoors (4) or outdoors (3)– our transmitter does not require any artificial source. A detailed comparison with SoA studies is presented in Table 4.2. Sunlight-Duo is the only system using sunlight for power and communication. The most relevant works are the ones working outdoors (bottom six rows), where the green and orange colors capture their main pros and cons[2]. In the next section, we analyze how a low-power IoT device can optimize harvesting and reception using a small solar cell array.

4.4. ANALYSIS OF CHARGER AND SOLAR CELL

Using the same solar cells for communication and energy harvesting, while relying solely on sunlight for both tasks, presents a complex scenario. Specifically, there are two main challenges, *(i)* the divergent optimal conditions for charging and communication; and *(ii)* the complexity of decoding the signal embedded under the high intensity of sunlight.

[2] A general trade-off between passive and active VLC (last column) is to reduce power consumption (by using ambient light) at the cost of reducing the data rate (due to the slow optical surfaces) [32, 42, 43, 40, 41, 17].

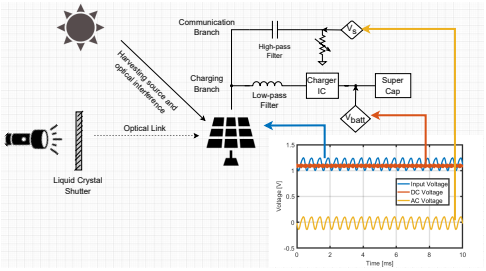


Figure 4.3: Controlled setup with solar cells

To tackle these challenges, we first perform an in-depth analysis of solar cell characteristics in a *controlled* scenario, focusing on two main components:

1. The type of charger, which runs the algorithm designed to optimize the energy harvesting of the solar cells.

2. The configuration of inter-cell connections, as this plays a pivotal role in optimizing the balance between harvesting and communication functionalities.

4.4.1. CONTROLLED EVALUATION SETUP AND METRICS

To design our system for varying sunlight conditions, we need to understand solar cell behavior under dynamic lighting. We conduct controlled experiments using two light fixtures for separate energy harvesting and communication purposes, allowing us to regulate harvesting, signal, and noise intensities independently. A 100 W LED array simulates sunlight *interference*, and a white light *source* behind an LC shutter acts as the data transmitter, with the *source*'s spectrum falling within the *interference*'s range to emulate data transmission via sunlight.

A diagram of the experimental setup is shown in Figure 4.3. The output of the solar cell goes through a high-pass filter (top branch, used for communication) and a low-pass filter (bottom branch, used for charging). Our design follows a battery-less approach, using a supercapacitor as energy storage, instead of a battery, due to the detrimental effects that batteries have on the environment. V_s represents the sensing voltage used to decode data, and V_{batt} represents the supercapacitor voltage. The signals received by both branches are shown in the bottom-right plot. We can observe a DC component used for energy harvesting (flat red line) and an AC component (yellow curve) containing the data.

Metrics. *The charging performance* is measured by the time it takes to charge the supercapacitor. *The communication performance* is measured by calculating the received signal strength (RSS) using a triangular wave within a time window of 10 ms.

Generalization. As described later, our dynamic reconfiguration requires some parameters to optimize harvesting and communication. These parameters depend on the type of solar cell and charger used. Since it is not possible to evaluate all possible combinations of solar cells and chargers, to generalize our method, we provide a step-by-step framework. The parts presented inside boxes are given as general guidelines to implement our approach.

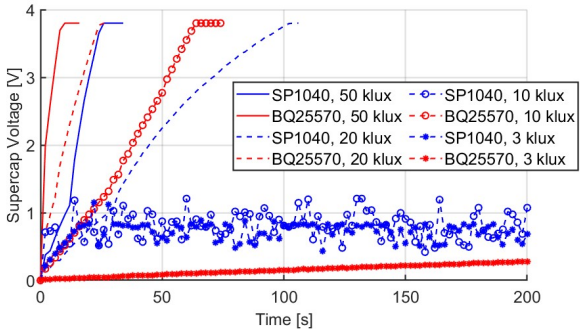


Figure 4.4: Charging a 22mF supercapacitor with different charger ICs under different light intensities

4.4.2. STEP 1: CHOOSING A SOLAR CELL CHARGER

Solar cells need to be connected to a charger IC to manage the energy harvesting process. Given that IoT sensors have limited surface areas, the first step is to select a charger IC that ensures maximum charging efficiency within the spatial constraints and under different amounts of ambient light.

Charger ICs run algorithms that consume part of the power harvested by the cells. With large solar panels, the power consumed by the charger is a tiny fraction of the power generated by the solar cells [76]. Since IoT devices operate on a significantly smaller scale, the energy consumption of some algorithms can offset their benefits. Our design adopts a solar cell area of 3000 mm^2, which is commonly used in this area [14]. In this first step, the focus is solely on the harvesting aspect of the system. Therefore, only the LED sunlight emulator in Figure 4.3 is utilized.

Among maximum power point tracking (MPPT) algorithms, the Perturb and Observe (P&O) and Constant Voltage (CV) methods are the most prevalent. To better understand which algorithm is better suited for small IoT devices, we evaluate one solar cell charger with a P&O algorithm (the SPV1040) and one with a CV (the BQ25570). The results in Figure 4.4 reveal that the CV algorithm (red curves) consistently outperforms the P&O (blue curves) across all light conditions. With small solar cells, the power consumed by the more accurate algorithm (P&O) outweighs the gains obtained from it. Furthermore, under low light intensities (10 klux and 3 klux), P&O even fails to store enough power to run itself, failing to charge the supercapacitor beyond 1 V.

After this step, the design will be guaranteed to have the best charger. In our case, we utilize the BQ25570 charger due to the superior performance of the CV algorithm.

4.4.3. STEP 2: DEFINING SOLAR CELL CONFIGURATIONS

After selecting the best charger, the next step is to define the different solar cell *configurations*. Denoting n as the number of cells that can be placed on the device's surface, we need to analyze the best configuration for those n cells, from serial to parallel. These configurations play a central role in defining the performance of energy harvesting and reception.

We populate the available area (3000 mm^2) with 16 Anysolar KXOB25-14X1F solar

Table 4.3: Solar Cell Reconfigurable Parameters

Parameter	Configuration
Solar Cell Connection	2s-8p, 4s-4p, 8s-2p
Operating point η_{voc}	80%, 50%, 30%, 10%

cells. With an efficiency of 25%, these cells capture the most popular technology in the market. For n solar cells, the *connection* refers to the number of cells connected in series and in parallel. To analyze the trade-off between communication and charging, we explore three configurations: 8 parallel sets of 2 solar cells in series (2s-8p), 4 parallel sets of 4 solar cells in series (4s-4p), and 2 parallel sets of 8 solar cells in series (8s-2p).

For a given area and number of solar cells, the configurations cannot be arbitrary, they need to satisfy two key criteria: 1. Equal current and voltage flow in each branch, maximizing the solar cell's efficiency, and 2. Ensuring the maximum current and voltage are within a valid range for chargers designed for low-power applications.

With our different configurations, we evaluate the harvesting and communication capabilities under varying light intensities. To benchmark the signal strength, the flashlight is turned on behind the LC, while the LC is modulated to transmit a triangular wave at a fixed frequency of 2 kHz. The power of the emulated sunlight ranges from 3k lux to 50k lux, which is typical during daylight. In our analysis, we consider two configuration parameters: the connection structure (whether it is more in series or parallel) and the operating point (represented by η_{voc} and described later in detail).

After this step, the design has a charger, two or more configurations depending on the number of cells, and different operating points η_{voc}. A summary of these parameters for our case is shown in Table 4.3. Next, we explain the values chosen for each parameter and evaluate their impact under the different operational stages of the charger.

4.4.4. STEP 3: ANALYZING THE PRE-CHARGING STAGE

When the system begins operating from a cold start, the supercap does not have sufficient energy to run the MPPT algorithm in the charger IC. The charger can harvest energy but in a suboptimal manner. Thus, in the pre-charging stage, the main requirement is to identify the solar cell *connection* that can charge the supercap as fast as possible.

To analyze this stage, we consider four ambient light intensities depicted with different colors in Figure 4.5: white (50 klux), light grey (20 klux), dark grey (10 klux), and black (3 klux). To leave the pre-charging stage, the supercap's voltage needs to go above the operational threshold of 1.8 V. Each connection is represented by a different shape: a square for the more *parallel* connection (2s-8p), a triangle for the *mixed* connection (4s-4p), and a circle for the more *serial* connection (8s-2p). The metrics are *normalized for each lighting condition.* The closer to the right a symbol is, the faster the charging; and the closer to the top, the better the communication.

Ideally, we want a single configuration (triangle, circle or rectangle) to deliver the best performance for all lighting conditions (all colors in the top right corner, blue region). This would indicate that a single configuration could simultaneously optimize charging and communication regardless of the intensity of sunlight. However, Figure 4.5 shows that this is not the case. There is only one light condition, 10 klux, where there exists

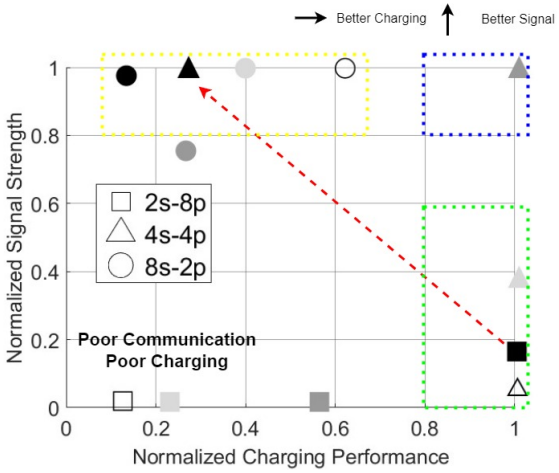


Figure 4.5: Communication and charging in the *precharging* stage. Colors denote varying light intensities: black - 3 klux; dark grey - 10 klux; light grey - 20 klux; and white - 50 klux

an optimal configuration for charging and communication, the *mixed* (triangle) setup 4s-4p.

In Figure 4.5, we identify two key regions: one (yellow rectangle) with configurations favoring communication over charging, and another (green rectangle) with the opposite trade-off. This Pareto frontier suggests that the receiver would need to switch configurations that can only optimize one task. For example, under low light (3 klux, black markers), favoring communication over charging (red arrow) would increase the charging time fourfold, from a normalized performance of 1 (*parallel* setup, black square) to 0.25 (*mixed* setup, black triangle).

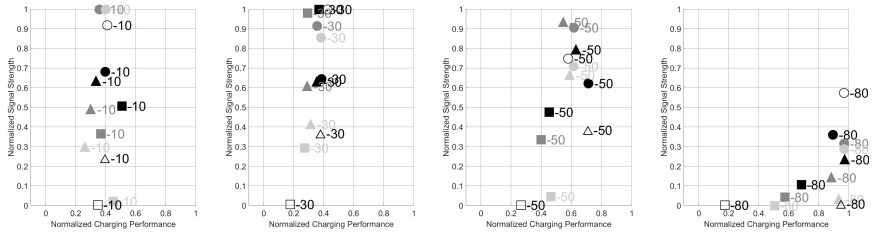
Overall, considering that in the pre-charging stage, the MPPT algorithm is not running optimally, it is better to use a connection that prioritizes charging over communication whenever possible.

4.4.5. STEP 4: ANALYZING THE CHARGING STAGE

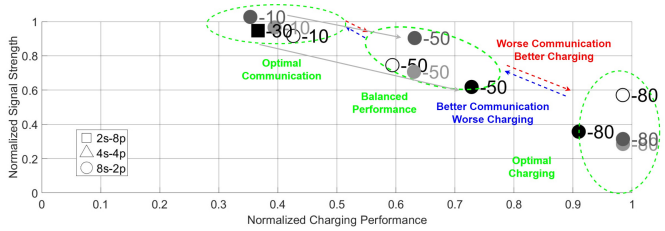
In the pre-charging stage, the analysis of solar cells includes only the connection (serial, mixed, parallel) because the harvesting algorithm could not run the operating point η_{voc}. In the charging stage, the algorithm is operational. Thus, we need a deep analysis of the critical influence of the operating point in tandem with the solar cell's connection.

The charging stage begins once the supercap's voltage exceeds 1.8 V. At this point, the MPPT algorithm is fully active. The receiver spends most of its operational time in this stage, hence, it is critical to optimize harvesting and communication. To achieve this optimization it is necessary a clear understanding of the MPPT algorithm and its parameter η_{voc}, Next, we explain how the CV algorithm changes the operating point η_{voc}, and then, present the results of our analysis under different configurations and lighting conditions.

Algorithm operation and operating point η_{voc}. The Constant Voltage (CV) algo-



(a) η_{voc} = 10% (b) η_{voc} = 30% (c) η_{voc} = 50% (d) η_{voc} = 80%



(e) Combined results

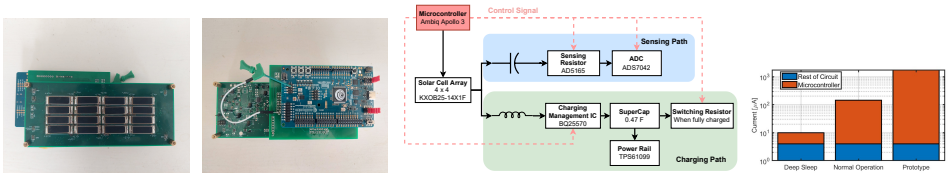
Figure 4.6: Communication and charging characteristics of the solar cell receiver during the *charging* stage. Colors denote varying light intensities: black - 3 klux; dark grey - 10 klux; light grey - 20 klux; and white - 50 klux

rithm starts by disconnecting the load to measure the *open circuit voltage* (V_{oc}). The system then regulates the charging process by maintaining the output voltage at a constant percentage of V_{oc}, represented by the variable η_{voc}. On the BQ25570, the algorithm temporarily halts the harvesting process every 16 s to sample the V_{oc} and then sets η_{voc} = 80%. While this percentage may be optimal for power output, lower values of η_{voc} could be better for communication. In this section, we assess the impact of deviating from the optimal charging point to improve communication. The notation used to describe a given connection and operating point is $Xs-Yp-\eta_{voc}$. For instance, a configuration labeled as 4s-4p-50 denotes a solar cell operating with a *mixed* connection at η_{voc} = 50%.

Charging and communication efficiency. The results of our analysis are presented in Figure 4.6. The performance of individual operating points (10%, 30%, 50%, 80%) is illustrated from Figure 4.6a to Figure 4.6d, while Figure 4.6e displays the combined Pareto frontier. Overall, our analysis provides three main results.

First, the range of the operating point η_{voc} should be between 10% and 80%. For η_{voc} =80% (Figure 4.6d), several configurations provide almost optimal charging (close to 100%) but low communication performances (mainly below 40%). As we reduce the value of η_{voc} (Figure 4.6c), the charging performance decreases (remaining below 70%) but the communication improves. For η_{voc} =30% and η_{voc} =10%, the trend continues, with communication giving a better performance than charging.

Second, similar to the pre-charging stage, there is no configuration (same connection and operating point) optimizing charging and communication simultaneously for all light intensities. At η_{voc} =30%, the best connections are parallel and serial; while at η_{voc} =50% and η_{voc} =80%, the best connections are mixed and parallel. This variabil-



(a) Receiver front (b) Receiver back (c) Receiver circuit (d) Measured receiver current

Figure 4.7: Receiver design and power consumption

ity occurs because there is a delicate balance between the type of connection, the value of the operating point, and the light intensity. The currents generated for charging and sensing need to be optimized for both tasks, while avoiding saturation, in particular at high-intensity levels.

Third, our analysis allows defining a **Pareto frontier** where one connection (serial, circles) plays the most critical role. In Figure 4.6e, we show the best Pareto frontier after combining all connections and operating points. While building a Pareto frontier, it is important to make sure that the entire boundary is populated with configurations that include all light intensities (color). In our Pareto frontier we can observe that, except for one marker, the boundary is covered completely by the serial connection (circles) with operating points ranging from 10% to 80%. *Adjusting the operating point can prioritize communication (η_{voc} =10%), charging (η_{voc} =80%), or maintain a balance (η_{voc} =50%). Our Pareto frontier can maintain an effective trade-off without requiring a significant compromise.*

The only exception for the serial configuration is when the receiver needs to optimize communication (top green ellipse) under low light conditions (3 klux). This exception is 2s-8p-30 (black square), a parallel setup with η_{voc} =30%. This exception, however, is not critical. At low light intensities, charging may be more relevant, and hence, the receiver could use the serial configuration with η_{voc} =50% to double the charging efficiency, from 36% to 72%, at the cost of reducing the communication efficiency from 95% to 60%, as depicted by the gray arrow between the black square and black circle.

Based on the charging stage analysis, our final design uses the serial connection with four operating points. Other combinations of chargers and solar cells may lead to different configurations. The analysis of connections and operating points is detailed but only needs to be done once.

4.4.6. STEP 5: OPERATION IN FULLY-CHARGED STAGE

When the supercapacitor is fully charged, the charger ensures that no further power flows into the supercapacitor to avoid overcharging it. As a result, communication cannot be carried out effectively because the system operates near the open circuit voltage. To enable communication we disconnect the supercapacitor and connect the DC branch to a fixed load to allow a flow of current in the high-frequency branch. When the supercapacitor voltage drops below a certain point, the supercapacitor is reconnected.

4.4.7. SUMMARY

Our analysis shows that it is possible to achieve energy harvesting and communication with natural light. In the precharging phase, the system focuses on charging instead of communication. This design choice is not a limiting factor because, for battery-less systems deployed outdoors, the precharging phase only takes a few seconds at the beginning of each day. It is only during that short period of time that communication is affected. During the charging phase, which is the most prevalent, the ability to reconfigure the *operating points* allows attaining a wide range of trade-offs, from near-optimal charging to near-optimal communication without penalizing either completely. During the fully-charged phase, the system can solely focus on optimizing communication. As shown later in our evaluation, these insights cover a design space that has not been tackled yet.

4.5. DESIGN OF RECONFIGURABLE RECEIVER

In the previous sections, the receiver configuration was analyzed for various controlled scenarios. In this section, we design a scheme to automatically adapt the receiver's configuration in real time depending on the ambient light intensity.

4.5.1. RECEIVER HARDWARE

The prototype and the circuit diagram are illustrated in Figure 4.7a, Figure 4.7b, and Figure 4.7c. The design employs low-power components, facilitating batteryless operation in outdoor conditions. In our prototype, the most power-intensive component is the microcontroller. We use the Ambiq Apollo 3 evaluation board, which features non-removable and non-disabling modules, thereby consuming a total of 2 mA [77]. However, the Ambiq Apollo3 microcontroller is documented to consume 140 µA under normal operation and 6 µA in deep sleep mode. Thus, with a custom design, the current power consumption of our prototype could be further reduced. The rest of the circuit draws 4 µA.

Modulation: The experiment setup is similar to section 4.4. But instead of sending a triangle wave, the transmitter continuously sends "Hello World" at 400 bps. We use binary frequency shift keying (BFSK) for signal modulation. Despite its lower data rate, FSK's inherent noise resistance proves beneficial for outdoor environments with dynamic light intensities [17]. We use a 1600 Hz signal to represent a '0' and a 2000 Hz signal to represent a '1'. We adopt a data link layer where the packet starts with an SYN symbol (01010101). The ASCII payload is preceded by an STX (Start of Text, 00000010), followed by ETX (End of Text, 00000011) and ETB (End of Transmission Block, 00010111).

Demodulation: The decoding is done as follows:

Preamble detection: A sliding window equivalent to one bit is applied to the received signal. Within this window, an FFT is applied to identify the frequency component with the largest magnitude.

Data demodulation: After a SYN byte is identified, the remaining bytes are decoded with the same process. If an ETX is identified, the received packet is recorded.

Phase correction: During preamble detection, if the decoded bit is different from the previous bit, the receiver adjusts the sliding window to synchronize to the phase of the

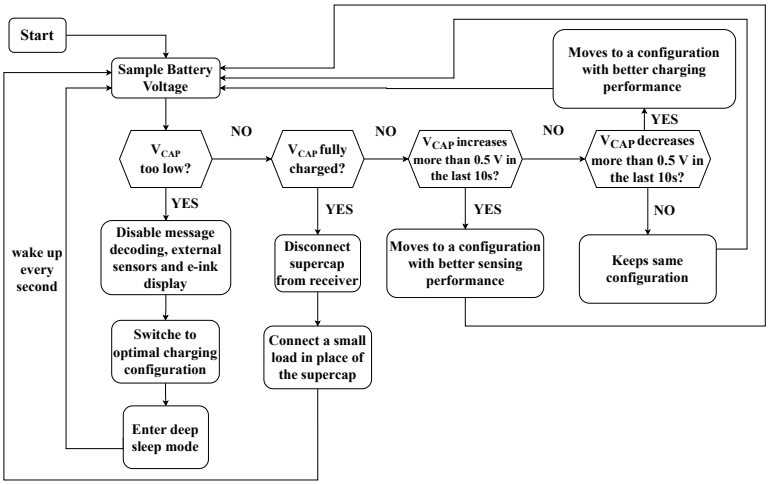
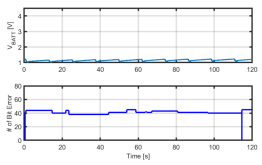
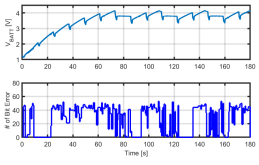


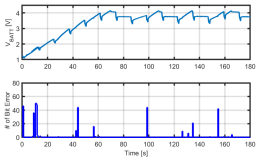
Figure 4.8: Receiver control loop



(a) SoA with 2s-8p-80 [14]
Supercap voltage: ≈1V
BER: above 40%
Packet success rate: 0%



(b) Sunlight-Duo with 4s-4p-80
Supercap voltage: ≈4V
BER: bursty
Packet success rate: 28.3%



(c) Sunlight-Duo with 8s-2p-80.
Supercap voltage: ≈4V
BER: mostly 0%
Packet success rate: 92.3%

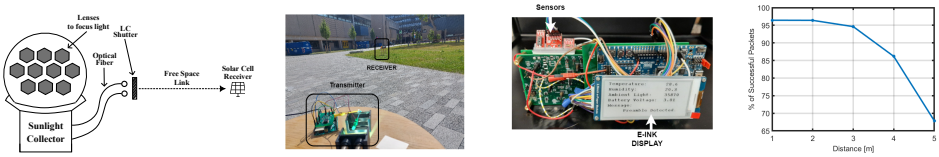
Figure 4.9: Comparing the SoA with Sunlight-Duo: supercap voltage and bit error rate with 50 klux interference. Under strong ambient light, the SoA guidelines cannot provide provide charging or communication, while Sunlight-Duo can provide both

transmitter.

FFT optimization: The CMSIS library on the Ambiq Apollo 3 facilitates FSK demodulation using efficient FFT algorithms, yet our experiments reveal significant demodulation time, leading to elevated power consumption [78]. Instead, the Goertzel algorithm offers faster decoding for messages with known transmitting frequencies [79]. To measure the decoding time, we run each algorithm 1000 times on the received data. On average, the CMSIS FFT takes 183400 cycles (1.91 ms), and the Goertzel implementation takes 27017 cycles (0.20 ms), which is almost a 10-fold improvement with the same decoding success rate. Therefore, a Goertzel algorithm is implemented on the microcontroller.

4.5.2. DYNAMIC RECONFIGURATION

Our dynamic, reconfigurable scheme employs a feedback control system to adjust the receiver's operating points and connections. Based on the insights outlined in previous sections, the feedback control design is showcased in Figure 4.8. The receiver samples



(a) System overview (b) Outdoor communication link (c) E-ink display and sensors (d) Packet success rate

Figure 4.10: Outdoor experiment setup and link range

the supercap voltage every second, which indirectly measures the ambient light intensity. Over a 10-second period, these samples are used to estimate the charging trend in order to determine if the receiver's configuration needs to be adjusted. The changes in configuration, however, can only take effect every 16 s because that is the period determined by the MPPT algorithm. *The goal of our control scheme is to prioritize communication as much as possible while maintaining a sufficient supercap voltage.* To achieve this goal, the control scheme works as follows.

Extreme cases: The supercap is drained or fully charged. *Panic mode: Voltage is lower than 1 V.* The microcontroller stops the communication process, sets the optimal charging configuration (4s-4p), and enters a deep sleep state. The receiver continues to sample the supercap voltage, but will only exit the deep sleep mode when V_{cap} is higher than 1.2 V. *Communication-only mode: Supercap is fully charged.* The supercap is disconnected, the solar cell configuration that was in place is maintained, and a shunt resistor is connected in place of the supercap to generate a current for sensing.

Receiver is in the precharging stage. *When the voltage is between* 1.2 V *and* 1.8 V, the system loops through two configurations (2s-8p, 4s-4p) every 30 s to determine the configuration that provides the highest charging efficiency. This mode is motivated by the insights obtained in section 4.4, where no fixed configuration provides the best charging performance under all light intensities in the precharging state. Therefore, the receiver periodically assesses the charging performance of the two best options, parallel and mixed.

Receiver is in the charging stage. The receiver operates in one of three configurations: 8s-2p-80 (optimal charging), 8s-2p-50 (balanced performance), or 8s-2p-30 (optimal communication). If the supercap voltage is steadily increasing, the configuration is changed to prioritize communication. If the voltage remains steady, no configuration changes are made. Conversely, a declining voltage prompts a shift towards a charging-focused configuration.

4.6. SYSTEM EVALUATION

Our system evaluation addresses two critical research questions: First, can sunlight be used simultaneously as a dual-source for energy and communication? Second, is it possible to create a stable passive link where solar cells operate as both data receivers and energy harvesters?

We first undertake an indoor assessment to show that the guidelines provided by prior SoA studies do not hold in the general case. Following this, we test our prototype outdoors under different conditions. We show that Sunlight-Duo is able to communicate

reliably outdoors, and further extend the system to facilitate bi-directional communication powered by sunlight. A potential application for such a system is smart farming, where sunlight coming into a greenhouse is used to collect local crop information from distributed batteryless sensors.

4.6.1. COMPARISON WITH THE SOA

The SoA study that is the most related to ours is the one performed by Mir et al., where an LED is used as a transmitter and solar cells simultaneously power the receiver and decode data [14]. That study suggests that a series connection holds an advantage for communication, while a parallel configuration is better for charging. *Those guidelines, however, are obtained indoors in a dark room, where the signal is transmitted by a stable LED without any interference.*

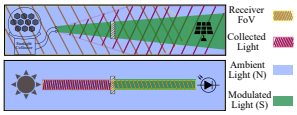
The SoA guidelines are valuable for a concrete scenario but do not hold universally. We use a controlled setup similar to the one presented in section 4.5, where we send packets, but with a key difference: To mimic a load condition representing sensors or other peripheral tasks, we use a 100˙ resistor. This resistor is connected to the supercap through an analog switch, which intermittently activates for one second every ten seconds. This setup captures a scenario where the receiver provides power for decoding and other sensing or computational tasks (intermittent load).

The transmitter (LC) is placed 1 m from the receiver. The intensity of the signal between the on and off states at the receiver is 1400 lux, strong enough to decode data with the SoA receiver. However, when we turn on the sunlight emulator, the ambient light introduces an interference of 50k lux at the receiver. We evaluate three configurations. The first configuration, suggested by the SoA [14], sets η_{voc}=80% and toggles between parallel (2s-8p-80) and serial (8s-2p-80) connections, contingent on whether the battery voltage (V_{batt}) is below or above 2.6V. The other two configurations are based on our analysis: mixed (4s-4p-80) and serial (8s-2p-80). Both configurations perform well in terms of charging, but the serial connection (8s-2p-80) outperforms the mixed one (4s-4p-80) in terms of communication.

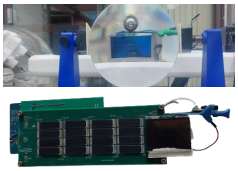
Results from Figure 4.9 reveal that the SoA configuration fails in both, energy harvesting and packet decoding due to high BER, especially under strong light conditions where its efficiency plummets to 20% for charging and 0% for communication, as shown in Figure 4.9a. This leads to insufficient power for load support and a nearly random BER (50%). Conversely, our near-optimal configurations (Figure 4.9b and Figure 4.9c) successfully charge the supercapacitor across all conditions. Specifically, the series configuration (8s-2p-80) achieves over 90% packet success rate, outperforming the mixed configuration (4s-4p-80) even amid strong ambient light. Temporary bit error spikes, due to the voltage sampling performed by the algorithm every 16 seconds, are quickly mitigated, allowing for successful packet reception. These observations underscore the importance of a thorough analysis. Our multi-step optimization shows that even with strong ambient light, the communication and harvesting capabilities of the solar cells can be preserved.

4.6.2. EXPERIMENT SETUP IN OUTDOOR EVALUATION

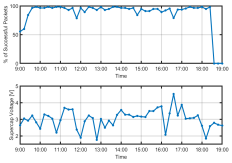
In the next phase, we test our system outdoors.



(a) Effect of FoV at the transmitter and receiver. Top: Sunlight-Duo. Bottom: System with PDs [17, 41]



(b) Top: Transmitter. Bottom: Receiver



(c) Simultaneous communication (downlink) and harvesting. Top: Packet Sucess Rate. Bottom: Supercap Voltage

Figure 4.11: System overview and experiment results

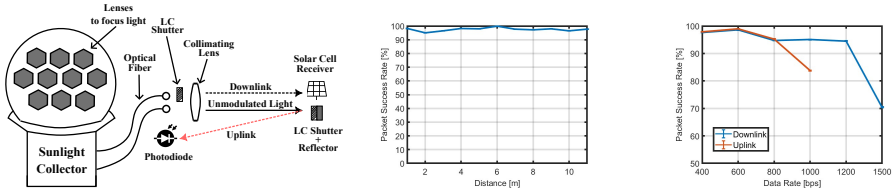
Transmitter: In the outdoor experiment, we use a sunlight collector from Himawari, as shown in Figure 4.2c. Commercial sunlight collectors are designed to bring natural light indoors to windowless areas, but we utilize them outdoors. A sunlight collector has two functions: *collection* and *tracking*. In *collection*, the device uses lenses to gather sunlight and channel it into optical fibers, which guide the light to the desired locations. This process does not consume any power. In *tracking*, since the sun changes its location throughout the day, the lenses rotate to point toward the sun. The tracking consumes between 1 W and 2 W when the lenses are moving. We place an LC shutter in front of the optical fiber output to modulate the collected light (as seen in Figure 4.10b). The transmitter continuously sends "Hello World" packets at a data rate of 400 bps, unless stated otherwise.

Receiver: Thanks to the design of our low-power receiver, as described in section 4.5, the decoding of data is only powered by the on-board solar cell array. In addition, the receiver has three sensors: a temperature sensor (TMP102), a humidity sensor (HIH-4030), an ambient light sensor (TEMT6000); and an e-ink display DEBO EPA 2.9, which are also powered by the receiver. The e-ink display shows the measurements obtained from the sensors. An image of the receiver is shown in Figure 4.10. *Note that our receiver obtains light from the sun and the beam coming from the collector. Both components contribute to charging, but only the collector's beam provides the signal, the light coming directly from the sun is noise.*

4.6.3. LINK RANGE AND RELIABILITY

Link range. In the first part of the experiment, the sunlight collector is placed on the ground at a fixed location, while we move the receiver to different distances. At each location, we collect the packets for a period of 30 seconds and repeat this experiment three times. At the same time, the receiver takes measurements of ambient light, temperature and humidity, and writes it to the e-ink display every 20 seconds. We also measure the average supercap voltage during the 30 second window and record it throughout the experiment. An overview of the system is provided in Figure 4.10a.

The packet reception rate is shown in Figure 4.10d. The experiment was conducted on a clear day with sunlight intensity around 60 klux. As shown, the packet success rate exceeds 85% at a distance of up to 4 m. The packet success rate does not reach 100% because communication is interrupted every 16 s when the MPPT algorithm samples the open circuit voltage. The communication distance achieved in this setup is smaller



(a) System overview

(b) Packet success rate over distance

(c) Packet success rate at 11 m

Figure 4.12: System and evaluation results of a bidirectional link

than previous passive systems using sunlight and PDs [41]. In the next subsection, we explain how we improve the range, but first let us use Figure 4.11a to describe why we achieve a shorter range than the SoA.

Communication performance hinges on three factors: signal intensity (S), interference (N), and field of view (FoV). For extended range, high SNR and narrow FoV are essential. Earlier systems used mirror-like surfaces for sunlight reflection, achieving collimated patterns with less attenuation and stronger signals (large S). However, the optical fibers of sunlight collectors have a 58° FoV, which yields a broader pattern and faster signal degradation (smaller S). To achieve more collimated beams, we later show the improved range by placing lenses on the collector's beams. Another important point is that the SoA uses PDs with narrow FoVs to reduce interference (small N). Solar cells have, inherently, a wide FoV. This wide-angle cannot be reduced without affecting the energy harvesting performance. Hence, solar cell receivers face greater noise challenges (larger N).

Reliability. To test reliability, we place the receiver at a distance of 2 m from the transmitter. Daytime conditions change based on the season and specific location, in our setup daylight was obtained from 9 am to 7 pm, we recorded the link's measurements every 10 minutes for 30 seconds. During this time, the receiver powers the sensors, e-ink display and sends backscattered data. The results, in Figure 4.11c, show that throughout the day, a reliable link is established despite the changing environmental conditions. It can also be observed that the supercap voltage fluctuates throughout the day, as a result of the dynamic reconfiguration of the receiver. However, the receiver is able to maintain a sufficient voltage to remain as a positive-energy link.

4.6.4. BI-DIRECTIONAL LINK AND LONGER RANGE

Bi-directional link. In our star topology, the sunlight collector acts as a hub, and sensors as nodes. Until now we have only tested the downlink, to send commands from the hub to nodes. To send sensing data to the hub (uplink), we exploit the fact that the sunlight collector provides two optical fiber bundles. This setup, depicted in Figure 4.12a, marks the first use of sunlight for backscattering. One optical bundle is used for the downlink and the other for the uplink. The uplink employs *unmodulated* light, backscattered by a mirror at the receiver to transmit sensor data back to the transmitter, where a photosensor and processor decode the uplink data.

Extended range. In the SoA, the range is extended by adding a lens to the receiver,

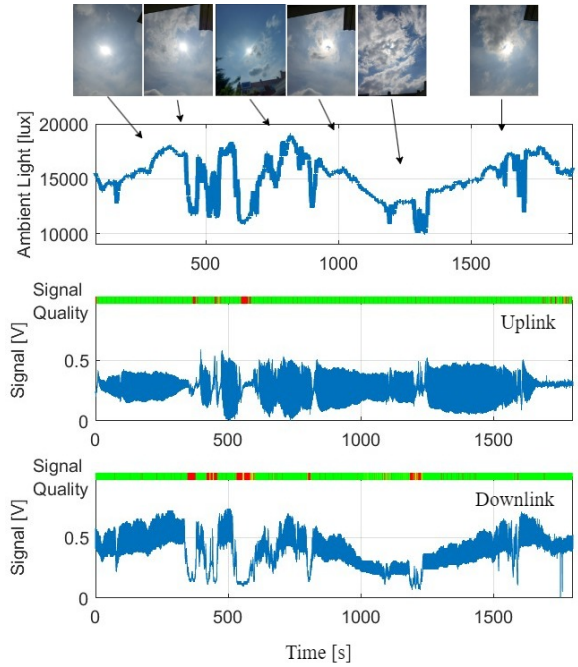


Figure 4.13: Link quality in a 30 minute window. Top: ambient light. Middle: uplink signal. Bottom: downlink signal

but this approach cannot be applied to solar cells without disrupting their energy harvesting capabilities. Instead, following basic optical principles, a lens is placed in front of the output of the sunlight collector. By incorporating a lens, we generate a narrow beam, which is roughly 120 mm when measured at 11 m, corresponding to a beam angle below 1°. In this way, we significantly reduce the signal dispersion as it travels over distance.

Results. The results for the communication range of the downlink are shown in Figure 4.12b. In our test area, we could only test up to a distance of 11 m, but it can be seen that for a data rate of 400 bps, the link is strong and a longer range can be achieved thanks to the added lens. To take advantage of the higher SNR, we increase the data rate at 11 m, which is shown in Figure 4.12c. It can be seen that for the downlink, a packet success rate of over 90% can be achieved for a data rate of up to 1000 bps. For the uplink, a packet success rate of over 90% can be achieved for a data rate of up to 800 bps. The uplink data rate is lower than the downlink's because the light has to travel double the distance, but they achieve a reliable bi-directional link at 11 m.

4.6.5. STABILITY OF BI-DIRECTIONAL LINK

We now assess the stability of a bi-directional communication link under fluctuating ambient light, particularly with intermittent sun blockage by clouds. We used a DFROBOT SEN0390 ambient light sensor alongside our receiver to track light intensity every second [80]. During the evaluation, the sunlight intensity ranged between 10 klux and 18klux, which are not high values because during clear days, sunlight can provide intensities

above 100 klux. In this experiment, we maintain the same setup as in the previous section, a 11 m bi-directional link, but over a 30-minute period.

The results, in Figure 4.13, depict the status of both uplink and downlink. The uplink showcases the AC signal post-filtering, thus excluding DC fluctuations. A color-coded system denotes the packet success rate within a one-second window: green represents a success rate over 80%, yellow between 60% and 80%, and red below 60%. For reference, we include photographs of the sky during the time. The results reveal similar stability for both uplink and downlink, although the downlink quality, affected by the double-distance travel, is slightly poorer. Total sun obstruction by clouds interrupts communication, yet during clear or moderately cloudy conditions, with the sun still visible, the link quality remains high, allowing effective communication. Over a 30-minute window, the uplink and downlink packet error rates are 90.7% and 77.8%, respectively.

4.6.6. DISCUSSION

Our work provides the first link that uses sunlight for communication and power, which opens several opportunities for improvement.

Range, data rate, and line of sight. An important parameter limiting the range and data rate is the slow switching speed of inexpensive liquid crystals. As shown in Figure 4.2e, a full transition between the on and off states takes around 3 ms. Modulations faster than that reduce the signal-to-noise ratio because the LC cannot reach its plateau. And a reduced SNR limits either the range or data rate. Besides LCs, one alternative is to use micro-mirror devices (DMDs), which can attain several 10 kbps [68], but the system would be more complex. Another general shortcoming of light communication, compared to RF, is that without a line-of-sight (LOS), the link degrades rapidly. In smart farming, small solar panels powering sensors are placed on bars to get LOS with the sun, but in applications without LOS the communication would be harder. To address this issue, the VLC community is investigating Intelligent Reflective Surfaces. That line of work would also benefit our system.

Comparison with alternative technologies. Sunlight-Duo leverages an abundant and sustainable resource: sunlight. However, its operation is constrained to daylight hours. While solar cells can power LEDs for active-VLC communication, this approach necessitates the use of batteries for energy storage. Moreover, converting sunlight to energy via solar cells and then converting that energy back to light through LEDs introduces inefficiencies that can be avoided by using sunlight directly, thereby eliminating the intermediary conversions. The lumen-to-watt efficiency of solar cells is 25%, and the watt-to-lumen efficiency of LEDs is 10 to 30% (around 95% of energy is lost). PassiveVLC achieves sub-μJ per bit [42], while LEDs use 30x more energy per bit [81]. Another option is to use low-power radio systems, which are a mature technology providing longer ranges and higher data rates, but the aim of using light is to use a part of the spectrum that is free and not crowded. The best use of Sunlight-Duo is to exploit it during daylight and complement it with other technologies at night or during cloudy days. Cost and deployment are also important considerations. The sunlight collector we use costs around 4.5k USD and it is bulky because it is designed to be placed on building roofs. Considering smart farming, a cheaper alternative would be to deploy a wider array of permanent static lenses on the already transparent roofs of greenhouses, minimizing

the cost and complexity of the hub. Compared to low-power RF systems, passive VLC exploits a free and open spectrum. While RF surpasses passive VLC in range, data rate, and energy efficiency, RF is well-established, whereas passive VLC is emerging. Passive VLC also eliminates double-energy conversion, offering better performance with 6 bits-per-µJ compared to lasers' 4 bits-per-µJ, without stringent regulations for eye safety and alignment. *Overall, it is important to note that our work does not aim at replacing existing technologies, but rather at presenting a complementary and novel research direction.*

4.7. CONCLUSION

This study investigates the use of sunlight as a dual-purpose medium for energy harvesting and communication. We identify and address the inherent challenges of this new type of link, especially the necessity to dynamically adjust solar cell parameters to optimize energy capture and communication effectiveness. Informed by these insights, we built a prototype that harnessed sunlight for bi-directional communication while simultaneously gathering energy. The system demonstrated a range of several meters throughout the day with a data rate of 1 kbps. To the authors' best knowledge, this is the first design that develops a complete communication and harvesting system relying only on sunlight.

5

CONCLUSION

The increasing reliance on IoT devices has significantly strained existing wireless communication infrastructure. VLC offers a compelling alternative by leveraging the unlicensed spectrum of light, thus bypassing the regulatory and interference challenges associated with RF communication. Despite its potential, VLC encounters several challenges that need to be addressed to ensure its viability. For active VLC, to be energy efficient, these systems must adapt light sources primarily intended for illumination to also function effectively as communication mediums. This dual-purpose use introduces limited ability to overcome blockage because its coverage can be easily obstructed by furniture, walls, and other obstacles. For passive VLC, optical modulators are used to encode data into natural light. However, these modulators are slow, limiting the effectiveness of passive VLC systems. Additionally, the variability in natural light sources, such as sunlight, introduces noise and reliability concerns. Addressing these challenges requires innovative solutions to maintain signal integrity and ensure consistent performance in diverse environments.

5.1. DISSERTATION WORK

To address these challenges, this thesis proposes several solutions to improve the efficiency and applicability of VLC systems.

ACTIVE VLC SYSTEMS

In this part of the dissertation, we address the research question: *"How can Intelligent Reflecting Surface (IRS) be tailored to overcome Non-Line-of-Sight (NLOS) communication and sensing challenges in active VLC?"*. We design the Dual-Mirrors platform, which uses both passive and active IRS to extend VLC coverage. Passive IRS divides light into multiple beams to cover various spots, while active IRS dynamically adjusts beam direction to maintain connectivity in mobile (with repeated and predictable patterns) and changing environments. This approach allows us to redirect light beyond the line of sight, effectively addressing VLC limitations caused by obstructions like walls and furni-

ture. We also integrate sensing capabilities using retro-reflectors to detect human presence, either worn by individuals or placed strategically in the target scenario. This allows us to sense movement and presence in areas not directly visible to the light source, extending the sensing range of VLC systems. Through practical testing, we demonstrate that our platform can provide communication coverage in NLOS areas. For instance, we show how a single light bulb combined with reflective surfaces can facilitate both communication and sensing in an apartment-sized area. Our findings confirm that IRS can significantly enhance the functionality and applicability of VLC systems, providing a practical solution to the inherent challenges when light is used for both communication and illumination.

PASSIVE VLC SYSTEMS

In the second part of the dissertation, we address the research questions: *"How can the transmitter design in passive VLC systems be optimized to increase data transmission rates using ambient light?"* and *"How can passive VLC receivers optimize the system's overall performance and energy efficiency?"*. To do this, we explore various approaches to enhance the efficiency and applicability of passive VLC components.

In our first contribution to passive VLC systems, we focus on improving the transmitter design to boost communication efficiency. We introduce a novel approach using DMDs as transmitters, achieving data rates up to 30 times faster than conventional methods. By integrating DMD technology, we demonstrate how VLC systems can more effectively utilize ambient light. Additionally, we develop an optical model to understand the fundamental limits and opportunities of ambient light communication. Our model reveals that maintaining directional light patterns is crucial for passive links, and DMDs, with their specular reflective properties, are ideally suited for this purpose. We demonstrate that DMDs can maintain high data rates even in the presence of ambient light noise, making them a robust solution for real-world applications. Through this research, we learned that optimizing passive VLC systems involves both enhancing transmitter designs and understanding the optical properties of the system components. Our findings provide a pathway for future developments in passive VLC technology, ensuring that ambient light can be harnessed more efficiently for communication purposes.

We then shift our focus to the receiver side of the passive VLC system. Our system, named Sunlight-Duo, explores methods to use solar cells for both communication and energy harvesting. We address the fundamental trade-off between energy harvesting and communication by analyzing various solar cell configurations suitable for embedded IoT devices. Our thorough analysis reveals that solar cells can indeed be used for both purposes, but the receiver must dynamically adjust key solar cell parameters on the fly. The prototype we developed includes a self-powered receiver capable of maintaining a bi-directional link for up to 11 meters, with data rates of 1200 bps for downlink and 800 bps for uplink. Additionally, our system can maintain a stable link over a distance of 2 meters throughout the day, even under varying sunlight conditions. From this work, we learned that optimizing VLC systems to efficiently utilize ambient light involves balancing energy harvesting and data communication. Our findings confirm that with dynamic reconfiguration, VLC systems can achieve stable communication and efficient energy use, even under varying light conditions.

LESSONS LEARNED

By addressing different aspects of VLC systems, our research offers practical solutions to the challenges faced by both active and passive VLC systems.

- **The Importance of Integrated Design**: Efficient VLC systems require careful consideration of all components (transmitters, receivers, and the environment) as an integrated whole. This is particularly evident in the Dual-Mirrors platform, where external passive and active surfaces help transmitters extend coverage to NLOS areas. Similarly, our work on passive VLC highlights opportunities to improve efficiency and performance in various components, such as transmitters and receivers, to make better use of the energy from sunlight. Effective VLC designs necessitate a holistic approach that considers the interplay of all system elements.

- **Analytical Foundation for Robust Design**: Having a strong analytical foundation in VLC system design is important. While ad-hoc designs may yield initial results, a thorough understanding of the underlying principles (e.g., optical propagation, modulation schemes, energy harvesting mechanisms) is essential for creating robust, efficient, and scalable systems. Our work with the light propagation analysis for ambient light communication and the solar cell configuration analysis for the Sunlight-Duo system exemplifies the value of theoretical insights in guiding practical implementation.

- **Synergy of Disciplines**: The development of VLC technology anchors at the intersection of embedded systems and optical engineering. Successful implementations, like the Dual-Mirrors platform, demand a strong understanding of both embedded control systems and the behavior of optical components. Future VLC advancements will rely on closer collaboration between these traditionally distinct fields, fostering a multidisciplinary approach that combines expertise in hardware, software, and optics.

5.2. FUTURE WORK

VLC is still in its early stages, leaving many open research questions. For future work, further research is needed to fully realize the capabilities of VLC systems.

- **Active VLC: IRS in an Integrated Smart Environment.** In our work with Dual-Mirrors, we explored the use of IRS to extend active VLC coverage to NLOS areas. Future work can build upon these demonstrations to investigate how IRS can be leveraged to dynamically create diverse lighting environments tailored for specific tasks and activities. For example, these surfaces could redirect and concentrate light onto work areas that require focused illumination, while simultaneously dimming or redirecting light away from areas that need less brightness. This concept can be extended to the realm of communication as well. IRS could be used to create or reconfigure focused communication zones within a larger space, catering to different needs and activities. For example, during meetings, IRS could establish a concentrated communication zone around a conference table, ensuring optimal signal strength and minimizing interference for participants. By dynamically

shaping the light field for both illumination and communication, IRS-enhanced VLC systems can create highly flexible and adaptable environments that cater to the evolving needs of users and applications.

- **Passive VLC: From Point-to-Point Communication to Network Infrastructure.** Passive VLC systems primarily operate on one-to-one (point-to-point) communication, effectively demonstrating its potential in terms of range and speed. However, for passive VLC systems to be viable in real-world applications, it needs to transition beyond this model, as point-to-point configurations limit the system's scalability, adaptability, and application range. Future work could focus on developing a comprehensive network infrastructure for passive VLC. This transition introduces challenges, such as increasing the reliability of the link as sunlight varies and facilitating seamless connections as devices move. Addressing these challenges will enable seamless communication experiences, transforming passive VLC into a more well-rounded communication method capable of supporting various applications in dynamic environments.

Recent advancements have shown great potential of VLC, but they also highlight the need for a multidisciplinary approach involving embedded systems, optics, and microelectronics to address current limitations in data rate, power consumption, and scalability. By pursuing these research directions, we can improve the maturity of VLC technologies, overcome existing challenges, and expand their applications, ultimately making VLC a viable and efficient alternative to conventional RF communication methods.

ACKNOWLEDGMENTS

I would like to thank Marco, first and foremost, for being an inspiring role model for me as a researcher. As a mentor, he has consistently encouraged my ideas, even in their early, underdeveloped stages. Marco provides me with the academic freedom to explore independently, while also being someone I can rely on for honest and constructive feedback. Throughout my PhD journey, Marco has shown immense patience and unwavering support as I've worked to develop both my academic and personal skills. I am sincerely grateful to him for everything.

I would like to thank my co-promoter, Qing, for guiding me through the more practical, yet equally important, aspects of academia, and for consistently (and rightly) emphasizing the value of networking and building connections. Qing has always been available when I needed advice, and I am truly grateful for his support. I would like to thank the other faculty members of the group — I appreciate the opportunity to learn from their diverse research perspectives over the years. I would especially like to thank Koen and Fernando for fostering a group culture that values both academic excellence and personal well-being.

I would like to thank my committee members, Prof. dr. Langendoen, Prof. dr. Markham, Prof. dr. Boano, and Prof. dr. Flores, for serving on my PhD committee and providing valuable comments and feedback on my dissertation.

I would like to extend my gratitude to the master's students I had the pleasure of working with: Ricardo Ampudia Hernandez, Oxana Oosterless, Lucan de Groot, Jasper de Zoete, Jasper Jonk, Jasper-Jan Lut, Floor Joosen, and Zhanhe Lou. I've learned much from working with you.

I would like to thank Eric for always being there in 2023. Eric taught me, through example, that it's possible to remain true to oneself, regardless of how strange others may perceive you. This is a compliment. I would like to thank Miguel for his ability to stay calm in any situation and for introducing me to the essence of true Peruvian life. I would like to thank Naram for his relentless efforts to offer advice to someone older than him. I would like to thank Dimitra for the enjoyable conversations about academic careers, life in Delft, and many other topics. I would like to thank others in the group—Girish, Gabe, Adrian, Vito, Belma, Fatih, Mikhail, Suryansh, Kees, Mengyuan, Anup, Jasper, Jorik, Lingyu, James, Mingkun, Ran, Xiaozhe—and our wonderful secretaries, Minaksie, Kim, and Pam, without whom nothing could ever be done in this group. If I've missed anyone, it's probably not because I'm already seven days late in submitting my thesis.

I would like to thank Ciaran for patiently answering all my random questions without ever questioning why I ask them, and Jason for providing the most sensible advice I never followed when it comes to social interactions.

I would like to thank Charles' family for spending time with us when we are in Toronto and abroad. Charles, it's difficult to pinpoint something I am thankful for when it comes to the person most special to me. I thank you for being you, for making me be with

someone who is, and will always be, a better person than I am. You are always Pebble's preferred human. You hold yourself to the highest moral standards and always try to be kind and fair to others. You are always confident in who you are and never compromise or change to please others. You have moved across the world for me, but never once made it seem like a sacrifice. I thank you for all our treasured memories, and for being someone who I can trust to share my dreams with.

Growing up, my mom and dad always told me that their only wish was for me to be happy. I once thought happiness was overrated, and I'm still not entirely convinced otherwise, but even so.. maybe they have a point. I thank my parents for their understanding and acceptance as my worldview developed to be different from theirs. Last but not least, I am grateful for what they didn't say—for never telling me what I should or shouldn't do because I'm a girl, and for never suggesting that there was anything I couldn't achieve.

Lastly, I want to thank Pebbles, who is sitting ~~on top of my keyboard between me and my laptop~~ right next to me as I type these words.

Talia
Auckland, October 2024

BIBLIOGRAPHY

[1] Lifang Feng, Rose Qingyang Hu, Jianping Wang, Peng Xu, and Yi Qian. Applying VLC in 5G Networks: Architectures and Key Technologies. *IEEE Network*, 30(6):77–83, 2016.

[2] National Telecommunications and Information Administration (NTIA). United States Frequency Allocations: The Radio Spectrum Chart, January 2016.

[3] Dobroslav Tsonev, Hyunchae Chun, Sujan Rajbhandari, Jonathan J. D. McKendry, Stefan Videv, Erdan Gu, Mohsin Haji, Scott Watson, Anthony E. Kelly, Grahame Faulkner, Martin D. Dawson, Harald Haas, and Dominic O'Brien. A 3-Gb/s Single-LED OFDM-Based Wireless VLC Link Using a Gallium Nitride μLED. *IEEE Photonics Technology Letters*, 26(7):637–640, 2014.

[4] Chien-Hung Yeh, Yen-Liang Liu, and Chi-Wai Chow. Real-time white-light phosphor-LED visible light communication (VLC) with compact size. *Opt. Express*, 21(22):26192–26197, Nov 2013.

[5] Dobroslav Tsonev, Stefan Videv, and Harald Haas. Towards a 100 Gb/s visible light wireless access network. *Opt. Express*, 23(2):1627–1637, Jan 2015.

[6] Harald Haas, Liang Yin, Yunlu Wang, and Cheng Chen. What is lifi? *Journal of Lightwave Technology*, 2016.

[7] M. Najafi and R. Schober. Intelligent Reflecting Surfaces for Free Space Optical Communications. In *IEEE GLOBECOM*, 2019.

[8] Amr M. Abdelhady, Ahmed K. Sultan Salem, Osama Amin, Basem Shihada, and Mohamed-Slim Alouini. Visible Light Communications via Intelligent Reflecting Surfaces: Metasurfaces vs Mirror Arrays. *IEEE Open Journal of the Communications Society*, 2021.

[9] Shiwei Fang, Ron Alterovitz, and Shahriar Nirjon. Non-Line-of-Sight Around the Corner Human Presence Detection Using Commodity WiFi Devices. In *Proceedings of the 1st ACM International Workshop on Device-Free Human Sensing*, 2019.

[10] Youwei Zeng, Dan Wu, Jie Xiong, Jinyi Liu, Zhaopeng Liu, and Daqing Zhang. MultiSense: Enabling Multi-Person Respiration Sensing with Commodity WiFi. *ACM IMWUT*, 2020.

[11] Asif Hanif, Mazher Iqbal, and Farasat Munir. WiSpy: Through-Wall Movement Sensing and Person Counting Using Commodity WiFi Signals. In *IEEE SENSORS*, 2018.

[12] F Bryant. Snell's law of refraction. *Physics Bulletin*, 9(12):317, 1958.

[13] Osama Zwaid Aletri, Mohammed T. Alresheedi, and Jaafar M. H. Elmirghani. Infrared Uplink Design for Visible Light Communication (VLC) Systems with Beam Steering. In *IEEE CSE and EUC*.

[14] Muhammad Sarmad Mir, Borja Genoves Guzman, Ambuj Varshney, and Domenico Giustiniano. Passivelifi: Rethinking lifi for low-power and long range rf backscatter. ACM MobiCom, 2021.

[15] Giuseppe Sellaroli. An algorithm to reconstruct convex polyhedra from their face normals and areas, 2017.

[16] Roger Fletcher. *Practical methods of optimization.* John Wiley & Sons, 2000.

[17] Rens Bloom, Marco Zúñiga Zamalloa, and Chaitra Pai. Luxlink: Creating a wireless link from ambient light. In *Proceedings of the 17th Conference on Embedded Networked Sensor Systems*, SenSys '19, page 166–178, New York, NY, USA, 2019. Association for Computing Machinery.

[18] Sylvester Aboagye, Alain R. Ndjiongue, Telex M. N. Ngatched, Octavia A. Dobre, and H. Vincent Poor. RIS-Assisted Visible Light Communication Systems: A Tutorial. *IEEE Communications Surveys Tutorials*, 2023.

[19] Alain R. Ndjiongue, Telex M. N. Ngatched, Octavia A. Dobre, and Harald Haas. Design of a Power Amplifying-RIS for Free-Space Optical Communication Systems. *IEEE Wireless Communications*, 2021.

[20] Shiyuan Sun, Fang Yang, Jian Song, and Zhu Han. Optimization on Multiuser Physical Layer Security of Intelligent Reflecting Surface-Aided VLC. *IEEE Wireless Communications Letters*, 2022.

[21] Danya A. Saifaldeen, Bekir S. Ciftler, Mohamed M. Abdallah, and Khalid A. Qaraqe. DRL-Based IRS-Assisted Secure Visible Light Communications. *IEEE Photonics Journal*, 2022.

[22] Sifat Ibne Mushfique, Ahmad Alsharoa, and Murat Yuksel. MirrorVLC: Optimal Mirror Placement for Multielement VLC Networks. *IEEE Transactions on Wireless Communications*, 2022.

[23] Alain Richard Ndjiongue, Telex. M. N. Ngatched, Octavia A. Dobre, and Harald Haas. Double-Sided Beamforming in OWC Systems Using Omni-Digital Reconfigurable Intelligent Surfaces, 2022.

[24] Sylvester Aboagye, Telex M. N. Ngatched, Octavia A. Dobre, and Alain R. Ndjiongue. Intelligent Reflecting Surface-Aided Indoor Visible Light Communication Systems. *IEEE Communications Letters*, 2021.

[25] Binghao Cao, Ming Chen, Zhaohui Yang, Minghui Zhang, Jingwen Zhao, and Mingzhe Chen. Reflecting the Light: Energy Efficient Visible Light Communication with Reconfigurable Intelligent Surface. In *2020 IEEE 92nd Vehicular Technology Conference (VTC2020-Fall)*, 2020.

[26] Shiyuan Sun, Weidong Mei, Fang Yang, Nan An, Jian Song, and Rui Zhang. Optical Intelligent Reflecting Surface Assisted MIMO VLC: Channel Modeling and Capacity Characterization. *IEEE Transactions on Wireless Communications*, 2023.

[27] Amr M. Abdelhady, Osama Amin, Ahmed K. Sultan Salem, Mohamed-Slim Alouini, and Basem Shihada. Channel Characterization of IRS-Based Visible Light Communication Systems. *IEEE Transactions on Communications*, 2022.

[28] Shiyuan Sun, Fang Yang, and Jian Song. Sum Rate Maximization for Intelligent Reflecting Surface-Aided Visible Light Communications. *IEEE Communications Letters*, 2021.

[29] Shiyuan Sun, Fang Yang, Jian Song, and Zhu Han. Joint Resource Management for Intelligent Reflecting Surface–Aided Visible Light Communications. *IEEE Transactions on Wireless Communications*, 2022.

[30] Alain R. Ndjiongue, Telex M. N. Ngatched, Octavia A. Dobre, and Harald Haas. Re-Configurable Intelligent Surface-Based VLC Receivers Using Tunable Liquid-Crystals: The Concept. *Journal of Lightwave Technology*, 2021.

[31] Susan Chan, Ryan E. Warburton, Genevieve Gariepy, Jonathan Leach, and Daniele Faccio. Non-line-of-sight tracking of people at long range. *Opt. Express*, 2017.

[32] Jiangtao Li, Angli Liu, Guobin Shen, Liqun Li, Chao Sun, and Feng Zhao. *Retro-VLC*: Enabling battery-free duplex visible light communication for mobile and iot applications. In Justin Manweiler and Romit Roy Choudhury, editors, *Proceedings of the 16th International Workshop on Mobile Computing Systems and Applications, HotMobile 2015, Santa Fe, NM, USA, February 12-13, 2015*, pages 21–26. ACM, 2015.

[33] Dingtian Zhang, Jung Wook Park, Yang Zhang, Yuhui Zhao, Yiyang Wang, Yunzhi Li, Tanvi Bhagwat, Wen-Fang Chou, Xiaojia Jia, Bernard Kippelen, Canek Fuentes-Hernandez, Thad Starner, and Gregory D. Abowd. Optosense: Towards ubiquitous self-powered ambient light sensing surfaces. *ACM IMWUT*, 2020.

[34] M. S. Amjad and F. Dressler. Using Visible Light for Joint Communications and Vibration Sensing in Industrial IoT Applications. In *IEEE ICC*, 2021.

[35] Lina Shi, Bastien Béchadergue, Luc Chassagne, and Hongyu Guan. Joint Visible Light Sensing and Communication Using m-CAP Modulation. *IEEE Transactions on Broadcasting*, 2023.

[36] Cisco. Cisco annual internet report - cisco annual internet report (2018–2023) white paper, 2020. https://www.cisco.com/c/en/us/solutions/collateral/executive-perspectives/annual-internet-report/white-paper-c11-741490.html.

[37] Nils Ole Tippenhauer, Domenico Giustiniano, and Stefan Mangold. Toys communicating with leds: Enabling toy cars interaction. In *2012 IEEE Consumer Communications and Networking Conference (CCNC)*, pages 48–49, 2012.

[38] Maury Wright. Philips lighting deploys led-based indoor positioning in carrefou, 2015. https://goo.gl/a0tGIj.

[39] PureLiFi. http://purelifi.com/, 2021.

[40] Purui Wang, Lilei Feng, Guojun Chen, Chenren Xu, Yue Wu, Kenuo Xu, Guobin Shen, Kuntai Du, Gang Huang, and Xuanzhe Liu. Renovating road signs for infrastructure-to-vehicle networking: A visible light backscatter communication and networking approach. In *Proceedings of the 26th Annual International Conference on Mobile Computing and Networking*, MobiCom '20, New York, NY, USA, 2020. Association for Computing Machinery.

[41] Seyed Keyarash Ghiasi, Marco A. Zúñiga Zamalloa, and Koen Langendoen. A principled design for passive light communication. In *Proceedings of the 27th Annual International Conference on Mobile Computing and Networking*, MobiCom '21, page 121–133, New York, NY, USA, 2021. Association for Computing Machinery.

[42] Xieyang Xu, Yang Shen, Junrui Yang, Chenren Xu, Guobin Shen, Guojun Chen, and Yunzhe Ni. PassiveVLC: Enabling practical visible light backscatter communication for battery-free iot applications. In *Proceedings of the 23rd Annual International Conference on Mobile Computing and Networking*, MobiCom '17, page 180–192, New York, NY, USA, 2017. Association for Computing Machinery.

[43] Yue Wu, Purui Wang, Kenuo Xu, Lilei Feng, and Chenren Xu. Turboboosting visible light backscatter communication. In *Proceedings of the Annual Conference of the ACM Special Interest Group on Data Communication on the Applications, Technologies, Architectures, and Protocols for Computer Communication*, SIGCOMM '20, page 186–197, New York, NY, USA, 2020. Association for Computing Machinery.

[44] Zixiong Wang, Dobroslav Tsonev, Stefan Videv, and Harald Haas. On the design of a solar-panel receiver for optical wireless communications with simultaneous energy harvesting. *IEEE Journal on Selected Areas in Communications*, 33(8):1612–1623, 2015.

[45] A.M. Ramirez-Aguilera, J.M. Luna-Rivera, V. Guerra, J. Rabadan, R. Perez-Jimenez, and F.J. Lopez-Hernandez. A review of indoor channel modeling techniques for visible light communications. In *2018 IEEE 10th Latin-American Conference on Communications (LATINCOM)*, pages 1–6, 2018.

[46] Yury Petrov. Optometrika, howpublished = `https://github.com/caiuspetronius/optometrika`, 2014.

[47] Bui Tuong Phong. Illumination for computer generated pictures. *Commun. ACM*, 18(6):311–317, June 1975.

[48] Rens Bloom, Marco Zuniga, Qing Wang, and Domenico Giustiniano. Tweeting with sunlight: Encoding data on mobile objects. In *IEEE INFOCOM 2019 - IEEE Conference on Computer Communications*, pages 1324–1332, 2019.

[49] Zhice Yang, Zeyu Wang, Jiansong Zhang, Chenyu Huang, and Qian Zhang. Wearables can afford: Light-weight indoor positioning with visible light. In *Proceedings of the 13th Annual International Conference on Mobile Systems, Applications, and Services*, MobiSys '15, page 317–330, New York, NY, USA, 2015. Association for Computing Machinery.

[50] Texas Instrument. Dlp2000 (.2 nhd) dmd datasheet, 2019. https://www.ti.com/lit/ds/symlink/dlp2000.pdf.

[51] Benjamin Lee. Introduction to ±12 degree orthogonal digital micromirror devices (dmds), 2018. https://www.ti.com/lit/an/dlpa008b/dlpa008b.pdf.

[52] Roy Blokker. Communication with ambient light using digital micromirror devices. Master's thesis, Delft University of Technology, 2021.

[53] Motoi Kodama and Shinichiro Haruyama. Visible light communication using two different polarized dmd projectors for seamless location services. In *Proceedings of the Fifth International Conference on Network, Communication and Computing*, ICNCC '16, page 272–276, New York, NY, USA, 2016. Association for Computing Machinery.

[54] Motoi Kodama and Shinichiro Haruyama. Pulse width modulated visible light communication using digital micro-mirror device projector for voice information guidance system. In *2019 IEEE 9th Annual Computing and Communication Workshop and Conference (CCWC)*, pages 0793–0799, 2019.

[55] Yu-Xuan Ren, Rong-De Lu, and Lei Gong. Tailoring light with a digital micromirror device. *Annalen der Physik*, 527(7-8):447–470, 2015.

[56] Tilahun Zerihun Gutema, Harald Haas, and Wasiu O. Popoola. Bias point optimisation in lifi for capacity enhancement. *Journal of Lightwave Technology*, 39(15):5021–5027, 2021.

[57] Pamela Rae Patterson, Dooyoung Hah, Makoto Fujino, Wibool Piyawattanametha, and Ming C. Wu. Scanning micromirrors: an overview. In Yoshitada Katagiri, editor, *Optomechatronic Micro/Nano Components, Devices, and Systems*, volume 5604, pages 195 – 207. International Society for Optics and Photonics, SPIE, 2004.

[58] Dana Dudley, Walter Duncan, and John Slaughter. Emerging digital micromirror device (dmd) applications, 2003. https://www.ti.com/pdfs/dlpdmd/152_NewApps_paper_copyright.pdf.

[59] Farshad Miramirkhani and Murat Uysal. Channel modeling and characterization for visible light communications. *IEEE Photonics Journal*, 7(6):1–16, 2015.

[60] Francisco J. Lopez-Hernandez, Rafael Perez-Jiminez, and Asuncion Santamaria. Ray-tracing algorithms for fast calculation of the channel impulse response on diffuse IR wireless indoor channels. *Optical Engineering*, 39:2775–2780, October 2000.

[61] Vincent Liu, Aaron Parks, Vamsi Talla, Shyamnath Gollakota, David Wetherall, and Joshua R. Smith. Ambient backscatter: Wireless communication out of thin air. *SIGCOMM Comput. Commun. Rev.*, 43(4):39–50, aug 2013.

[62] Dinesh Bharadia, Kiran Raj Joshi, Manikanta Kotaru, and Sachin Katti. Backfi: High throughput wifi backscatter. volume 45, page 283–296, New York, NY, USA, aug 2015. Association for Computing Machinery.

[63] Nguyen Van Huynh, Dinh Thai Hoang, Xiao Lu, Dusit Niyato, Ping Wang, and Dong In Kim. Ambient backscatter communications: A contemporary survey. *IEEE Communications Surveys Tutorials*, 20(4):2889–2922, 2018.

[64] Luiz Eduardo Mendes Matheus, Alex Borges Vieira, Luiz F. M. Vieira, Marcos A. M. Vieira, and Omprakash Gnawali. Visible light communication: Concepts, applications and challenges. *IEEE Comm. Surveys & Tutorials*, 2019.

[65] Sovan Das, Enrique Poves, John Fakidis, Adrian Sparks, Stefan Videv, and Harald Haas. Towards energy neutral wireless communications: Photovoltaic cells to connect remote areas. *Energies*, 2019.

[66] Sovan Das, Adrian Sparks, Enrique Poves, Stefan Videv, John Fakidis, and Harald Haas. Effect of sunlight on photovoltaics as optical wireless communication receivers. *Journal of Lightwave Technology*, 2021.

[67] Qing Wang and Marco Zuniga. Passive visible light networks: Taxonomy and opportunities. In *Proceedings of the Workshop on Light Up the IoT*, LIOT '20, page 42–47, New York, NY, USA, 2020. Association for Computing Machinery.

[68] Talia Xu, Miguel Chávez Tapia, and Marco Zúñiga. Exploiting digital Micro-Mirror devices for ambient light communication. In *USENIX NSDI*, 2022.

[69] Nominoe Lorrière, Nathan Bétrancourt, Marcel Pasquinelli, Gilles Chabriel, Jean Barrère, Ludovic Escoubas, Jyh-Lih Wu, Veronica Bermudez, Carmen Maria Ruiz, and Jean-Jacques Simon. Photovoltaic solar cells for outdoor lifi communications. *Journal of Lightwave Technology*, 2020.

[70] Sung-Man Kim and Ji-San Won. Simultaneous reception of visible light communication and optical energy using a solar cell receiver. In *2013 International Conference on ICT Convergence (ICTC)*.

[71] Yichen Li, Tianxing Li, Ruchir A. Patel, Xing-Dong Yang, and Xia Zhou. Self-powered gesture recognition with ambient light. ACM UIST, 2018.

[72] Dong Ma, Guohao Lan, Mahbub Hassan, Wen Hu, Mushfika B. Upama, Ashraf Uddin, and Moustafa Youssef. Solargest: Ubiquitous and battery-free gesture recognition using solar cells. ACM MobiCom, 2019.

[73] Zixiong Wang, Dobroslav Tsonev, Stefan Videv, and Harald Haas. Towards self-powered solar panel receiver for optical wireless communication. In *IEEE ICC*, 2014.

[74] Gaofeng Pan, Panagiotis D. Diamantoulakis, Zheng Ma, Zhiguo Ding, and George K. Karagiannidis. Simultaneous lightwave information and power transfer: Policies, techniques, and future directions. *IEEE Access*, 2019.

[75] Panagiotis D. Diamantoulakis, George K. Karagiannidis, and Zhiguo Ding. Simultaneous lightwave information and power transfer. *IEEE Transactions on Green Communications and Networking*, 2018.

[76] Global progress in photovoltaic technologies and the scenario of development of solar panel plant and module performance estimation Application in Nigeria. *Renewable and Sustainable Energy Rev.*, 2015.

[77] Apollo3 Blue Plus. `https://wiki.dfrobot.com/Ambient_Light_Sensor_0_200klx_SKU_SEN0390#target_0`.

[78] CMSIS DSP software library. `https://www.keil.com/pack/doc/CMSIS/DSP/html/index.html`. Accessed: 2022-09-01.

[79] D. Jones. Goertzel's algorithm. *This recently updated page provides a concise mathematical treatment of the Goertzel Algorithm in its general form*, 2006.

[80] Dfrobot SEN0390. `https://ambiq.com/apollo3-blue-plus`.

[81] Borja Genoves Guzman, Muhammad Sarmad Mir, Dayrene Frometa Fonseca, Ander Galisteo, Qing Wang, and Domenico Giustiniano. Prototyping Visible Light Communication for the Internet of Things Using OpenVLC. *Comm. Mag.*, 61(5):122–128, may 2023.